THESIS APPROVAL

GRADUATE SCHOOL, KASETSART UNIVERSITY

Master of Engineering (Chemical Engineering)

DEGREE

Chemical Engineering	Chemical Engineering
FIELD	**DEPARTMENT**

TITLE: Catalytic Cracking of Heavy Oil in a Downer Reactor with Heat Loss Through the Wall

NAME: Mr. Chanin Sraphet

THIS THESIS HAS BEEN ACCEPTED BY

THESIS ADVISOR

(Associate Professor Terdthai Vatanatham, Ph.D.)

THESIS CO-ADVISOR

(Associate Professor Sunun Limtrakul, D.Sc.)

DEPARTMENT HEAD

(Associate Professor Phungphai Phanawadee, Ph.D.)

APPROVED BY THE GRADUATE SCHOOL ON

DEAN

(Associate Professor Gunjana Theeragool, D.Agr.)

THESIS

CATALYTIC CRACKING OF HEAVY OIL IN A DOWNER REACTOR WITH HEAT LOSS THROUGH THE WALL

CHANIN SRAPHET

A Thesis Submitted in Partial Fulfillment of
the Requirements for the Degree of
Master of Engineering (Chemical Engineering)
Graduate School, Kasetsart University
2010

Chanin Sraphet 2010: Catalytic Cracking of Heavy Oil in A Downer Reactor with Heat Loss Through the Wall. Master of Engineering (Chemical Engineering), Major Field: Chemical Engineering, Department of Chemical Engineering. Thesis Advisor: Associate Professor Terdthai Vatanatham, Ph.D. 149 pages.

A mathematical model of catalytic cracking of heavy oil in a downer reactor with heat loss through the wall was developed based on the dispersion model and 4-lump kinetics. The model was used to predict the product yield and the temperature distribution in non-isothermal, isothermal, and adiabatic cases. In this work, the effect of heat loss through the wall was included into the dispersion model of catalytic cracking of heavy oil in the downer reactor. The rate of heat losses through the wall was obtained from the heat transfer experiments. The overall heat transfer coefficient obtained experimentally was used to calculate the rate of heat loss and added in to the energy balance equation. The correlation of overall heat transfer coefficient is in the form of $U = 0.000408 G_g^{3.31} G_s^{1.37}$ kW/m^2.K. This equation is applicable in the temperature range of 300 - 560 ^{o}C, the solid flux of 2.2 - 5.6 kg/m^2.s, and the gas flux range of 3.8 - 5.8 kg/m^2.s. Simulation results show that the heat loss effect causes the axial temperature profiles in the simulated non-isothermal reactor to be lower than the adiabatic and isothermal cases. The reduction in temperature gives lower reactant conversion at the same feed conditions. At the ambient inlet solid temperature (35 ^{o}C), the reaction does not occur in the reactor. A high inlet solid temperature leads to a higher conversion. The conversion to products is affected by inlet gas temperature, inlet solid temperature, gas flux, and solid flux. The highest gasoline yield is obtained with isothermal downer reactor with high solid catalyst temperature and feeding rate and the length of 3 m.

______________________ ______________________ ___ /___ /___

Student's signature Thesis Advisor's signature

ACKNOWLEDGEMENT

I would like to dedicate my sincere thank to people who have contributed either directly or indirectly to this thesis. Moreover, my appreciation extends to those who were involved in my study and research but whose names are not mentioned here.

First, I would like to express my sincere gratitude and deep appreciation to my advisor and co-advisor, Assoc. Prof. Dr. Terdthai Vatanatham, and Assoc. Prof. Dr. Sunun Limtrakul for all the guidance, supervision, comments, discussions and invaluable suggestions throughout this project. They also gives me many good opportunities. This work would not be accomplished without their help.

I deeply thank to the Kasetsart University Research and Development Institute (KURDI), and National Center of Excellence for Petroleum, Petrochemical, and Advanced Materials (NCE-PPAM) through the Post Graduate Education and Research Development Program in Chemical Engineering at Kasetsart University for their financial supports.

I would like to express my special thank to Plastic Cracking Laboratory members (Sanya, Chainurak, Pattarawan, Sanphet, Varanyu, Thitichai) and all colleagues in both Assoc. Prof. Dr. Terdthai's research group and Assoc. Prof. Dr. Sunun's research group for their warm friendship, suggestions, and all supports.

My deepest appreciation goes to my parents, family, and friends for their unconditional love, understanding, and supporting me.

Chanin Sraphet
April 2010

TABLE OF CONTENTS

Page

LIST OF TABLES

Appendix Table

LIST OF FIGURES

LIST OF FIGURES (Continued)

LIST OF FIGURES (Continued)

LIST OF FIGURES (Continued)

LIST OF FIGURES (Continued)

LIST OF FIGURES (Continued)

LIST OF FIGURES (Continued)

Figure **Page**

LIST OF FIGURES (Continued)

Figure **Page**

Appendix Figure

LIST OF FIGURES (Continued)

Appendix Figure **Page**

LIST OF ABBREVIATIONS

a = Surface area of particle per bed volume, [m^2m^{-3}]
A = Surface area, [m^2]
C = Concentration, [kg/m^3]
C_D = Drag coefficient, [-]
C_p = Heat capacity, [kJ/kg.K]
D_{im} = diffusion coefficient, [m^2/s]
G = Mass flux, [$kg/m^2.s$]
ΔH = heat of reaction, [kJ/kg]
h = Heat transfer coefficient, [$kW/m^2.K$]
i = The component of reaction
k = Thermal conductivity, [kW/m.K]
k_i = Kinetic rate constant
k_{ig} = Mass transfer coefficient between phases, [m/s]
L = Length of reactor, [m]
$\dot{m}$ = Mass flow rate, [kg/s]
M_n = Molecular weight, [kg/kmol]
P = Pressure, [atm]
Pe = Peclect Number, [-]
r = Reaction rate
Re = Reynolds Number, [-]
T = Temperature, [^oC]
u = Superficial velocity, [m/s]
U = Overall heat transfer coefficient, [$kW/m^2.K$]
v = velocity, [m/s]
y = Mass fraction, [-]
Z = Dimensionless of length, [m]

LIST OF ABBREVIATIONS (Continued)

Greek symbol

ρ = Density, [kg/m^3]

θ = Dimensionless of temperature, [-]

ε = Void fraction, [-]

μ = viscosity (Pa·s)

Subscripts

g = Gas phase

s = Solid phase

j = Jacket

w = Wall

The i-components of catalytic cracking of heavy oil

A = Heavy oil

B = Gasoline

C = Light gas

D = Coke

CATALYTIC CRACKING OF HEAVY OIL IN A DOWNER REACTOR WITH HEAT LOSS THROUGH THE WALL

INTRODUCTION

Nowadays, plastics are generally useful in the life styles. The waste plastics are also significant waste after its usage. The waste plastics are hard and long time for degradation and destruction. Everyone knows in it creates several environment problems and attempt to solve this problem together. The cracking process is developed to convert the structure of waste plastic to fuel. It can be converted by 2 main route, thermal cracking (pyrolysis) and catalytic cracking. Both cracking process has to be operated in the absence of oxygen and high temperature. The catalytic cracking require lower energy for cracking and can control the desire product when compare with the thermal cracking. The heavy oil is obtained from the thermal cracking then distilled to separate light compounds.

Many researchers experimented with several types of reactor. Circulating fluidized bed reactor has been proven that it is the highly effective reactor for catalytic cracking. Circulating fluidized bed (CFB) reactors have been widely used in many fields such as chemical industry, energy and materials. CFB include the gas-solid co-current up flow system (riser) and the gas-solid co-current down flow system (downer). The advantage of the flow of gas–solid suspension in CFB downer is that both gas and solid are in the same direction with gravity. Therefore the contact time is uniform and the extent of axial back mixing is reduced greatly in comparison to CFB risers. The flow inside the reactor approaches plug flow conditions. The radial profiles of velocity and solid concentration are also much more uniform across the downer cross-section.

The mixing behavior is important for heat transfer and mass transfer. The axial dispersion model is used to explain the flow pattern in the reactor. The dispersion model has considered the influence of mixing along the reactor by Peclect number. The Peclet number indicates the ratio of convection to dispersion which is quite similar to the real flow pattern of the downer reactor. The Peclect number in downer reactor can reach 100 which approach to the plug flow condition.

Normally, the heat transfers in the downer reactor are the heat conduction, the heat convection, heat transfer between phases, and heat of reaction. The heat transfer in the downer reactor is studied in experiments and modeling. Many researchers studied in the heat transfer between phases, heat convection, and the heat of reaction from the cracking reaction.

This work shows the simulations for catalytic cracking of heavy oil with the heat loss through the wall in the downer reactor. The heat losses through the wall were obtained from the heat transfer experiments. The data from hydrodynamic of downer reactor, the heat transfer in solid-gas and surrounding system are used to investigate and predict the gas temperature distributions along the length of reactor under various operating conditions.

OBJECTIVES

1. To study the temperature and mass distributions of heavy oil cracking in a downer reactor with heat loss through the wall and study the effect of various operating variables.

Scope of the Investigation

1. The rate of heat loss through the wall is obtained from experimental result.

2. Four-lump kinetic model is used in the modeling of heavy oil cracking.

3. Mathematical model for prediction of temperature and mass distribution in the downer reactor is done in terms of dispersion model.

4. The operating variables studied are gas flux, solid flux, inlet gas and solid temperatures as well as operating schemes in isothermal, adiabatic, and non- adiabatic modes.

Impact of research

1. Better prediction of temperature and mass distributions for catalytic cracking of heavy oil in downer reactor.

2. Mathematical model is available for development of better design of the downer reactor.

LITERATURE REVIEW

1. Plastics

Plastics play an important role in almost every aspect of our lives. Plastics are used in manufacturing of everyday products such as beverage containers, household items, and furniture. The widespread use of this valuable material demands proper management of waste plastics, as they have become a larger part of the municipal solid waste (MSW) stream in recent decades.

Plastics are polymers. The simplest definition of a polymer is something made up of many units. Polymers are chains of molecules. Each link of the chain is usually made of carbon, hydrogen, oxygen, and/or silicon to make the chain. Many links are hooked or polymerized, together.

To create polymers, petroleum and other hydrocarbon materials are heated under controlled conditions and broken down into smaller molecules called monomers. These monomers are the building blocks for polymers. Different combinations of monomers produce plastic resins with different characteristics, such as strength or molding capability.

Plastics can be divided in to two major categories; thermosetting and thermoplastic:

a) Thermosetting

Thermosetting is a polymer that solidifies or "sets" irreversibly when heated. They are useful for their durability and strength, and are therefore used primarily in automobiles and construction. Other uses are adhesives, inks, and coatings.

b) Thermoplastic

Thermoplastic is a polymer in which the molecules are held together by weak bonds, creating plastics that soften when exposed to heat and return to original condition at room temperature. Thermoplastics can easily be shaped and molded into products such as milk jugs, floor coverings, credit cards, and carpet fibers.

1.1 Municipal solid waste

Our trash, or municipal solid waste (MSW), is made up of the things we commonly use and then throw away. These materials range from packaging, food scraps, and grass clippings, batteries, tires, and etc. MSW does not include industrial, hazardous, or construction waste .In recent years, municipal waste increase very fast every year. In Thailand, municipal waste is about 14.6 million tons in 2004 but can be recycling and reuse 3.1 million tons per year or 21.23%. The most remaining waste is land filled Waste consumption is growing about 0.7-1.45% every year in Thailand. In 2010, the developing countries will increase the municipal solid waste at an annual rate of 2.7 percent. The municipal solid waste generation and recycle in Thailand, 1996-2004 is illustrated in Table 1. (Ministry of natural resource and environment, 2004)

Table 1 The municipal solid waste and recycle in Thailand, 1996-2004.

Year	Waste (million tons)	Recycle waste (million tons)	Recycle %
1996	13.1	1.4	10.69
1997	13.5	1.5	11.11
1998	13.6	1.6	11.76
1999	13.8	1.8	13.04
2000	13.9	2.0	14.39
2001	14.1	2.2	15.60
2002	14.3	2.6	18.18
2003	14.4	2.8	19.44
2004	14.4	3.1	21.23

Source: Ministry of natural resource and environment (2004)

The most common types of MSW materials are food scraps, plastics, papers, glasses, woods, metals, textures, rubbers/leathers, and another. The food scraps is the highest amount and the plastic waste is second as 63.57% and 16.83%, respectively. The management of the municipal solid waste in Thailand is shown in Figure 1. (Ministry of natural resource and environment, 2004)

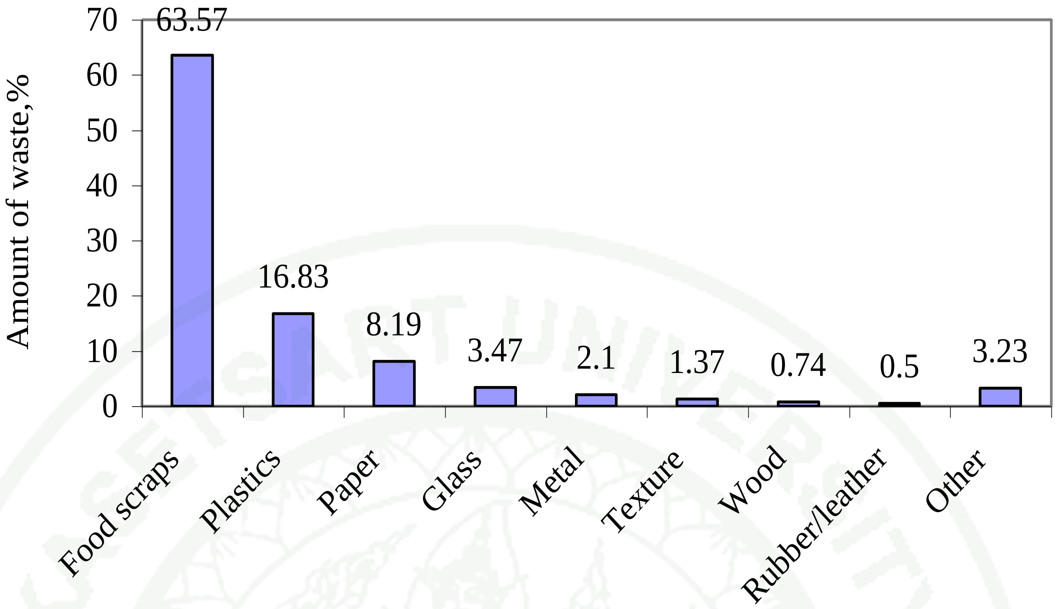

Figure 1 The management of the municipal solid waste in Thailand.

Source: Ministry of natural resource and environment (2004)

1.2 Plastics Cracking

Plastic can be converted from the large molecules to smaller molecules, which at room temperature become liquid and gas, by cracking with 2 main ways. They are thermal cracking and catalytic cracking.

1.2.1 Thermal cracking process

Thermal cracking or pyrolysis is a conversion of plastics into chemicals by high temperature, in the absence of the oxygen and catalyst. The mechanism of plastics pyrolysis has been presented in three types of mechanisms. They are: (Cullis and Hirschler, 1981)

a) End-chain scission or depolymerization: The polymer is broken up from the end groups successively yielding the corresponding monomers.

b) Random-chain scission: The polymer chain is broken up randomly into fragments of uneven length.

c) Chain-stripping: Elimination of reactive substitutes or side groups on the polymer chain, leading to evolution of a cracking product on the one hand, and a charring polymer chain on the other.

These different mechanisms and product distributions are to some extent related to bond dissociation energies, the chain defects of polymers, and the aromaticity degree, as well as the presence of halogen and other hetero-atoms in the polymer chains. For common plastics, the decomposition mechanisms and associated monomer yield are listed in Table 2. (Shoeter and Buekens, 1979)

Table 2 Decomposition mechanisms and monomeric yields of some polymer.

Polymers	Decomposition mechanisms	Monomeric yield (wt%)
Polymethylmetacrylate	End-chain scission	91-98
Polytetrafluorethylene	End-chain scission	95
Polymethacrylonitrile	End-chain scission	90
Polyethylstyrene	End-chain scission	82-94
Polystyrene	End-chain scission and Random-chain scission	42-45
Polyisobutene	End-chain scission and Random-chain scission	18-25
Polyethylene	Random-chain scission	0.03
Polypropylene	Random-chain scission	0-17
Polybutadiene	Random-chain scission	1
Polyvinylchloride	Chain-stripping	0-0.07
Polyvinyl fluoride	Chain-stripping	0
Polyacrylonitrile	Chain-stripping	5

Source: Shoeter and Buekens (1979)

1.2.2 Catalytic cracking process

The plastics are big molecules hydrocarbon compounds. Catalytic cracking is the reactions that reduce the size of high or long molecules into the smaller ones. The catalyst that used in the process will give more desire products (such as gasoline or oil, and LPG) when compared with the thermal cracking. Catalyst will reduce the reaction temperature and activation energy so the time, heat, and energy requirement decrease.

The catalytic cracking process can be divided according to main phase contacting as liquid phase and vapor phase. In liquid phase contact, the catalyst is contacted with melted plastics and acts mainly on the partially degraded oligomers from the polymer chains. In vapor phase contact, the polymer is thermally degraded into hydrocarbon vapors which are then contacted with the catalyst. Most of experiments and models are concentrated in vapor phase contact because the large scale industries work with this phase.

2. Reactor for plastic cracking

The reactors are the containers that load the reactants or initial agents that produce the reaction inside. The selection of reactor has to consider on the main products, by products, dimension of reactor, the physical properties, the capacity, the resident time, and etc. The reactors used in plastic cracking process have several designs but each of reactors has advantages and disadvantages depends on products or the condition that researcher’s desire. The general types of reactor were fluidized bed reactor, packed bed reactor, and etc.

2.1 Thermal cracking reactor

Thermal cracking reactors are the system used for transforming of the plastics or high hydrocarbon to the smaller hydrocarbon and other components. The main ideal conditions are in absence of oxygen and catalyst. The thermal cracking reactors also have several types, such as fluidized bed and heated vessels.

Fluidized bed reactor is a type of reactor that can be used to carry out a variety of multiphase chemical reactions. In this type of reactor, a fluid (gas or liquid) is passed through the bed of solid material such as sand, at high velocities to suspend the solid, which is heat carrier, and cause it to behave as though it is a fluid. The fluidized bed reactor is now used in many industrial applications.

For thermal cracking, fluidized bed reactor gives a great heat transfer between gas and solid in contact. The procedure in fluidized bed reactor is that fine plastics are dropped down from the top of reactor and nitrogen is pursed into the bottom of the reactor for fluidizing the fine solid (such as sand) inside the reactor. Inside the reactor, there are heating coils for controlling the temperature. The main heat transfers are heat conduction from solid to plastic and heat convection from gas-solid to plastics. When the product gas flows out from the reactor, it passes through the pipe to the condenser system to cool down and condense the big molecules into liquid form. The remaining gas can be collected with sampling bags for analysis of data and experiments. The fluidized bed reactor has advantage in very good heat transfer between gas-solid contacts but has long residence time and is difficult to control operation. It can be operated as batch or semi-batch. The fluidized bed system for thermal cracking is shown in Figure 2.

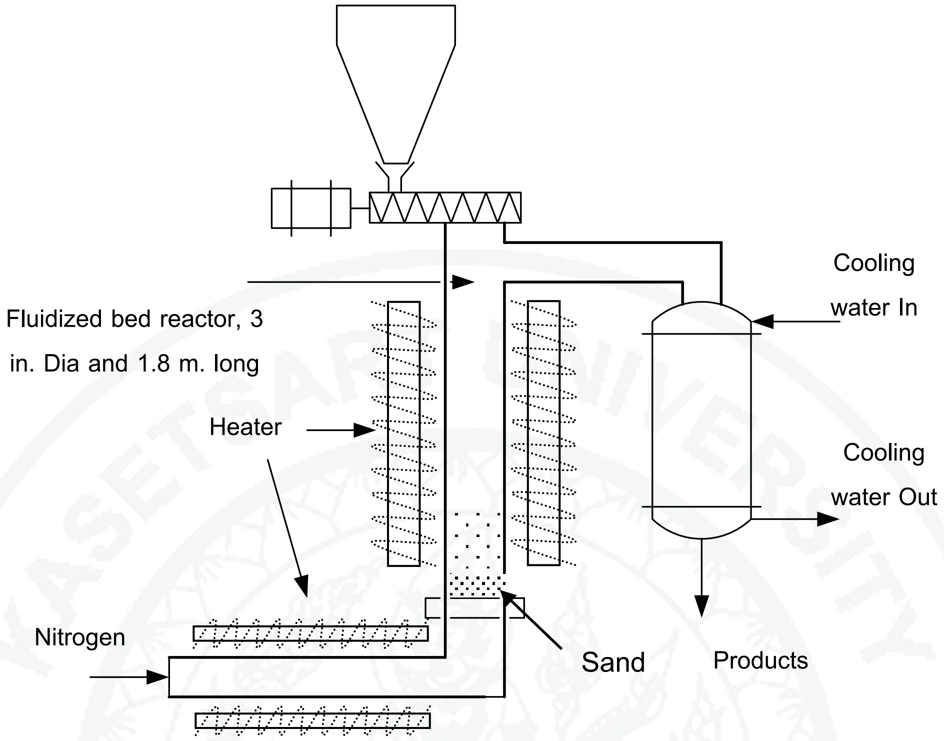

Figure 2 Schematic diagram of thermal cracking fluidized bed for polypropylene cracking.

Source: Klomklom (2009)

The most popular thermal cracking reactor is a heating chamber which is surrounded with heater or other energy supply. The plastics are put into the chamber with flow of nitrogen gas to eliminate the oxygen inside the reactor. The heat is supplied for cracking reaction inside. The plastic changes to plastic vapor at high temperature, then flow out to condenser unit or catalytic cracking unit. Furthermore, thermal cracking is also use in thermogravimetric analysis (TGA) analyzer for analysis of thermal decomposition of plastic. The heating chamber is illustrated in Figure 3.

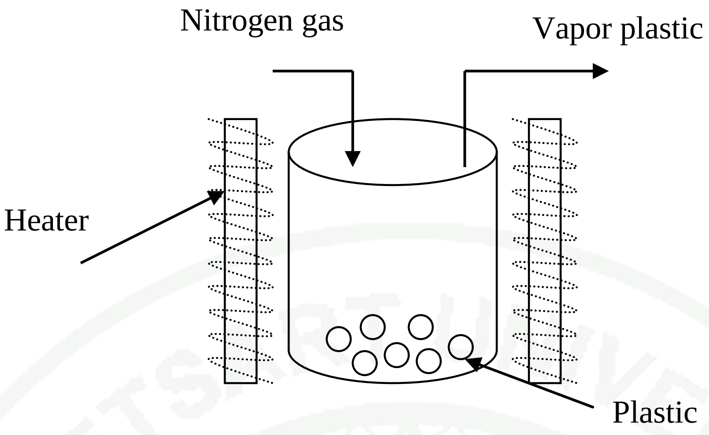

Figure 3 Schematic diagram of heating chamber reactor for thermal cracking.

Source: Pum-in (2006)

2.2 Catalytic cracking reactor

In recent years, catalytic cracking of hydrocarbon vapor is widely used in the chemical industry and is developed continuously. The catalytic cracking reactor is also used in absent of oxygen, the same as in thermal cracking process. There are several types of catalytic cracking reactors in current used.

Fluidized bed reactor in catalytic cracking is the same as one in thermal cracking except sand is replaced with catalyst. These reactors give more of desired product depending on types of catalyst. They also need lower energy. In this reactor, refreshing of the catalyst to maintain high conversion is more convenient than packed bed reactor. The fluidized bed reactor for catalytic cracking is illustrated in Figure 4.

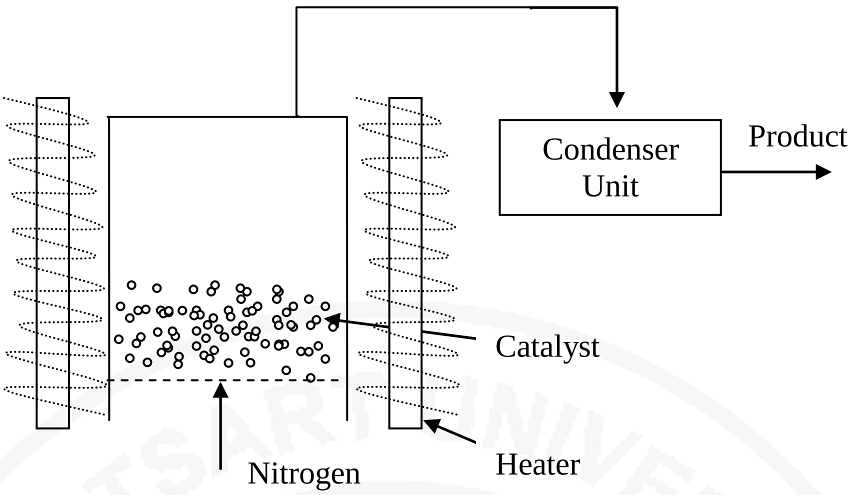

Figure 4 Schematic diagram of catalytic fluidized bed reactor.

Source: Lin and Yang (2007)

The packed bed reactor is one type of catalytic reactor that is generally used in chemical laboratories and industries. Normally, the fluid flows through the fixed bed of catalyst in a pipe. It has high conversion and easy to control. The disadvantages are low heat transfer between catalyst bed and the reactor wall and catalyst regeneration is not a continuous operation.

A schematic diagram of two-stage reaction systems, thermal cracking and catalytic cracking, is show in Figure 5. Plastics accumulate in a glass chamber at the bottom of the equipment with heating coils along its side to transfer heat into reactor. The plastic is vaporized and plastic vapor flows through a packed bed of catalyst region for reforming into the desired products. The products pass through the condenser system and are collected as gas and liquid.

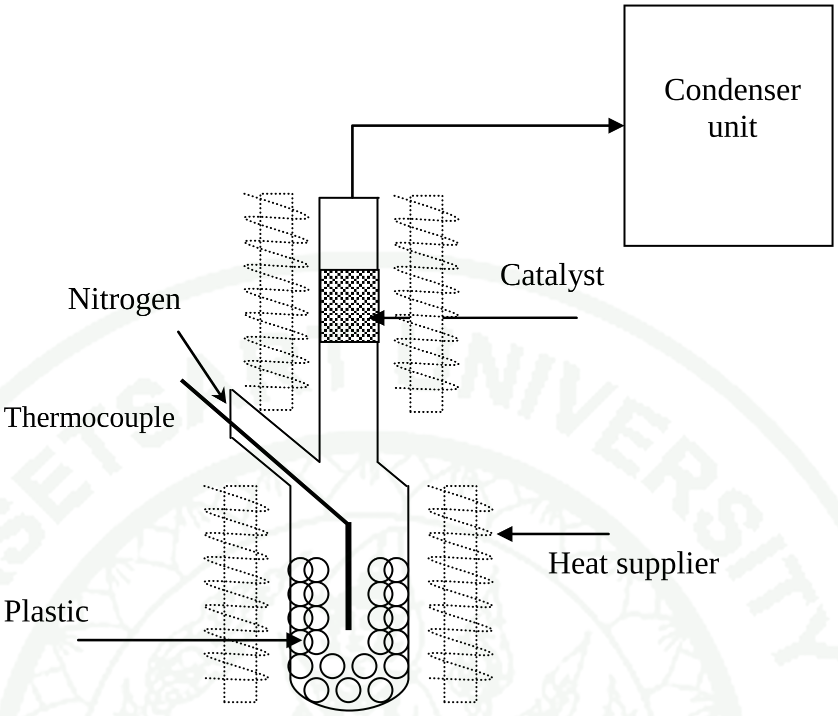

Figure 5 Schematic diagram of two stage reaction systems with thermal cracking and catalytic cracking (packed bed).

Source: Aguado *et al.* (2007)

A stirred batch reactor is a mobilized bed in a reactor. In the reactor, there is a catalyst basket which spins inside at a constant or variable. This type of reactor has advantage in the kinetic and mass transfer. The disadvantage is that there is a dead zone inside the reactor. In this process, plastic vapor flows though a mixing tank with spinning solid basket. The products flow out and go though the condenser for collection of liquid hydrocarbon and gas product. The schematic diagram of a stirred batch reactor is shown in Figure 6.

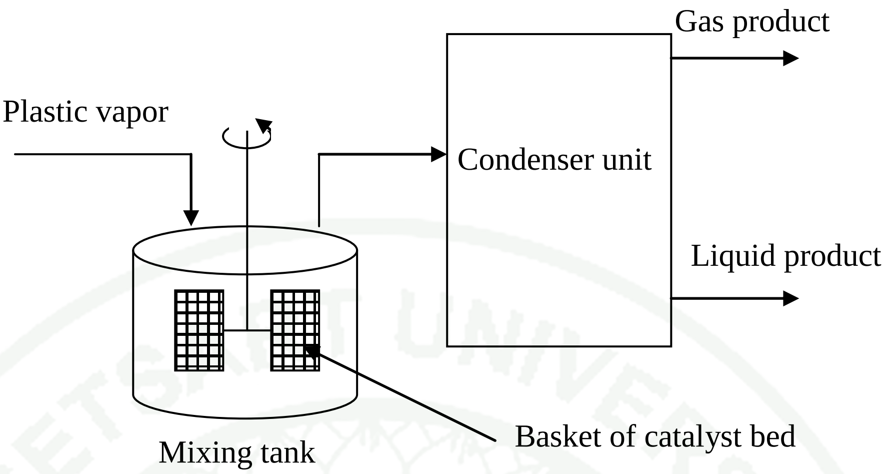

Figure 6 Schematic diagram of a stirred batch reactor with catalytic reaction.

Source: Pum-in (2006)

Circulating fluidized bed (CFB) reactor is a type of reactor with combination the good points. The circulating fluidized bed reactors have been long used in the fluid catalytic cracking (FCC) industry and applied in various types of processes involving gas–solid reactions because of their excellent mixing and transport characteristics. CFB can be divided into two types according to the gas–solid flow directions, the gas–solid co-current up flow circulating fluidized bed system (riser) and the gas–solid co-current down flow circulating fluidized bed system (downer). The advantage of the flow of gas–solid suspension in CFB downer is that gas and solid are in the same direction with gravity. Therefore the contact time is uniform and the extent of axial back mixing is reduced greatly in comparison to CFB risers. The flows inside the reactor approaches plug flow conditions. The radial profiles of velocity and solid concentration are also much more uniform across the downer cross-section.

Co-current down flow circulating fluidized bed diagram (downer) is illustrated in Figure 7. Gas and solid catalyst are fed from the top of the reactor through gas-solid distributor. Then solid flows downwards under the gravity force and gas flows under the momentum of the entering flows. Gas products are separated from the solid at the bottom of the reactor by a separator tank and cyclone. The products are fed to a condenser system immediately to stop further thermal reaction and separate the gas-liquid products. The catalyst section, which is deactivated, goes to the riser system in a co-current up flow circulating fluidized bed for regeneration and preparation to be fed into the distributor zone again. The solid in the riser is carried by hot air and fluidized during the movement. Several schematic diagrams of downer reactor for studying the flow pattern, solid distribution, temperature distribution, and etc. are demonstrated in Figure 7, 8, and 9. The gas and solid distributor of downer system is presented in Figure 10.

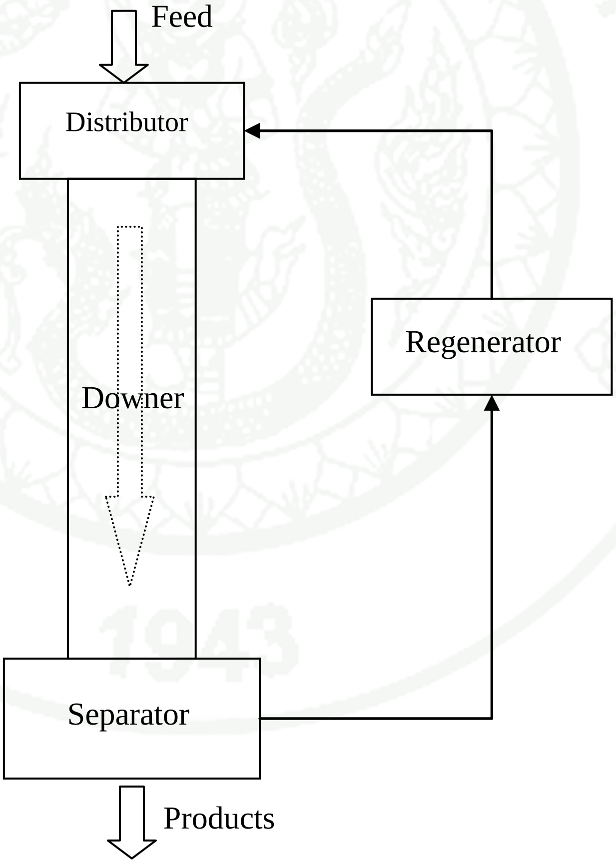

Figure 7 Pattern of co-current down flow fluidized bed reactor.

Source: Cheng *et al*. (2008)

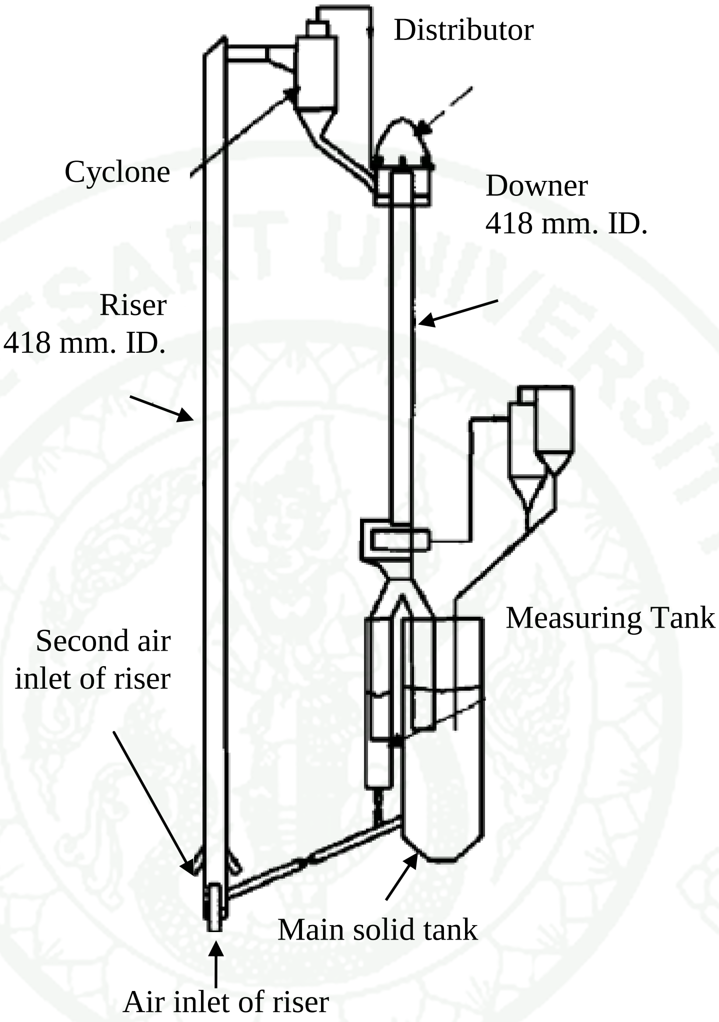

Figure 8 Schematic diagram of downer reactor (1).

Source: Chen and Li (2004)

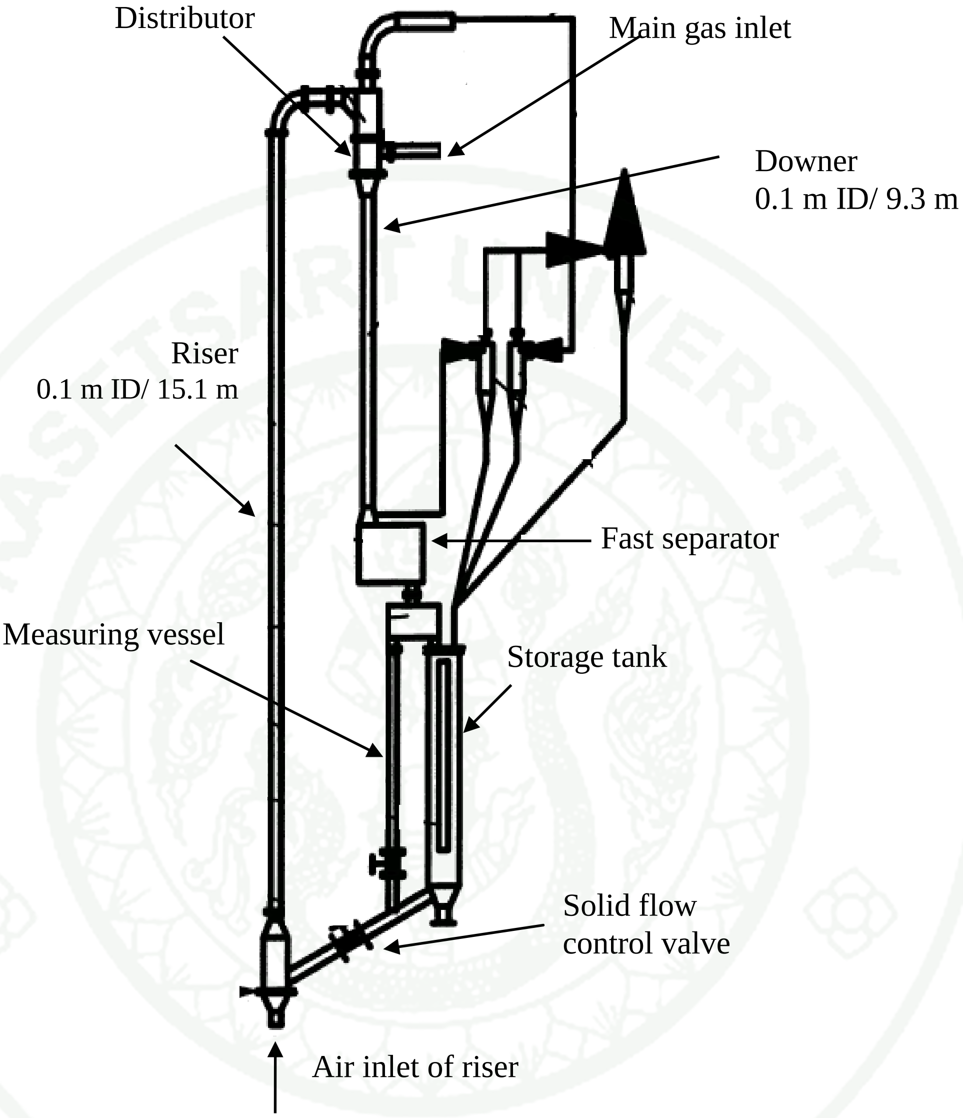

Figure 9 Schematic diagram of downer reactor (2).

Source: Bolkan *et al*. (2003)

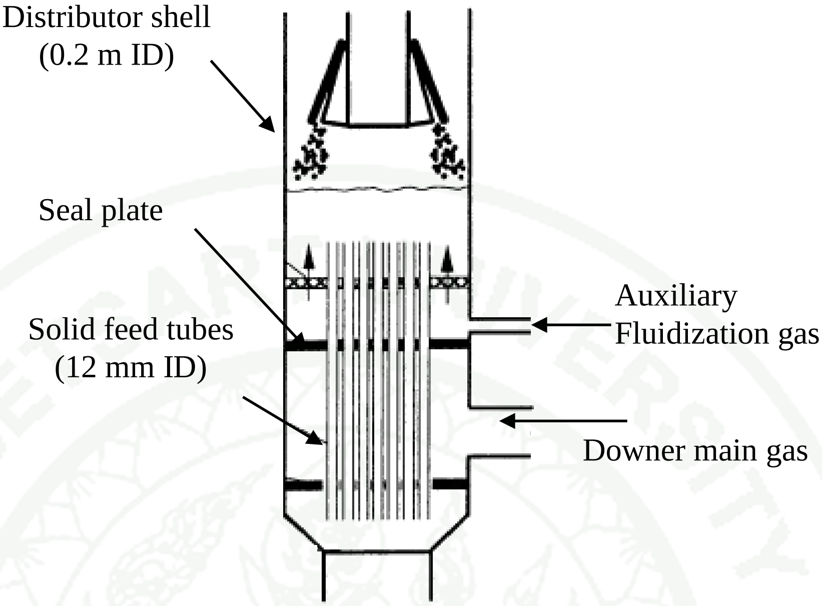

Figure 10 Schematic diagram of downer distributor.

Source: Bolkan *et al*. (2003)

3. Hydrodynamic of down flow fluidized bed

The co-current down flow fluidized bed is suitable for catalytic cracking process, many studies to improve hydrodynamic, thermal, and mixing behavior such as superficial velocity, solid flow rate, temperature gradient, dispersion, and etc. in downer reactor are going on. The hydrodynamic behaviors of gas-solid suspension represented in the reactor for both of the developing flow and fully developed flow. Behavior of gas-solid flowing along the direction of the gravity force in the developing flow phenomena are divided into 3 sections. They are the first acceleration section, the second acceleration section, and the constant velocity section. The developing flow phenomena in the downer reactor are illustrated in Figure 11. In the first acceleration section, noticed immediately below the distributor, the gas velocity is high and particle velocity is very low. Solid are accelerating by both the gas flowing and the gravity until the solid velocity is equal to the gas velocity. The pressure drop is negative in this section. In the second acceleration section, particles are further accelerating by gravity but resisted by the flowing gas. Particle velocity then over takes the gas velocity and increases further until the gas drag force (in the upward direction) counter balances the gravitational force. In this section, the pressure drop is positive and gradually increases. When the gravitational force is in balance with the drag force, both particle and gas velocities remain constant. The pressure drop also becomes constant. This section is the constant velocity section. (Liu *et al*., 2001)

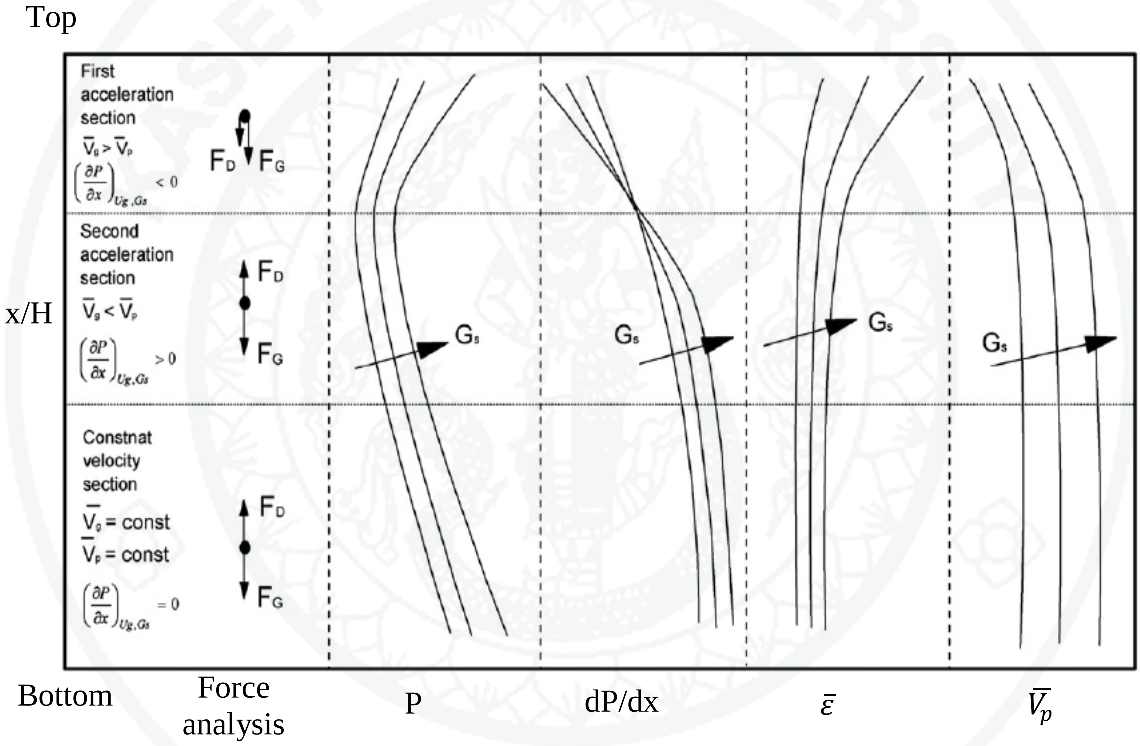

Figure 11 Illustration of typical axial flow structure in the downer reactor.

Source: Cheng *et al*. (2008)

Solid holdup is one of the key parameters which characterize a gas–solid system. In a co-current gas–solid system, both up flow and down flow, gas velocity and solid flux are the main operating variables influencing the solid holdup. Generally, an increase of gas velocity reduces the solid holdup at a constant solid flux and an increased solid flux results in an increase in the solid holdup when the gas velocity is fixed.

In a solid holdup case study in the fully developed region, the range of gas velocity was 0-7.82 m/s and range of solid flux was 0-1,600 kg/m^2.s. In the entire range of gas velocities, the solid holdup is seen to increase almost in linear relationship with the solid flux for any types of particles which are FCC particle, and glass beads. Furthermore, a higher velocity significantly lowers the solid holdup. For the large size of particle, the slope of solid holdup versus solid flux decreases. The larger particle size leads to lower ratio of drag force to gravitational force. The mean solid holdup in fully developed flow section with various solid flux at the difference gas velocity and types of particle are shown in Figure 12.

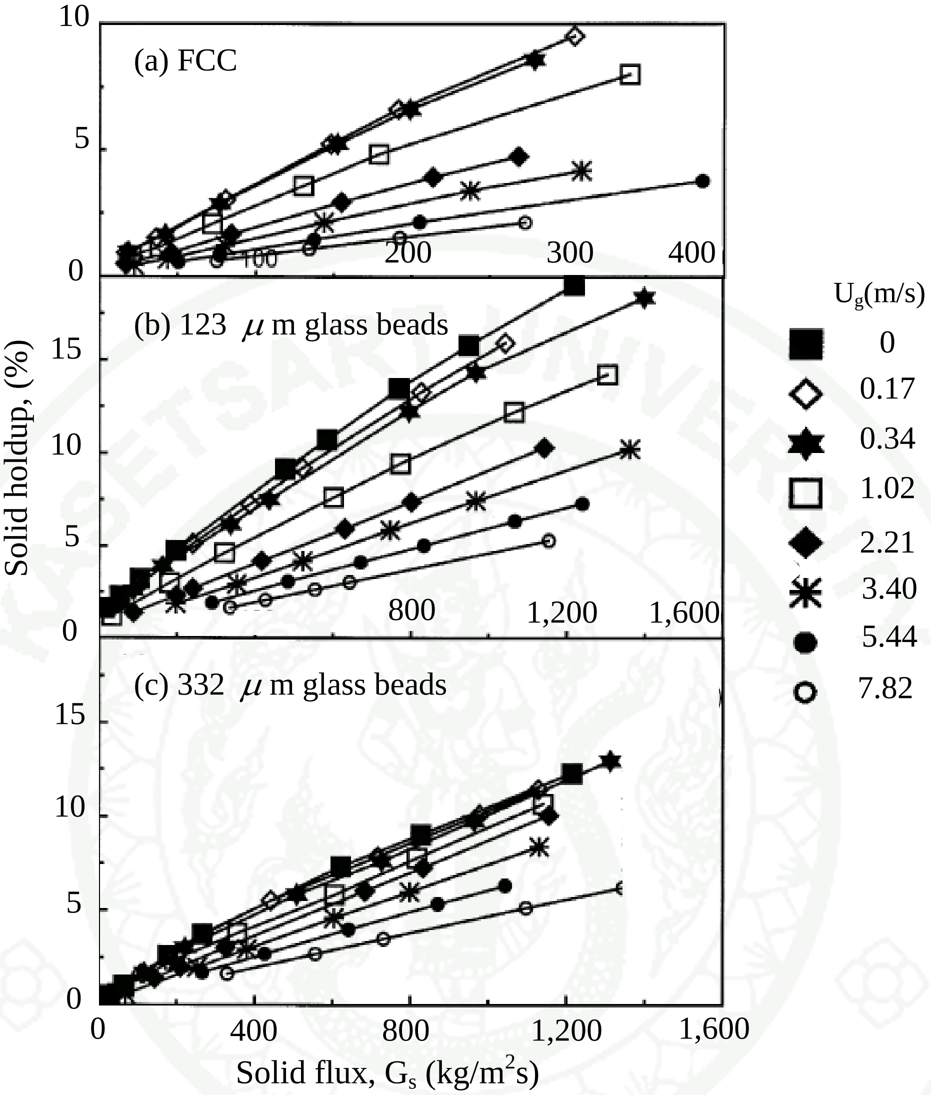

Figure 12 Solid hold up in the fully developed region as a function of solid flux at various gas velocity.

Source: Liu *et al*. (2001)

The solid holdup with various superficial gas velocity at the different solid flux were also replotted. The three particle types have similar trends that are the solid holdup decreases inversely with gas velocity at the same solid flux. This is reasonable since increasing of gas velocity increases the particle velocity which in turn results in lower solid holdup under fixed solid flux. Variation of the solid holdup with superficial gas velocity in fully developed region is illustrated in Figure 13.

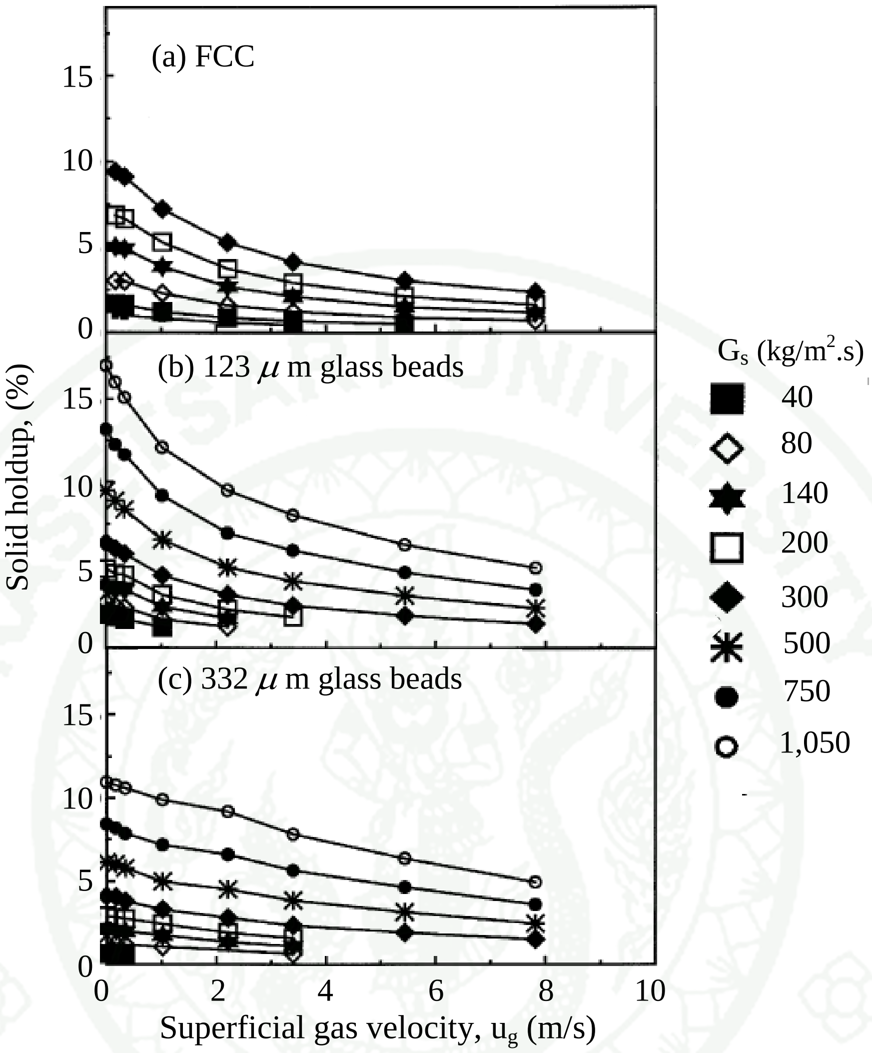

Figure 13 Solid holdup in the fully developed region as a function of superficial gas velocity at various solid flux.

Source: Liu *et al*. (2001)

In the developed zone, the variation of particle velocity with superficial gas velocity is nearly linear as shown in Figure 14. This figure also shows the influence of the particle characteristics on the particle velocity. Changing particle size seems not to change the high particle velocity, as shown by Figure 14 (b) and (c). For the lower-density FCC particles, on the other hand, particle velocity increases faster with the gas velocity and becomes higher than those of the two glass bead particles at higher U_g although they are similar at lower velocity.

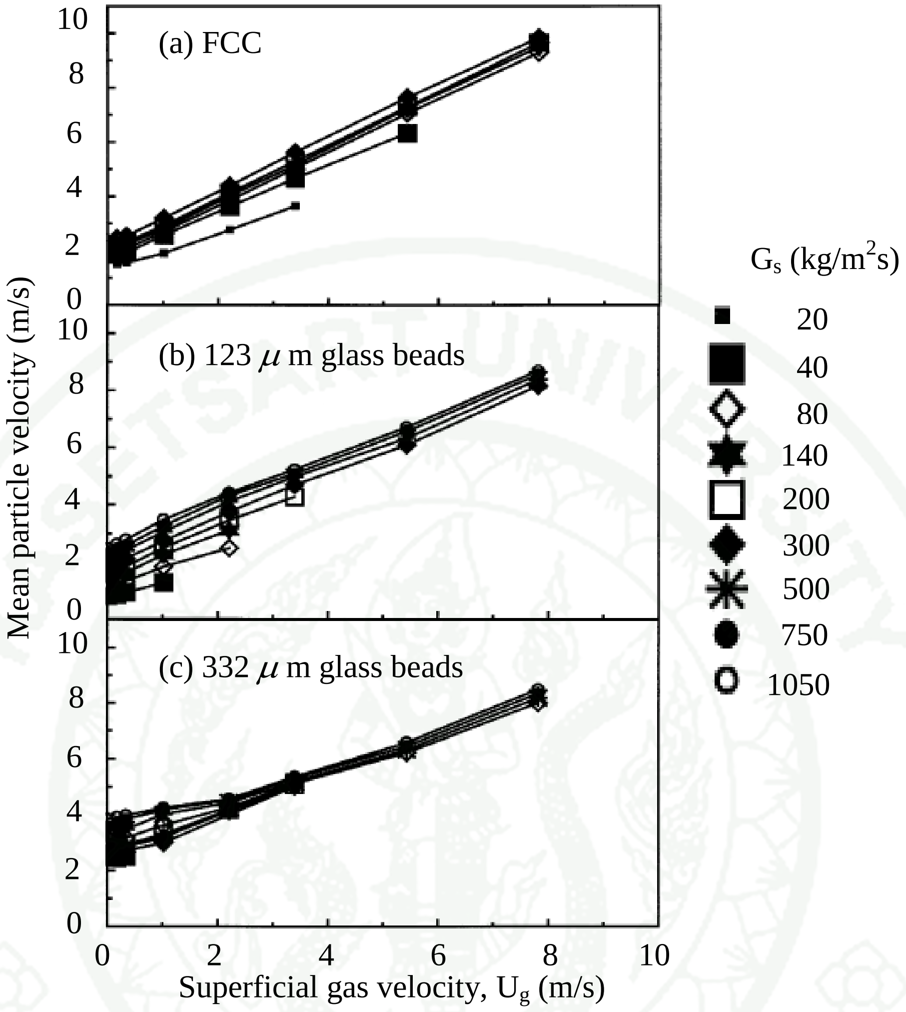

Figure 14 Mean particle velocity as a function of superficial gas velocity in fully developed zone at various particle size.

Source: Liu *et al*. (2001)

Furthermore, solid holdup in developing zone and fully developed zone in a downer reactor change axially but the pattern is the same. The radial distribution in downer at different height of the reactor shows that the uniform flow pattern occurs in the center region. The radial profiles are more uniform flow in the center region and the solid concentration is higher at the wall as shown in Figure 15 and 16.

The radial distributions of solid concentration $\left(\varepsilon^{*} = \varepsilon_s / \varepsilon_{av}\right)$ become more uniform with increasing length of axial position. The flow pattern changes from the acceleration and developing region to developed region after the entrance at the edge of the reactor. In the first region, most of solids accumulate near the wall, as both gas and solid flow downward. The solid concentration near the wall slowly decreases until nearly approach to the uniform pattern flow. (Chen and Li, 2004)

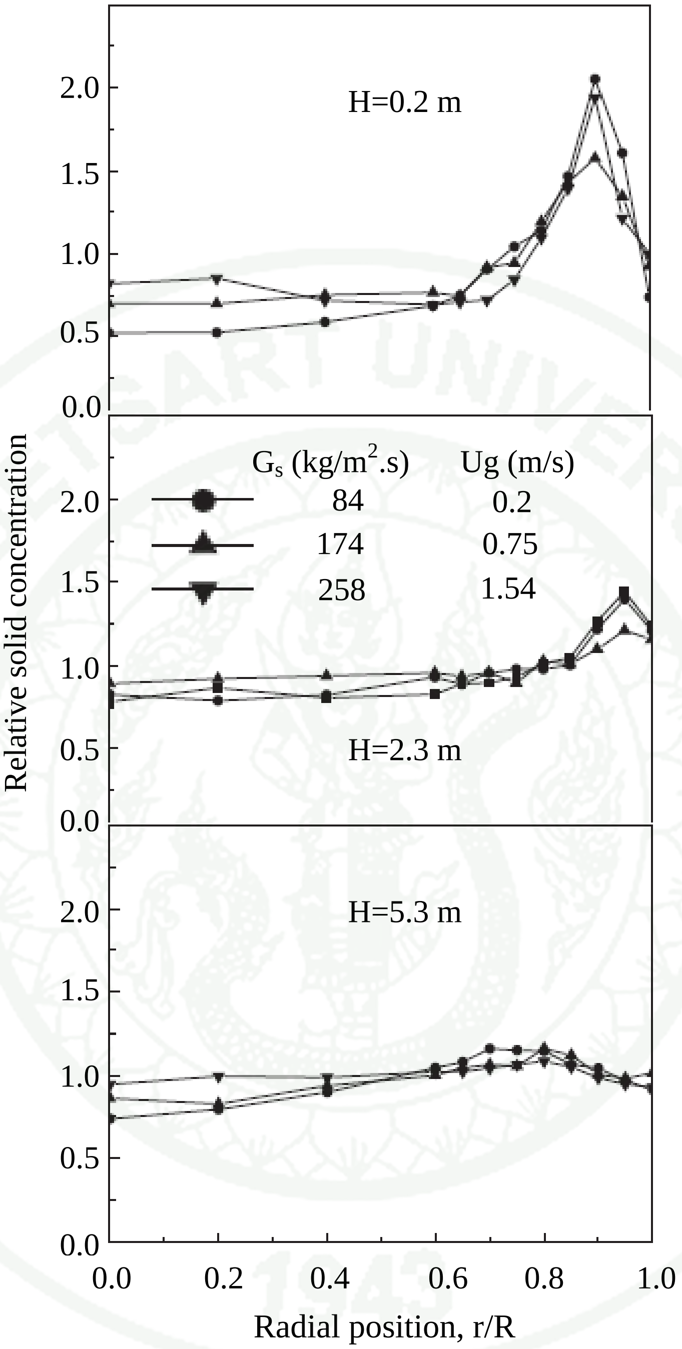

Figure 15 Radial profiles of relative solid concentrations for the downer at various height.

Source: Chen and Li (2004)

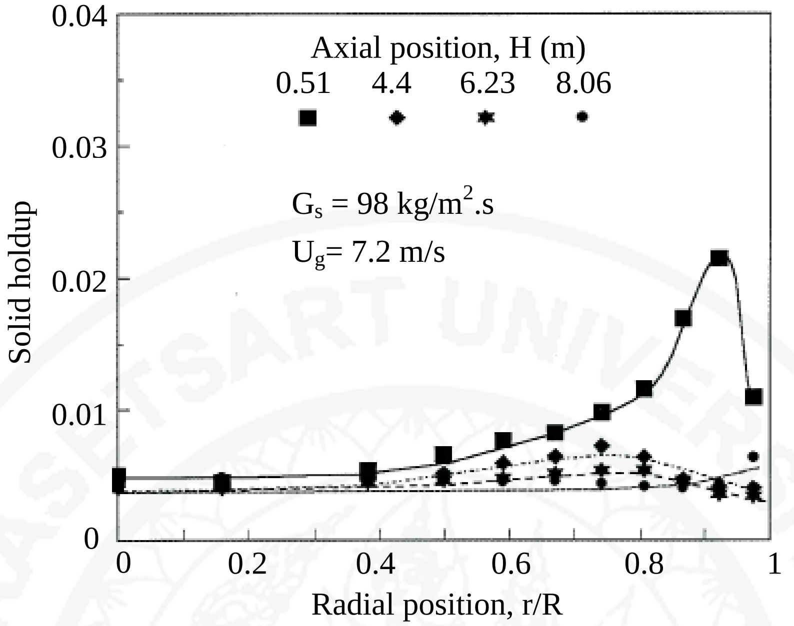

Figure 16 The radial distribution of the solid holdup in the downer reactor.

Source: Deng *et al*. (2001)

Solid fraction is $(1-\varepsilon)/\overline{(1-\varepsilon)}$. The wall of downer reactor has significant influence on the radial solid distribution and forming of near wall dense ring is closely related to the wall effect. The effect caused by the wall on the radial solid distribution in the downer is not related to the dimensionless distance r/R, but the absolute distance r. The effective range of the wall effect is relatively a constant value, which is very important to understand the scale-up feature of the downer. The solid holdup at various sizes of downer with the radial position is illustrated in Figure 17.

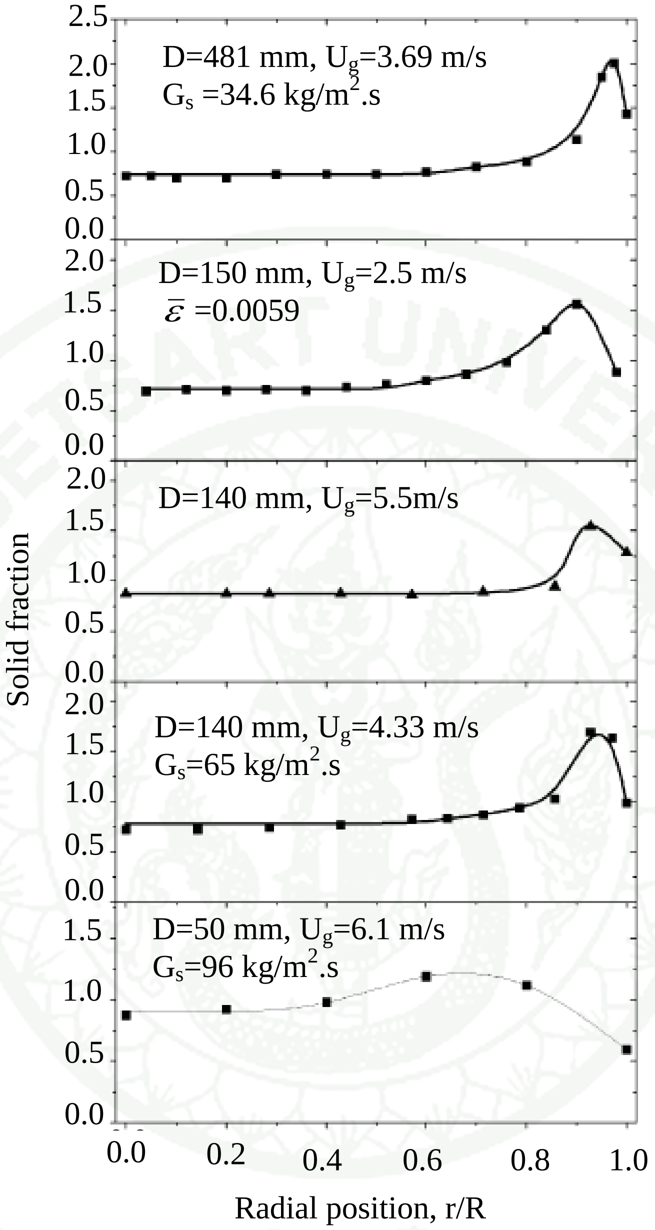

Figure 17 Comparison of radial solid density distribution in the downers with different diameter.

Source: Zhang *et al*. (2003)

Figure 18 shows the solid holdup profiles with difference radial and height in both riser and downer. Hydrodynamics studies have shown large differences in the gas-solids flow pattern between the riser and downer. At entrance of both CFB, dense solid hold up near the wall is formed and smoother flat profile is shown near the exit of the reactor. Downer reactor has smoother solid holdup profiles than the riser one.

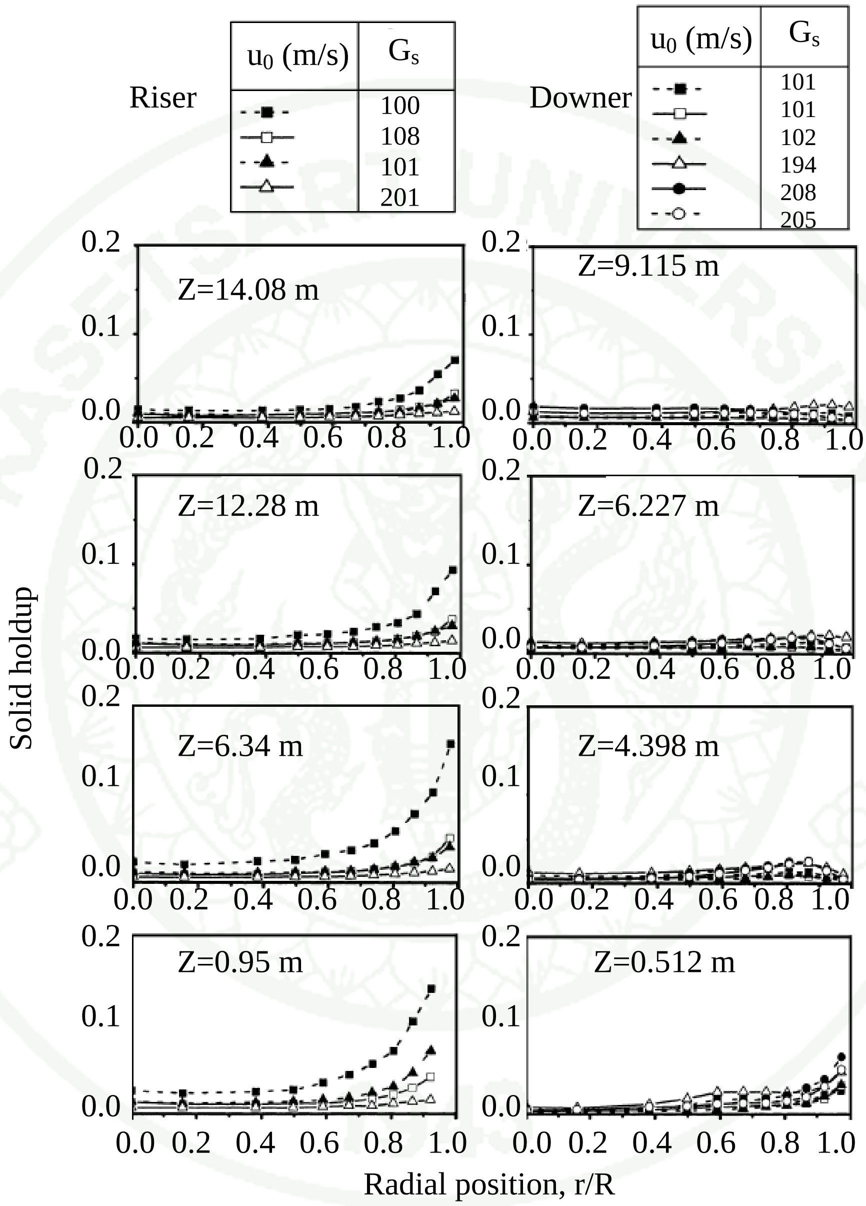

Figure 18 Radial solid holdup profiles along the riser and the downer.

Source: Zhang *et al*. (2003)

The results in axial direction are non uniform in the early regime (the entrance zone, 0-2 m.) and smooth in the middle regime to the exit. In the early regime, the solid and gas illustrate the developing flow and become fully developed after 2 m. The high solid flux increases solid holdup at all locations in comparing to the lower cases. When gas velocity increases, the average solid holdup has similar trends as the axial solid holdup profiles but the solid holdup consistently decreases at all axial positions. The solid flux is the key factor to affect the solid holdup in both developing region and fully developed region. High solid fluxes give high solid holdup as show in Figure 19.

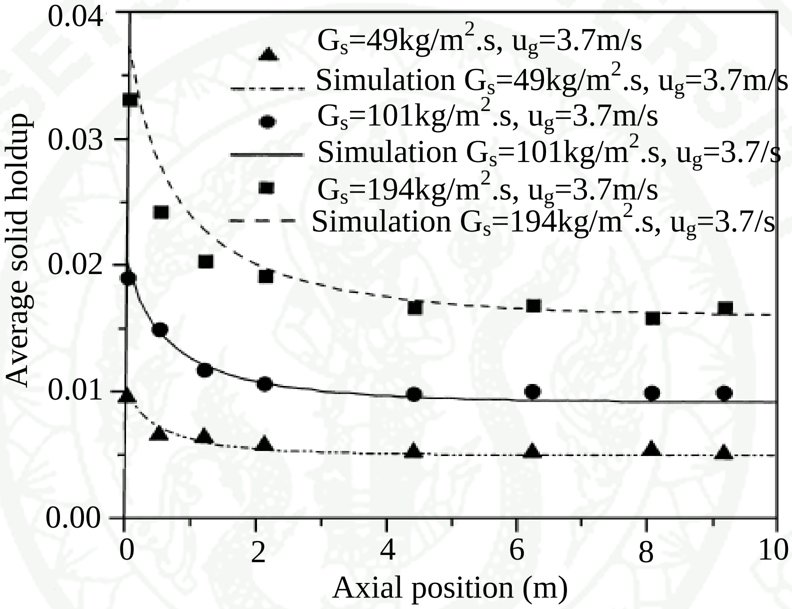

Figure 19 Model predictions compared to experimental data for solids holdup along the downer.

Source: Bolkan *et al*. (2003)

The particles leave from a distributor. The solid velocity is minimal at early point and continuously accelerating until it reaches a constant velocity at 5 m of height. The value of fully developed particle velocity exceeds the actual gas velocity due to the gravity effect. The particle velocity is directly related to the superficial gas velocity. The solid velocity is calculated from the mass conservation, $G_s = (1-\varepsilon)\rho_s v_s$. The axial profile of average particle velocity is illustrated in Figure 20.

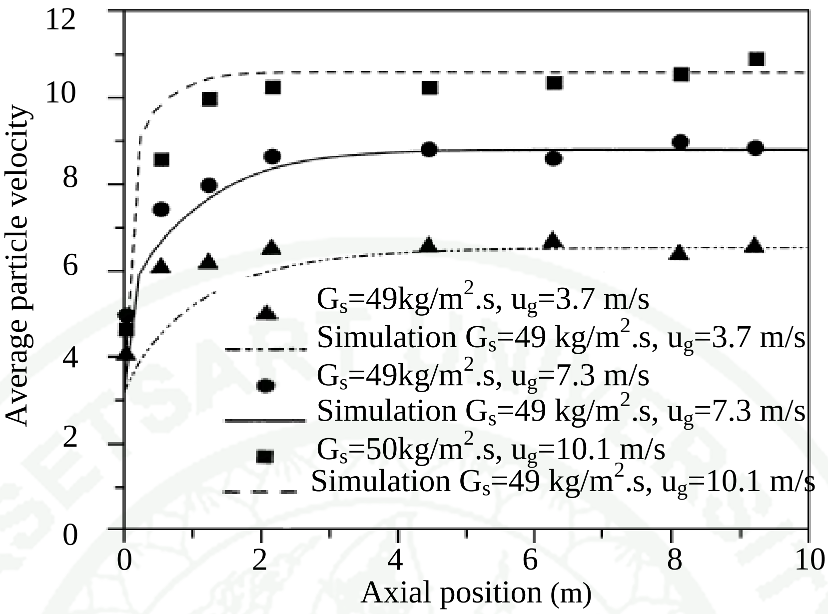

Figure 20 Model predictions compared to experimental data for particle velocity along the downer, G_s = 49 kg/m^2.s

Source: Bolkan *et al*. (2003)

The solid fraction in a gas-solid system depends on the hydrodynamics and gas expansion in the reactor. The solid fraction in a downer reactor can be derived from slip velocity definition (Zhu *et al*., 1995). The slip velocity in a downer is equal to the difference of particle velocity and gas velocity which is equal to terminal velocity of a single particle. The slip velocity is related to the solid superficial velocity, u_s, and the gas superficial velocity, u_g , as in equation (1).

$$v_{sl} = v_t = \frac{u_s}{(1-\varepsilon)} - \frac{u_g}{\varepsilon} \tag{1}$$

Void fraction can be derived from equation (2).

$$\varepsilon = \left[\frac{(v_{t-}u_g - u_s) + \sqrt{(u_g + u_s - v_t)^2 + 4u_g v_t}}{2v_t}\right] \tag{2}$$

The terminal velocity of a single particle can be calculated from equation (3). (Welty *et al.*, 1984)

$$v_t = \sqrt{\frac{4gd_s(\rho_s - \rho)}{3\rho C_D}} \tag{3}$$

where

$$\begin{array}{ccc} C_D = 24/Re_p & \text{at} & Re_p < 1 \\ C_D = 18.5/Re_p^{0.6} & \text{at} & 1 < Re_p < 1{,}000 \\ C_D = 0.44 & \text{at} & Re_p > 1{,}000 \end{array}$$

where C_D is the drag coefficient and Re_p is the particle Reynolds number $\left(Re_p = \frac{\rho v_{sld_s}}{\mu}\right)$

4. Heat transfer in down flow fluidized bed

Heat transfer is the transition of thermal energy from a hotter object to a cooler object. When there is a gradient of temperature between surrounding or another object, transfer of thermal energy, also known as heat transfer or heat exchange, occurs in such a way that the body and the surroundings finally reach thermal equilibrium. Heat transfer always occurs from a higher-temperature to a cooler-temperature one as described by the second law of thermodynamics or the Clausius statement. When there is a temperature difference between objects in proximity, heat transfer between them can never be stopped. It can only be slowed down. Heat transfer mechanisms can be grouped into 3 broad categories:

4.1 Conduction or heat conduction is the transfer of thermal energy between neighboring molecules in a substance due to a temperature gradient. It always takes place from a region of higher temperature to a region of lower temperature and acts to equalize temperature differences. Conduction takes place in all forms of matter (solids, liquids, gases, and plasmas) without any bulk motion of matter. In solids, it is due to the combination of vibrations of the molecules in a lattice and the energy transport by free electrons. In gases and liquids, conduction is due to the collisions and diffusion of the molecules during their random motion.

The basic relation for heat flow by conduction is the proportionality between heat flux and the temperature gradient called Fourier's law, with simplification for steady one-dimensional flow in the x direction, which is given in equation (4). (Welty *et al*., 1984)

$$\left(\frac{dq}{qA}\right) = -k\left(\frac{dT}{dx}\right) \tag{4}$$

where

q = rate of heat flow in the direction normal to surface
A = surface area
T = temperature
x = distance measured normal to surface
k = thermal conductivity

The general expressions of Fourier's law for heat flow in three dimensions in an isotropic material are shown in equation (5).

$$\frac{dq}{dA} = -k\left(\frac{\partial T}{\partial x} + \frac{\partial T}{\partial y} + \frac{\partial T}{\partial z}\right) = -k\nabla T \tag{5}$$

Equation (5) applies to conduction in cylindrical coordinates as:

$$\frac{\partial q}{\partial A} = -k\left(\frac{\partial T}{\partial r} + \frac{1}{r}\frac{\partial T}{\partial \theta} + \frac{\partial T}{\partial z}\right) = -k\nabla T \tag{6}$$

In Fourier’s law, k is independent of the temperature gradient. The thermal conductivity of metal is generally nearly constant or decreases slightly as the temperature is increased. For most liquids and gases, k is lower than solid due to the large distance between atoms in molecules. For ideal gas, thermal conductivity is proportional to the average molecular velocity, the mean free path, and the molar heat capacity.

4.2 Convection is the transfer of heat energy between a solid surface and the nearby liquid or gas in motion. As fluid motion goes faster, the convective heat transfer increases. The presence of bulk motion of fluid enhances the heat transfer between the solid surface and the fluid. There are two types of Convective heat transfer:

4.2.1 Natural Convection occurs when the fluid motion is caused by buoyancy forces that result from the density variations due to variations of temperature in the fluid. For example, the absence of an external source of flow, when the mass of the fluid is in contact with the hot surface, its molecules separate and scatter causing the mass of fluid to become less dense. When this happens, the fluid is displaced vertically or horizontally while the cooler fluid is denser and the fluid sinks. Thus the hotter volume transfers heat towards the cooler volume of that fluid. Normally, the natural heat transfer coefficient of air is about 10-50 W/m^2.K. The natural convection gradient is shown in Figure 21.

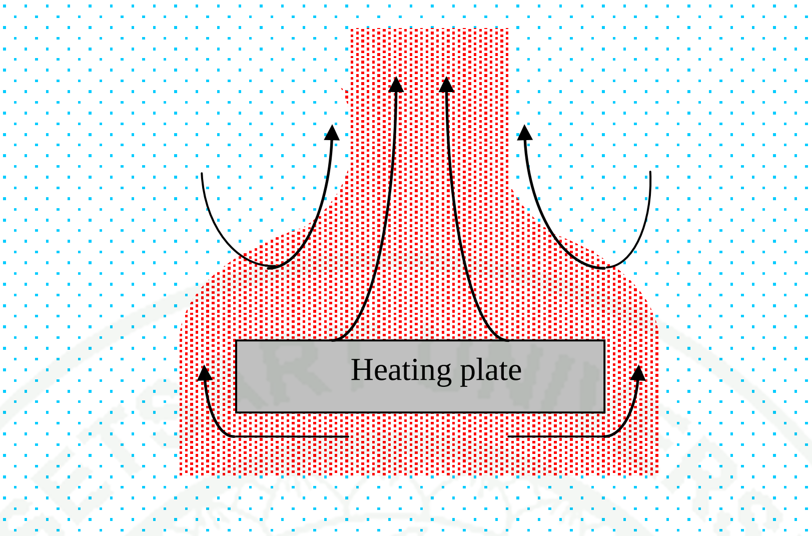

Figure 21 Natural convection of hot plate.

The natural convection in the vertical cylinder can be corelated with Nusselt number, Rayleigh number, and Prandtl number as in equation (7). (Wilty *et al.*, 1984)

$$N_u \equiv \frac{hL}{k} = \left[0.825 + \frac{0.387R \propto^{1/6}}{\left[1 + \left(\frac{0.492}{Pr}\right)^{9/16}\right]^{8/27}} \right]^2 \tag{7}$$

where

$$\frac{D}{L} \geq \frac{35}{Gr_L^{0.25}} \tag{8}$$

where $Ra = Gr.Pr$ is the Rayleigh number, $Pr = \frac{v}{\propto} = \frac{\mu c_p}{k}$ is the Prandtl number, and $Gr_L = \frac{L^3 \rho g \Delta\rho}{\mu^2}$ is Grashof number.

4.2.2 Forced Convection occurs when the fluid is forced to flow over the surface by external source such as fans and pumps. It creates an artificially induced convection current. Internal and external flow can also classify types of convection.

Internal flow occurs when the fluid is enclosed by a solid boundary such as a flow through a pipe. An external flow occurs when the fluid extends indefinitely without encountering a solid surface.

Both of these convections, either natural or forced, can be internal or external as they are independent of each other. The formula for rate of convective heat transfer is expressed in equation (9).

$$q = hA(T_s - T_b) \tag{9}$$

where A isthe surface area of heat transfer. T_s is the surface temperature and T_b is the temperature of the fluid at bulk temperature. However, T_b varies with each situation and is the temperature of the fluid far away from the surface. The parameter h is the constant heat transfer coefficient which depends upon physical properties of the fluid such as temperature and the physical situation in which convection occurs. Therefore, the heat transfer coefficient must be derived or found experimentally for every system analyzed. Formulae and correlations derived from experimental data are available in many references to calculate heat transfer coefficients for typical configurations and fluids. For laminar flows the heat transfer coefficient is rather low compared to the turbulent flows. This is due to the fact that turbulent flows have a thinner stagnant fluid film layer on heat transfer surface. The force convection gradient of the hot surface is shown in Figure 22.

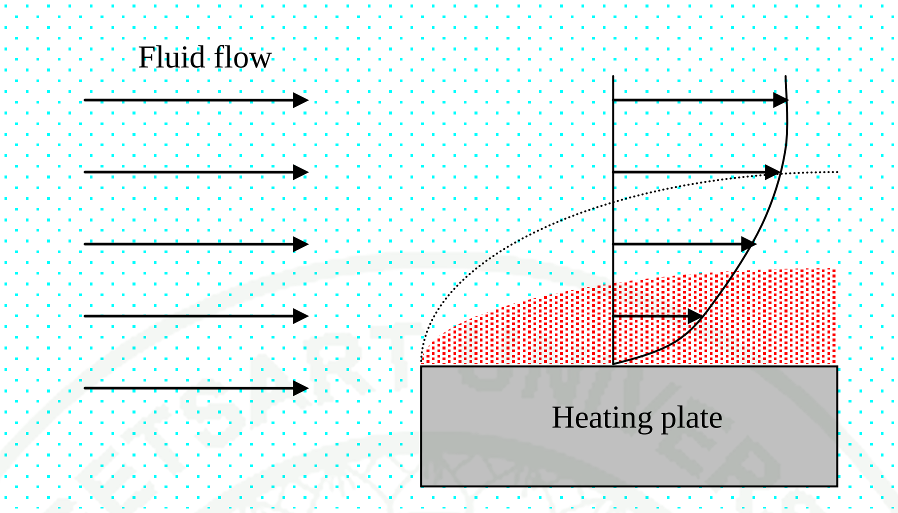

Figure 22 Force convection velocity gradient on the hot plate.

The force convection for laminar flow in the tube is the ratio of fluid viscosity at bulk temperature and at wall temperature. Sieder and Tate have shown the Nusset1 correlation as equation (10). (Wilty *et al*., 1984)

$$Nu_D \equiv \frac{hL}{k} = 1.86\left(Pe\frac{D}{L}\right)^{1/3}\left(\frac{\mu_b}{\mu_w}\right)^{0.14} \tag{10}$$

where μ_b and μ_w are the viscosity at bulk and wall temperature, respectively, [Pa.s].

4.3 Radiation all materials radiate thermal energy in amounts determined by their temperature. The energy is carried by photons of light in the infrared and visible portions of the electromagnetic spectrum. When temperatures are uniform, the radiative flux between objects is in equilibrium and no net thermal energy is exchanged. The balance is upset when temperatures are not uniform, and thermal energy is transported from surfaces of higher to surfaces of lower temperature.

4.4 Overall heat transfer coefficient

The three modes of heat transfer, a conduction, convection, and radiation, can be considered in one term which is overall heat transfer coefficient. Sometime, considerations of each heat transfer mechanism at the multiwall layer are complex. Therefore, overall heat transfer coefficients are considered. The composite wall with three material layers is shown in Figure 23.

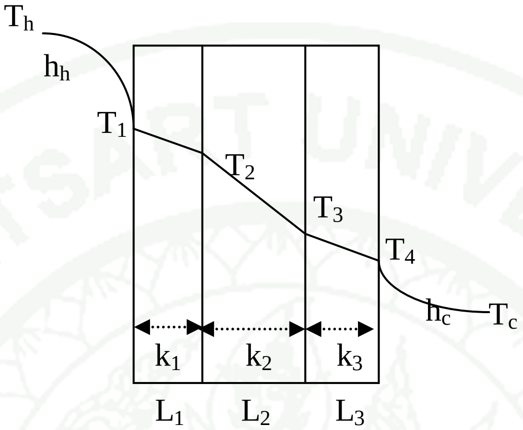

Figure 23 Heat transfer through the composite wall.

Source: Wilty *et al*. (1984)

In Figure 23, the hot temperatures pass through the composite wall to the cold temperature. All mechanisms comprise of convection, three conductions, and convection. The heat transfer rate of the composite wall is expressed in equation (11).

$$q_x = \frac{T_h - T_c}{1/h_h A + L_1/k_1 A + L_2/k_2 A + L_3/k_3 A + 1/h_c A} \tag{11}$$

where the q_x is the heat transfer rate. The heat transfer resistance can be correlated as in Ohm’s law. So, the heat transfer rate can be rewritten as equation (12).

$$q = \frac{\Delta T}{\sum R_{thermal}} \tag{12}$$

where $R_{thermal}$ is the thermal resistant from conduction or convection.

The heat transfer rate can be calculated in terms of overall heat transfer coefficient as show in general form in equation (13),

$$U = \frac{q_x}{A\Delta T} = \frac{\Delta T/\sum R}{A\Delta T} = \frac{1}{A\sum R} \tag{13}$$

or for the cylindrical tube can be shown in equation (14).

$$U = \frac{1}{A\{1/A_i h_i + [ln(r_o/r_i)]/2\pi kL + 1/A_o h_o\}} \tag{14}$$

where U is the overall heat transfer coefficient, [kW/m^2.K].

Heat transfer between gas-solid flow and heat transfer surface in fluidized bed comprises mainly of three components: particle convection, gas convection, and radiation. At low temperature, the radiation component can be neglected. Normally, the particle convection is the primary heat transfer mechanism, given the large heat capacity of solids, as compared to the gas. Gas convection may become important when the gas velocity is high and the solid holdup is low. (Ma and Zhu, 1999)

4.5 Heat distribution in the downer reactor

However, the axial distribution temperature profile for downer reactor is illustrated in Figure 24. In early regime, the gas temperature decreases along the axial direction of the downer reactor. The temperature decreases rapidly near the distributor and gradually approaches a constant value further down. The higher solid flux gives lower axial gas temperature profile when compared with lower solid flux. The high solid flux is high in mass flow rate so that more heat in the gas is transferred to solid. (Zhu *et al.*, 1999)

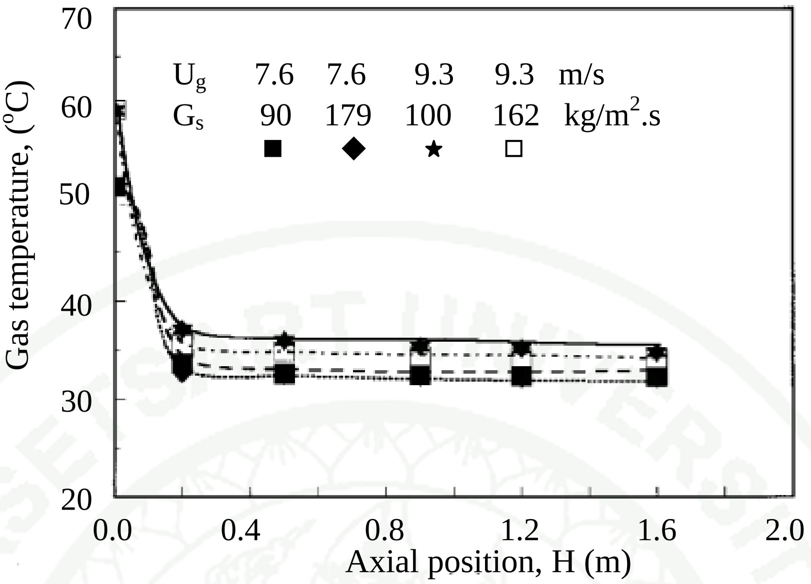

Figure 24 The axial average gas temperature of the top of downer with solid mixing through the distributor.

Source: Zhu *et al*. (1999)

The average heat transfer coefficient decreases along the downer. At the top of the reactor, the average heat transfer coefficient is higher when the solid circulating rate is higher or the gas velocity is lower due to dominant factor of the solid concentration on heat transfer in this regime. In the developing zone along the axial direction, the heat transfer coefficient is smoothly constant because solid concentration is in more uniform pattern. In this zone, gas convection is more significant than the particle convection. The heat transfer coefficient is higher at higher gas velocity at the same solid flow rate. This shows that the heat transfer can also be significantly affected by the gas velocity. The axial distribution of average heat transfer coefficients for downer reactor is shown in Figure 25.

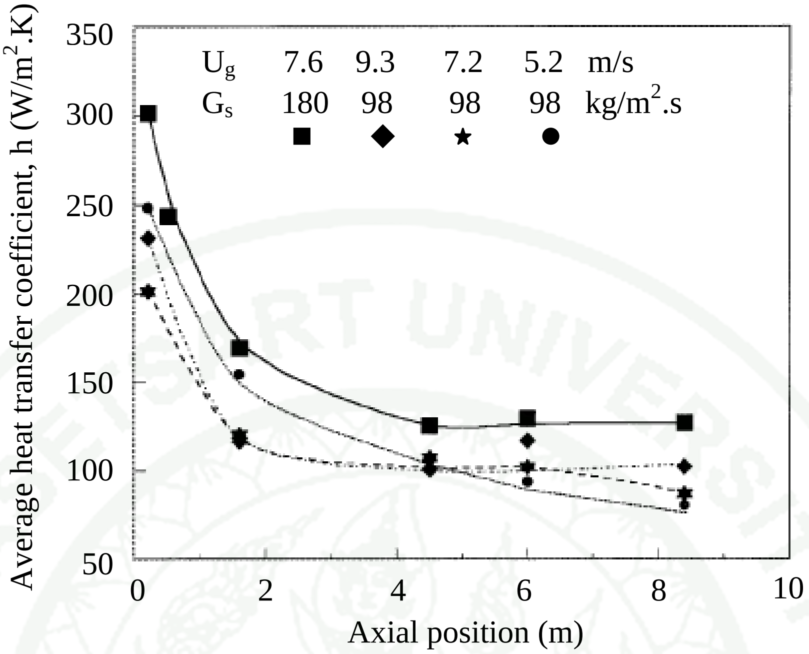

Figure 25 The average heat transfer coefficient as a function of solid flux and gas velocity for the downer reactor.

Source: Ma and Zhu (1999)

The experimental profiles of local heat transfer rate also change with the radial position. At the wall region (r/R=0.85-9), the heat transfer coefficient decreases sharply along the axial direction in the first section or accelerating zone. This variation becomes less significant in the developing zone and finally becomes negligible in the fully developed zone. Near the centre region (r/R=0-0.6), the heat transfer coefficient increases along the column in the accelerating zone. The reason for the low heat transfer coefficient at the top center of the downer come from the initial particle velocity is very low and the solid concentration is more dilute than in the annular region. In the developing and fully developed zones, the particle velocity and concentration become more uniformly distributed in the radial direction so that heat transfer coefficient at various radial position approach a constant in this section. The heat transfer coefficient in axial position with various radial positions is shown in Figure 26.

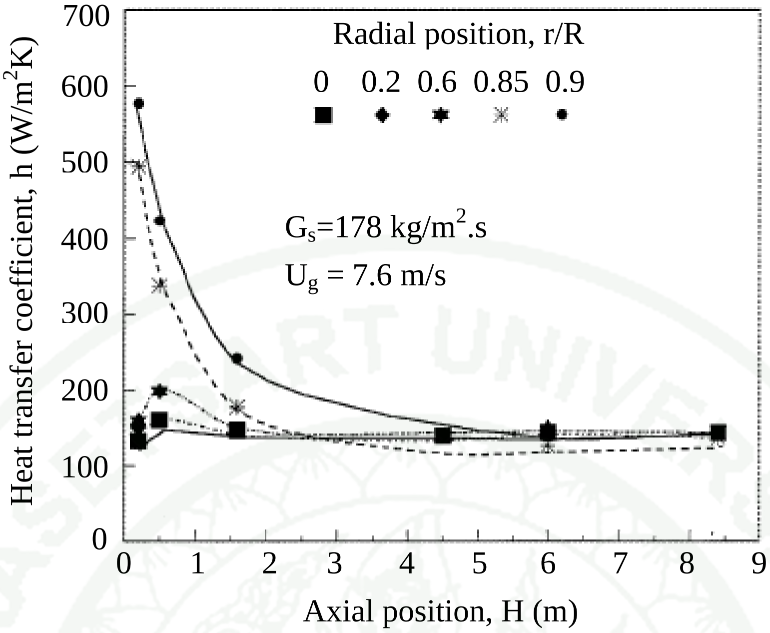

Figure 26 Heat transfer coefficient profiles at various radial position in the downer reactor.

Source: Ma and Zhu (1999)

A different view of heat transfer coefficient is plotted versus the radial position at the various axial positions under the same superficial gas velocity and solid flow rate as shown in Figure 27. In the first acceleration section, the heat transfer coefficient is high and its radial distribution is very non-uniform. It remains fairly constant in the central region of this section. The heat transfer coefficient increases dramatically to form a significant peak near the wall, and then decreases toward the wall. Further down in the second acceleration section or developing zone, this radial distribution becomes much more uniform. In the fully developed zone, the heat transfer coefficient becomes almost constant along the radial direction.

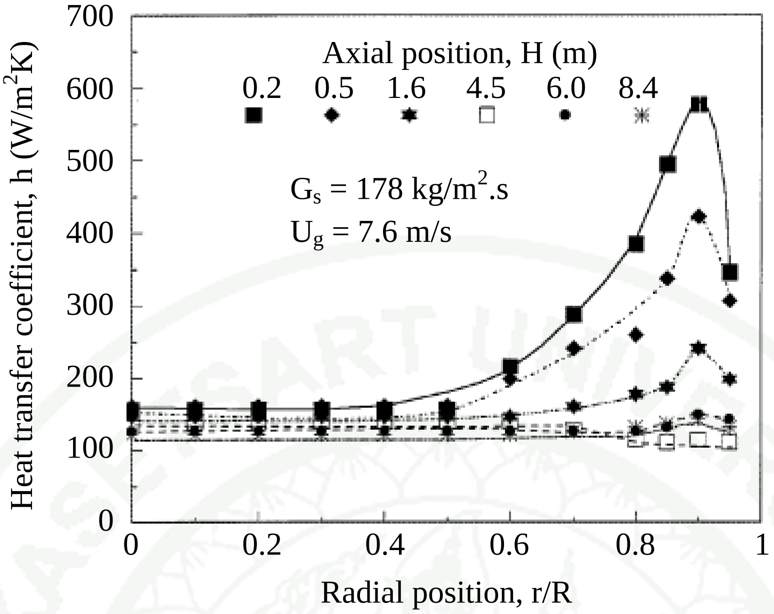

Figure 27 Radial profiles of heat transfer coefficient at various axial position in the downer reactor.

Source: Ma and Zhu (1999)

The effect of the solid circulating rate on the heat transfer coefficient and the effect of the solid circulating rate on the radial distribution of heat transfer coefficient along the downer reactor are illustrated in Figure 28 and 29, respectively. The average heat transfer coefficient at various axial position always increase with solid flow rate under the same superficial gas velocity as shown in Figure 28. The high solid flow rate results in a high suspension density. The radial distributions of heat transfer coefficients at the same axial location under constant superficial gas velocity become more uniform with decreasing solid flow rate, where the radial structure of solid concentration becomes more uniform as shown in Figure 29. The effect of solid flow rate on heat transfer coefficient is significantly higher in the lower region of the downer than that near the distributor region because the solids concentration is always very high at the top of the downer reactor, as the particles are at low velocity. A changing in solid flow rate may not cause a dramatic change in solid concentration in this region. In the fully developed region below, gas and particle velocity remain constant and the bed void is much higher. In this case, a change in solid flow rate will lead to a more significant change in solid concentration so that the effect of solid flow rate on heat transfer becomes more significant.

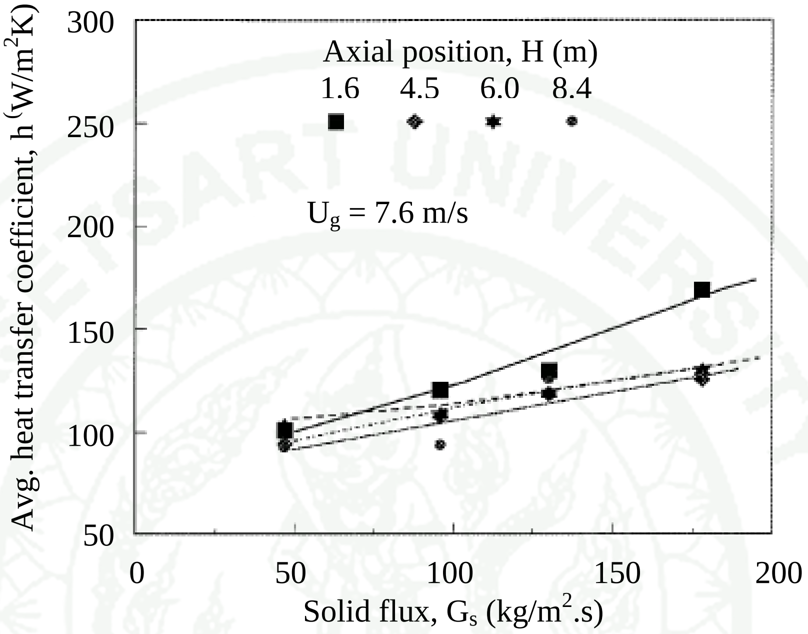

Figure 28 The effect of the solid flow rate on the heat transfer coefficient in a downer reactor.

Source: Ma and Zhu (1999)

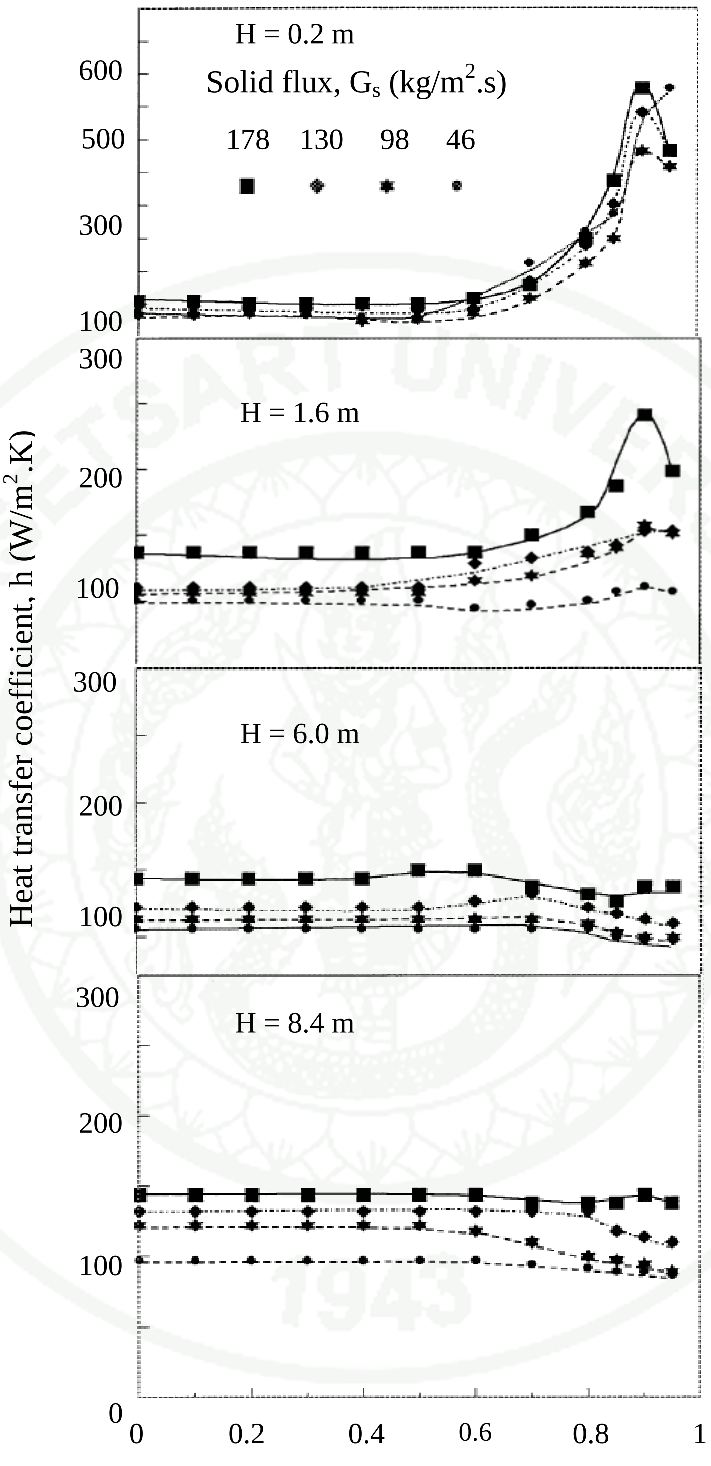

Figure 29 The effect of solid flux on the radial distribution of the heat transfer coefficient for the downer reactor.

Source: Ma and Zhu (1999)

In downer reactor model, the solid concentration or solid holdup is the main factor on the heat transfer coefficient. The heat transfer coefficient with suspension density is shown in equation (15). (Kim *et al*., 1999)

$$h = 12(\rho_{sus}^{0.43}) \tag{15}$$

where $p_{sus} = \rho_s(1-\varepsilon)$, p_{sus} is density of suspension (kg/m^3).

5. Axial dispersion model

Dispersion model explains the flow pattern in the reactor. Normally, the flow pattern usually is viewed as ideal plug flow or idea mixed flow for convenient consideration. However, most of reactors have the flow patterns between plug flow and mixed flow. Co-current down flow fluidized bed is developed to reduce the back mixing problem of other types of fluidized bed reactor. The solid - gas flow downward with gravity force direction. The dispersion of solid and gas in reactor become close to the plug flow.

The ideal plug flow in a tubular reactor is flat in velocity and concentration profiles with no back mixing. Noticed dispersion coefficient is zero. In fact, the flow behavior inside a pipe reactor is rough flow because the velocity and concentrations profiles are affected from the slippage, backmixing, fluid materials, reactor materials, and etc. The ideal plug flow and dispersed plug flow is shown in Figure 30.

Figure 30 The characteristic of ideal plug flow and dispersed plug flow.

Source: Levenspiel (1999)

Axial dispersion model is studied by pulsing the tracer into the fluid flowing in the vessel. The dispersion in radial is neglected. The dispersion coefficient (D) is obtained by following the characteristic and spreading of tracer inside reactor. The concentration and time of tracer are measured from the entrance of reactor along to the exit of reactor only the x-direction. The dispersion coefficient is calculated with Fick's law equation as show in equation (16).

$$\frac{\partial C}{\partial t} = D\frac{\partial^2 C}{\partial x^2} \tag{16}$$

where D is axial dispersion coefficient or degree of back mixing. The high D is rapid spreading of the tracer. Low D is slow spreading and D =0 is no spreading, hence ideal plug flow. (levenspiel, 1999)

While the fluids flow through the pipe, axial mixing is mainly due to fluid velocity gradients, whereas radial mixing is due to molecular diffusion alone. In dimensionless from where $z = (ut + x)/L$ and $\theta = t/\bar{t} = tu/L$, the basic differential equation representing dispersion model becomes equation (17).

$$\frac{\partial C}{\partial \theta} = \left(\frac{D}{uL}\right)\frac{\partial^2 C}{\partial z^2} - \frac{\partial C}{\partial z} \tag{17}$$

Replace $\frac{1}{Pe} = \left(\frac{D}{uL}\right)$ in equation (18).

$$\frac{\partial C}{\partial \theta} = \left(\frac{1}{Pe}\right)\frac{\partial^2 C}{\partial z^2} - \frac{\partial C}{\partial z} \tag{18}$$

The Peclect number indicates the ratio of convection to dispersion which is quite similar to the real state of flow in the downer reactor.

$$Pe = \frac{uL}{D_z} = \frac{convection}{dispersion} \tag{19}$$

In dispersion model, the influence of gas-solid back mixing is considered by Peclect number. Increasing the mixing behavior can be seen by decreasing Peclect number (under 100). The plug flow reflected by high Peclect number (over 100). The axial gas and solid Peclect number in downer reactor can reach 100 which approaches a plug flow condition.

6. Kinetic model

The kinetic model is the path ways of the reactions. The lumps illustrate the groups of reactants and products. The lump model is useful to reduce the complicacy of complex reaction by substitute the main similar reactants and products into one. The assemblages are separated with same range of boiling points or the number of carbon atoms or the main structure of molecules.

The kinetic model of heavy oil catalytic cracking reaction is studied in several lump kinetic models such as 3-lump, 4-lump, and other lumps depend on the range of the groups of reactants and products. The main lump kinetic model for heavy oil catalytic cracking is heavy oil, gasoline, light gas, and coke. The several lump model of catalytic cracking is shown in Figure 31 and 32.

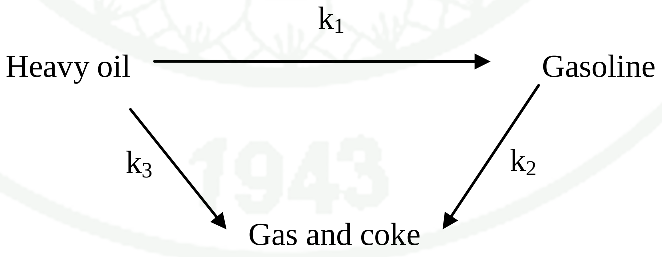

Figure 31 Proposed 3-lump kinetic model of heavy oil catalytic cracking.

Source: Weekman (1969)

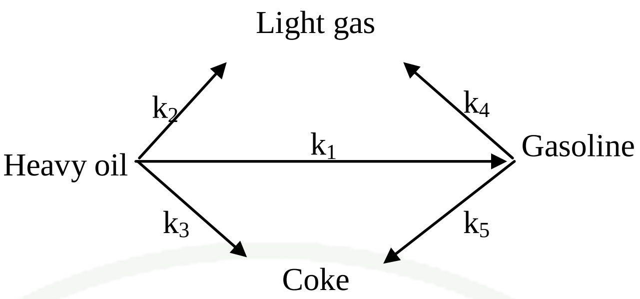

Figure 32 Proposed 4-lump kinetic model of heavy oil catalytic cracking.

Source: Songip *et al*. (1994)

The kinetic rate constant (k) is a function of the temperature (T), frequency factors (k_0) and activation energies (E_a). The kinetic rate constant is calculated from Arrhenius equation as show in Equation (20).

$$k = k_0 e^{-E_a/RT} \tag{20}$$

The catalytic cracking of heavy oil was studied (Songip *et al*., 1994). Catalytic cracking of heavy oil proposed into 4-lump model as shown in Figure 32. The components are heavy oil (above C_{12}), light gas (C_1-C_4), gasoline(C_5-C_{11}) and coke. The heavy oil cracking was done with REY zeolite a packed bed reactor. The kinetic rate of 4-lump model were obtained from experiments at various temperature in the form of the frequency factor and activation energy by using the Arrhenius equation. The frequency factor and activation energies for heavy oil catalytic cracking are shown in Table 3.

Table 3 Frequency factors and activation energies for catalytic cracking of heavy oil.

Second order reaction	k_0 (m^6/kg.kg$_{cat}$.s)	Ea (kJ/mol)
$A \longrightarrow B$	1,237	50.7
$A \longrightarrow C$	23,776	75.7
$A \longrightarrow D$	1.29×10^{-2}	18.5
First order reaction	**k_0 (m^3/kg$_{cat}$.s)**	**Ea (kJ/mol)**
$B \longrightarrow C$	0.975	35.1
$B \longrightarrow D$	4.7×10^{-2}	42.1

Source: Songip *et al*. (1994)

The reaction rate of catalytic cracking of heavy oil and products from 4-lump model in Figure 32 are shown with the second order and first order reaction as in equation (21) to (24). (Songip *et al*., 1994)

$$r_A = -(k_1 + k_2 + k_3)C_A^2 \tag{21}$$

$$r_B = k_1 C_A^2 - (k_4 + k_5)C_B \tag{22}$$

$$r_C = k_2 C_A^2 + k_4 C_B \tag{23}$$

$$r_D = k_3 C_A^2 + k_5 C_B \tag{24}$$

where C_A and C_B are the concentration of heavy oil (A) and gasoline (B), respectively.

7. Modeling of catalytic cracking of heavy oil in a downer reactor

The model of catalytic cracking in the downer reactor is developed to reduce the complication of equation by using the no backmixing in radial direction. (Promsan, 2005). The modeling of axial dispersion model for catalytic cracking of heavy oil in a downer reactor was developed by Promsan with using the 4-lump reaction model proposed by Songip above as shown in Figure 32. The axial dispersion models for adiabatic and isothermal operations were simulated. The mass balance equation and energy balance equations with the continuity of gas and solid were developed as shown in equation (25) to (28).

The mass balance equations for catalytic cracking of heavy oil in the downer reactor are shown for individual component in the gas phase and solid phase as in equation (25) and (26). The mass balances of both phases are in diffusion term, convection term, and mass transfer between phases written in dimensionless form of axial direction. In addition for solid phase, the heavy oil cracking reaction term to account for the reactions that occur on the solid catalyst surface only.

Solid phase:

$$\frac{1}{Pe}\frac{d^2y_{is}}{dZ^2}-\frac{dy_{is}}{dZ}+\frac{k_{ig}aL}{u_s}\left(y_{ig}-y_{is}\right)+\frac{(1-\varepsilon)\rho_s L}{C_{A0}u_s}r_i=0 \qquad (25)$$

Gas phase :

$$\frac{1}{Pe}\frac{d^2y_{ig}}{dZ^2}-\frac{dy_{ig}}{dZ}-\frac{k_{ig}aL}{u_g}\left(y_{ig}-y_{is}\right)=0 \qquad (26)$$

The energy balances of catalytic cracking of heavy oil in a downer reactor are also shown in the gas phase with the conduction term, convection term, and heat transfer between phases. The energy balance of solid phase contains 3 terms as in the solid phases with addition of heat consumption term from endothermic reaction on the solid surface. The energy balances equations are used in the adiabatic operate calculation. The energy balance equation is neglected in simulation of isothermal operation. The axial energy balance equation in dimensionless of solid and gas phases are shown in equation (27) and (28).

Solid phase:

$$\frac{1}{Pe_{Hs}}\frac{d^2\theta_s}{dZ^2}-\frac{d\theta_s}{dZ}-\frac{haL}{G_sC_{ps}}\left(\theta_s-\theta_g\right)+\frac{(1-\varepsilon)\Delta H_A L}{G_sC_{ps}T_{s0}}r_A=0 \qquad (27)$$

Gas phase:

$$\frac{1}{Pe_{Hg}}\frac{d^2\theta_g}{dZ^2}-\frac{d\theta_g}{dZ}+\frac{haL}{G_gC_{pg}}\left(\theta_s-\theta_g\right) \qquad (28)$$

The hydrodynamics of the downer reactor is related to the mass flux of gas and solid defined as follow.

For solid phase:

$$G_s=(1-\varepsilon)\rho_s v_s \qquad (29)$$

For gas phase:

$$G_g=\varepsilon\rho_g v_g \qquad (30)$$

where v_g, v_s, G_g, and G_s are gas velocity, solid velocity, gas flux, and solid flux, respectively. The ε is void fraction of the bed in the downer reactor which can be calculated from slip velocity as in equation (2).

The axial dispersion model was solved simultaneously by COLNEW software. The simulated results are the temperature and mass distributions on the axial position of downer reactor with variation of inlet gas temperature, inlet solid temperature, gas flux, and solid flux. (Promsan, 2005)

8. Numerical approach

The numerical solution is used to approximate the solution of ordinary differential equations that cannot be solved by directly integration or analytical solution, e.g. Eurler method, Runge-Kutta methods, IVP. The solutions of nonlinear equations for catalytic cracking reactor model can be obtained with the orthogonal collocation method.

The orthogonal collocation method has found widespread applications in sciences and chemical engineering. These methods have to calculate with orthogonal polynomial. This method is used for the dimensionless equation at the boundary of [0,1]. Other points inside the boundary are solved by finding the root of Jacobi polynomials.

The Jacobi polynomial is a class of orthogonal polynomials. It’s used to separate the boundary with the weight function and calculate the root finding at each collocation points. There are N interior points or collocation points plus one at each end and the domain is always transformed to lie on 0 to 1. The root finding and collocation points by Jacobi polynomial is illustrated in Figure 33.

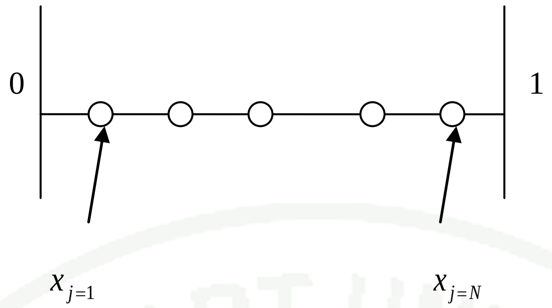

Figure 33 The root finding from the N collocation points by Jacobi polynomial.

Source: Rice and Do (1995)

The Jacobi polynomial with N collocation points is shown in equation (31).

$$J_N(x) = \sum_{i=0}^{N} (-1)^{N-i}\, \gamma_{N,i}x^{i} \tag{31}$$

when $\gamma_{N,i}$ is a constant coefficient from calculation.

The root finding of the various collocation points is shown following.

N=1 $x_j = 0.500000000$

N=2 $x_j = 0.2113248654, 0.7886751346$

N=3 x_j =0.1127016654, 0.5000000, 0.8872983346

In general equation, the 1st order derivative equation and the 2nd order derivative equation of the orthogonal collocation method are expressed in equation (32).

$$y(x_j) = \sum_{i=1}^{N+2} d_i x_j^{i-1} \qquad \frac{dy}{dx}(x_j) = \sum_{i=1}^{N+2} d_i (i-1) x_j^{i-2}$$
$$\frac{d^2y}{dx^2}(x_j) = \sum_{i=1}^{N+2} d_i (i-1)(i-2) x_j^{i-3} \qquad (32)$$

Put these formulas in matrix notation, where **Q**, **C**, and **D** are N+2 by N+2 matrices.

$$y = Qd \qquad \frac{dy}{dx} = Cd \qquad \frac{d^2y}{dx^2} = Dd$$
$$Q_{ij} = x_j^{i-1} \qquad C_{ij} = (1-i)x_j^{i-2} \qquad D = (i-1)(i-2)x_j^{i-3}$$

Solving the first equation for **d,** we can rewrite the first and second derivatives as $y = QD$.

$$d = Q^{-1}y \qquad \frac{dy}{dx} = CQ^{-1}y = Ay \qquad \frac{d^2y}{dx^2} = DQ^{-1}y = By$$

The example of calculation matrix A and B is shown in Table 4.

Table 4 The example of calculation of matrix A and B.

N	A	B
1	$\begin{bmatrix} -3 & 4 & -1 \\ -1 & 0 & 1 \\ 1 & -4 & 3 \end{bmatrix}$	$\begin{bmatrix} 4 & -8 & 4 \\ 4 & -8 & 4 \\ 4 & -8 & 4 \end{bmatrix}$
2	$\begin{bmatrix} -7 & 8.196 & -2.196 & 1 \\ -2.732 & 1.732 & 1.732 & -0.7321 \\ -0.732 & 1.732 & -1.732 & 2.732 \\ -1 & 2.196 & -8.196 & 7 \end{bmatrix}$	$\begin{bmatrix} 24 & -37.18 & 25.18 & -12 \\ 16.39 & -24 & 12 & -4.392 \\ -4.392 & 12 & -24 & 16.39 \\ -12 & 25.18 & -37.18 & 24 \end{bmatrix}$

Source: Rice and Do (1995)

9. Software

COLNEW or COLSYS is the program, which was developed from British Columbia University by Ascher, Christiansen and Russel. The COLNEW program is the groups of mathematic equations and numerical techniques. COLNEW is used for solving boundary value problems (BVPs) for linear or nonlinear ordinary differential equations (ODEs). With these advances, COLNEW can considered the initial value problems case or without. The COLNEW program use for solving the linear and nonlinear equations of less than the 4th order.

$$1 \leq m_1 \leq m_i \leq \cdots \leq 4 \tag{33}$$

where m_i is the order of the differential equation i. The general formats of ordinary differential equation have to array as follow below in equation (34).

$$u_n^{(m_n)}(x) = F_n\big(x; Z(u)\big) \qquad a < x < b \qquad n = 1, \dots, d, \tag{34}$$

where m_n is the highest order, n is the number of differential equations which is not over than 20. a and b are the left and right boundary. Then, equation (35) is an isolated solution vector.

$$u(x) = \big(u_1(x), \dots, u_d(x)\big) \tag{35}$$

The vectors of unknowns are shown in equation (36).

$$z(u) = \Big(u_1, u_1', \dots, u^{(m_1-1)}, u_2, \dots, u_d^{(m_d-1)}\Big) \tag{36}$$

The total number of boundary equations is equal to the summary of the order of every differential equation, also not over 40, as shown in equation (37).

$$m^* = \sum_{n=1}^{d} m_n \tag{37}$$

The nonlinear function used to represent boundary condition is expressed in equation (38).

$$g_j\left(\xi_j; z(u)\right) = 0 \qquad\qquad j = 1, \dots, m^* \tag{38}$$

where ξ_i is location of the j th boundary (or side) condition. The value has to be between a and b in equation (39).

$$a \le \xi_1 \le \xi_1 \le \cdots \le \xi_{m^*} \le b \tag{39}$$

The following is the subroutines that supply the evaluation duty to the main program are shown in Table 5.

Table 5 The subroutines which work with the main program.

Names	Description
fsub	name of subroutine for evaluating the ordinary differential equations
dfsub	name of subroutine for evaluating the jacobian of ordinary differential equations in fsub.
gsub	name of subroutine for evaluating the i-th component of the boundary.
dgsub	name of subroutine for evaluating the equation for gsub subroutine.
solutn	name of subroutine to evaluate the initial approximation for unknown vector $z(u(x))$.
read_my_data	name of subroutine for read the initial value of parameters and simple equations.

MATERIALS AND METHODOLOGY

Materials

1. Co-current down flow fluidized bed System

The full system of co-current down flow fluidized bed reactor and material for the experiments are show in the heat transfer experiment of the methods topic and the schematic diagram of co-current down flow fluidized bed reactor is illustrated in Figure 34.

2. Computer and operating system

2.1 Personal computers: Pentium IV

2.2 Windows XP operation system

3. Software for Simulations

3.1 Visual Fortran

Methods

This research studied the gas-solid heat transfer in the co-current down flow fluidized bed reactor (downer). The methods are divided into 2 main categories. They are the experiment of heat transfer (heat loss) in the downer system and the simulations of catalytic cracking of heavy oil in downer reactor with heat loss in the downer system. Both cases were compared at similar operating conditions to explore the heat transfer behavior in the downer.

1. The heat transfer experiments

The heat transfer experiment was conducted in the downer fluidized bed made from stainless steel with 7.62 centimeters in inside diameter and 9.30 meters in height. The outside of reactor was covered with a large cavity iron jacket and the insulator as shown in Figure 34. Ambient air flew along the outside reactor wall from the bottom of reactor by natural convection. It left the outside wall of the reactor at the top where the temperature was measure.

The air flow was generated from the single blower that has maximum capacity of 1 m^3/min. The air feed stream went through a 5 kW heater before feeding into the top part of the downer reactor. The solid were fed into the downer through a solid distributor under the screw feeder. The solid feed rates were controlled by a pulse width modulator (PWM) which changes the rotating speed of the screw feeder. Gas and solid mixed below the distributor and subsequently flow downward together to the bottom of the reactor. At the bottom of the reactor, gas and solid were separated with a large diameter conical separator tank and the exit gas flew through a cyclone. The solid were collected in the storage tank and cooled down.

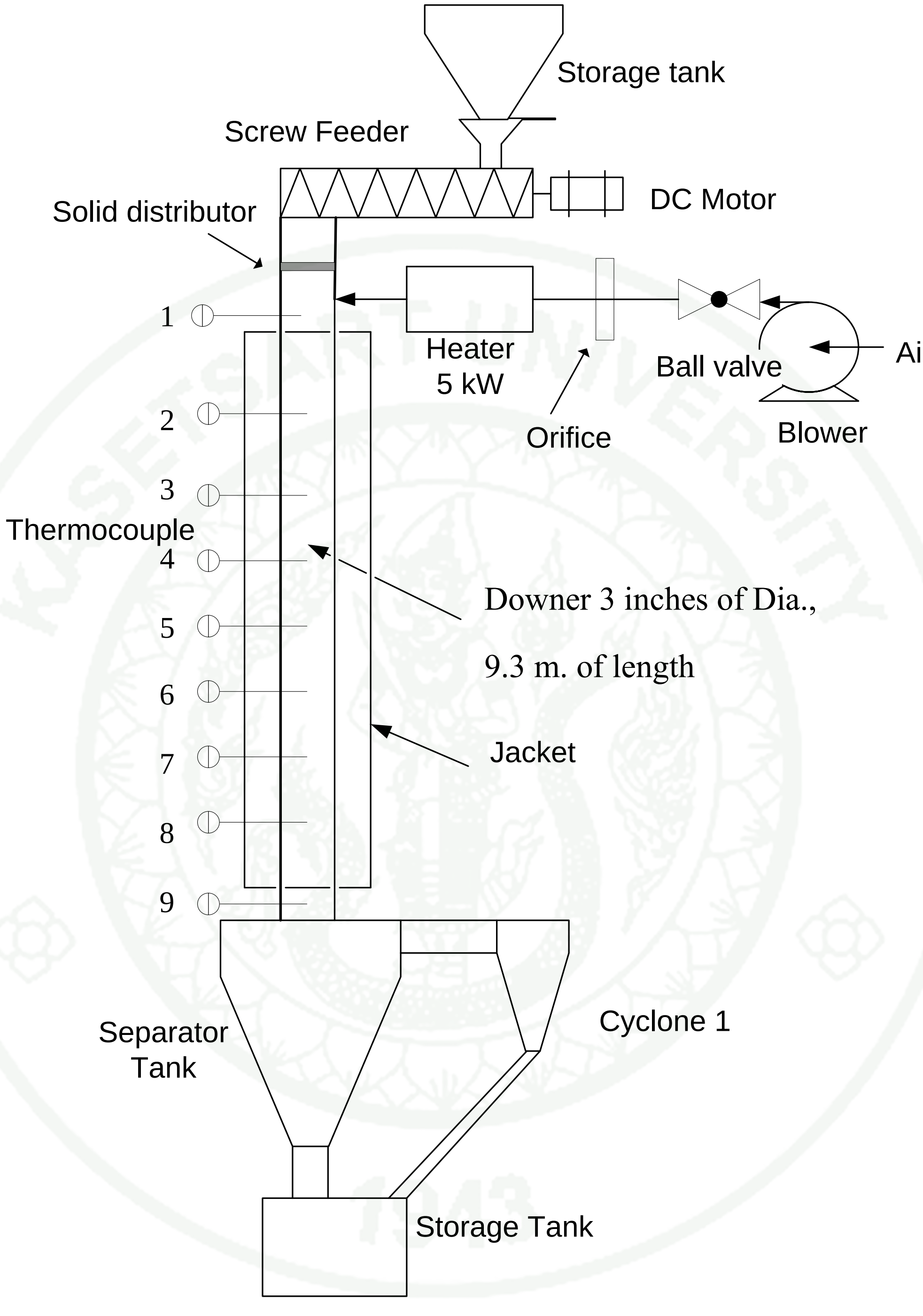

Figure 34 Schematic diagram of co-current down flow fluidized bed reactor (downer).

The solids used were FCC particles (E-cat) of 75 micrometers mean diameter and a bulk density of 1,800 kg/m^3. The main compositions of solid particles were SiO_2 and Al_2O_3 with 64.49 and 32.10%, respectively. The properties of solid catalyst are shown in Table 6.

Table 6 Properties of solid catalyst.

Properties		Value
Chemical composition (wt.%)		
	SiO_2	64.49
	Al_2O_3	32.10
	Re_2O_3	2.08
	Na_2O	0.48
	C	0.38
	Fe	0.47
Particale Size Distribution (PSD) (wt.%)		
	<40 (microns)	2
	<50 (microns)	12
	<60 (microns)	26
	<70 (microns)	43
	<80 (microns)	57
	<105 (microns)	84
Average Particle size (APS) (microns)		75
Physical properties		
	surface area (SA), m^2/g	130
	Pore volume (PV), ml/g	27
	Apparent bulk density (ABD), g/ml	0.95
ASTM micro activity		70.1

The gas velocity was measured with an orifice and manometer which installed between the blower and heater. The orifice was calibrated using an anemometer. The calibration curve is illustrated in Figure 35._The calibration curve is linear. The superficial air velocity and orifice pressure drop can be correlated as $v_g = 0.022(\Delta P) + 1.6063$ where v_g is in m/s and ΔP is in mm.H_2O.

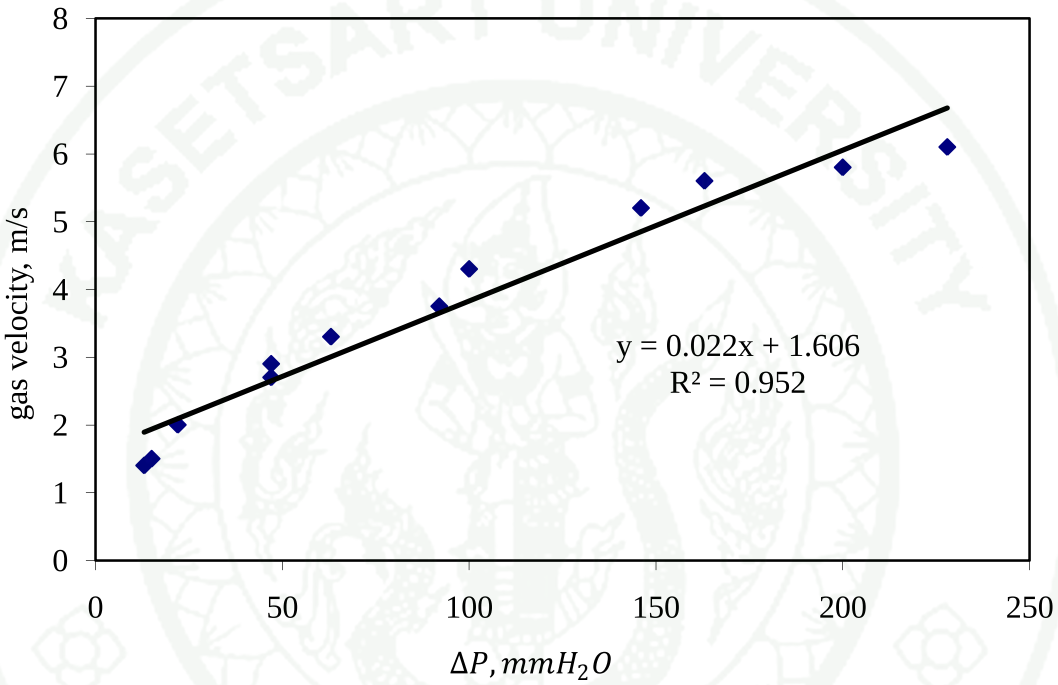

Figure 35 Calibration curve of superficial velocity with pressure dropped through flow meter (orifice).

The gas velocity changes with the difference temperature but the mass flux is not. So the orifice measurement was done at ambient temperature and the mass flux of gas was calculated in relation to the cross sectional area of the feeding tube. The gas mass flux at various pressure drops across the orifice is shown in Figure 36. The calibration curve is linear. The gas mass flux and orifice pressure drop can be correlated as $G_g = 0.026(\Delta P) + 1.876$.

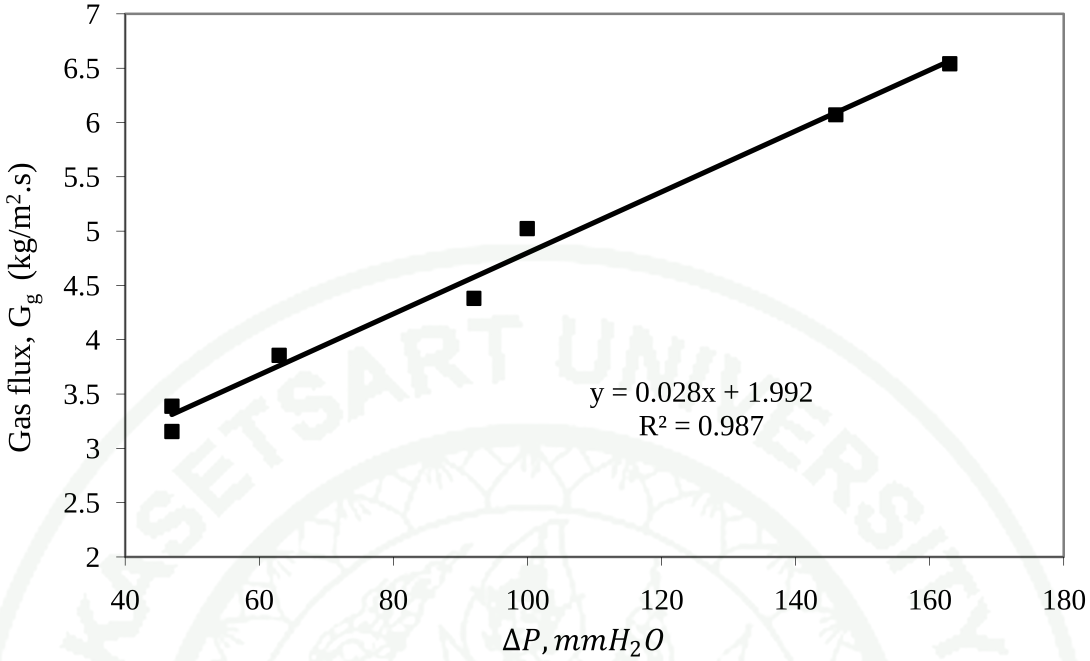

Figure 36 The gas mass flux at various pressure drop across the orifice at the feeding point.

The adjustment of solid flow rate or solid flux was controlled by pulse width modulator (PWM). The PWM is an electronic circuit board for controlling and adjusting the direct voltage (DCV) input to the DC motor that drives the screw feeder. The straight sign input is converted to the band width of fish teeth wave. The average output voltage is the average of the peak and the bottom voltages. The advantage of a PWM is that it doesn't effect to the torque of motor and easier to control than a gearbox. The alteration of direct voltage to the fish teeth wave is shown in Figure 37.

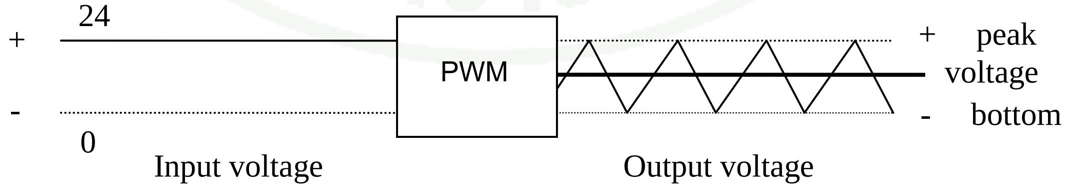

Figure 37 Alteration of direct voltage to fish teeth wave by PWM.

The screw feeder is used to convey solid to the distributor. The screw feeder is driven by 24 direct current voltage motor. The adjustment of direct voltage by pulse width modulator has effect to increase or decrease the rotation speed in round per min (rpm). The variation of voltages relate directly to the solid flow rate or solid flux. The solid flux increases with direct voltage. The solid flux flowing through the screw feeder was calibrated with variation in direct voltage as shown in Figure 38.

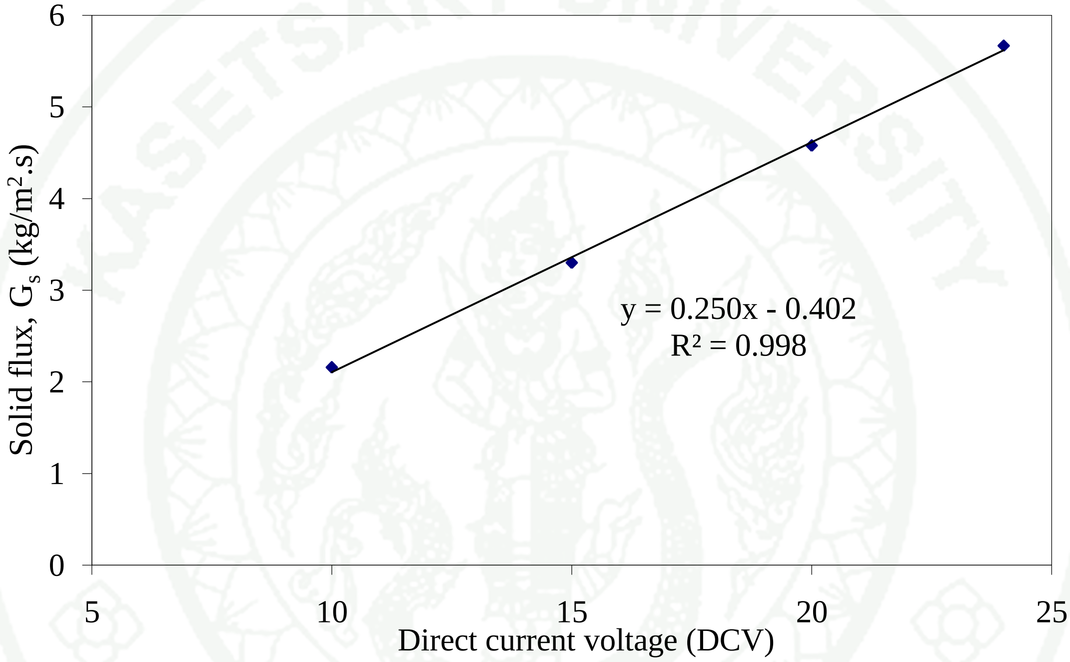

Figure 38 The calibration curve of solid flux at various direct voltage supplied to screw feeder.

The measurements of temperature along the downer reactor were done by 10 thermocouples (type K) that were installed in axial positions at the entering and every 1.125 meters to the bottom of reactor. The temperature data from the thermocouples is analog signal which were converted to digital signal by Wisco data logger. Then digital data were sent to the computer and recorded.

2. Mathematical model and simulation

This work studied the gas temperature distribution in the downer reactor. The dispersion model is applied to the gas solid flow from entering to the bottom of the reactor. The effect of heat loss is included in the mathematical model. The simulation of down flow reactor (Figure 34) was done for catalytic cracking of heavy oil with heat loss through the wall.

Modeling was done with the following assumptions.

a. Axis symmetry.
b. Low solid dispersed in the radial position.
c. Without radial temperature gradient
d. Steady state.
e. Pe = 100.
f. Heat loss through the wall from solid phase is neglected.
g. Heat transfer outside the reactor wall is under natural convection.
h. Outside temperature near the reactor wall varies linearly with the reactor length.

The model resembles the dispersion model developed previously (Promsan, 2005). It was modified to account for the heat loss through the wall of the reactor. Therefore, the energy balance was modified with the addition of heat loss term to the gas phase energy balance equation.

2.1 Hydrodynamics

The continuity equations of gas and solid phase for downer reactor obtained G_g and G_s as equation (29) and (30).

For solid phase:

$$G_s = (1-\varepsilon)\rho_s v_s \tag{21}$$

For gas phase:

$$G_g = \varepsilon \rho_g v_g \tag{22}$$

where ε, v_g, v_s, G_g, and G_s are void fraction, gas velocity, solid velocity, gas flux, and solid flux, respectively.

The solid fraction in a gas-solid system in a downer reactor can be derived from slip velocity definition as shown previously in equation (1).

$$v_{sl} = v_t = \frac{u_s}{(1-\varepsilon)} - \frac{u_g}{\varepsilon} \tag{1}$$

Void fraction can be derived from equation (2).

$$\varepsilon = \left[\frac{\left(v_{t-}u_g - u_s\right) + \sqrt{\left(u_g + u_s - v_t\right)^2 + 4u_g v_t}}{2v_t}\right] \tag{2}$$

The terminal velocity of a single particle can be calculated as shown previously from equation (3).

$$v_t = \sqrt{\frac{4gd_s(\rho_s - \rho)}{3\rho C_D}} \tag{3}$$

where

$C_D = 24/Re_p$	at	$Re_p < 1$
$C_D = 18.5/Re_p^{0.6}$	at	$1 < Re_p < 1{,}000$
$C_D = 0.44$	at	$Re_p > 1{,}000$

2.2 Energy balance

Dispersion model is used to describe the heat transfer in downer reactor. The energy balance is considered in non - adiabatic case with gas phase and solid phase. Both phase compose with heat conductions, heat convection, heat transfer between gas-solid phase. In catalytic cracking, the endothermic reactions occur at the surface of solid catalyst. Therefore, the heat of reaction occurs in solid phase only. The heat transfer to the surrounding systems or heat loss through the wall is added in the dispersion model. The heat loss through the wall is determined in gas phase only because most of the surface area of the reactor is in contact with gas phase. The heat loss through the wall from solid phase is neglected. The ambient air temperature is 35 ^{o}C. The temperature of the outside air near the wall exit at the top of reactor is obtained from the experimental data. The diagram of heat transfer in downer reactor is shown in Figure 39.

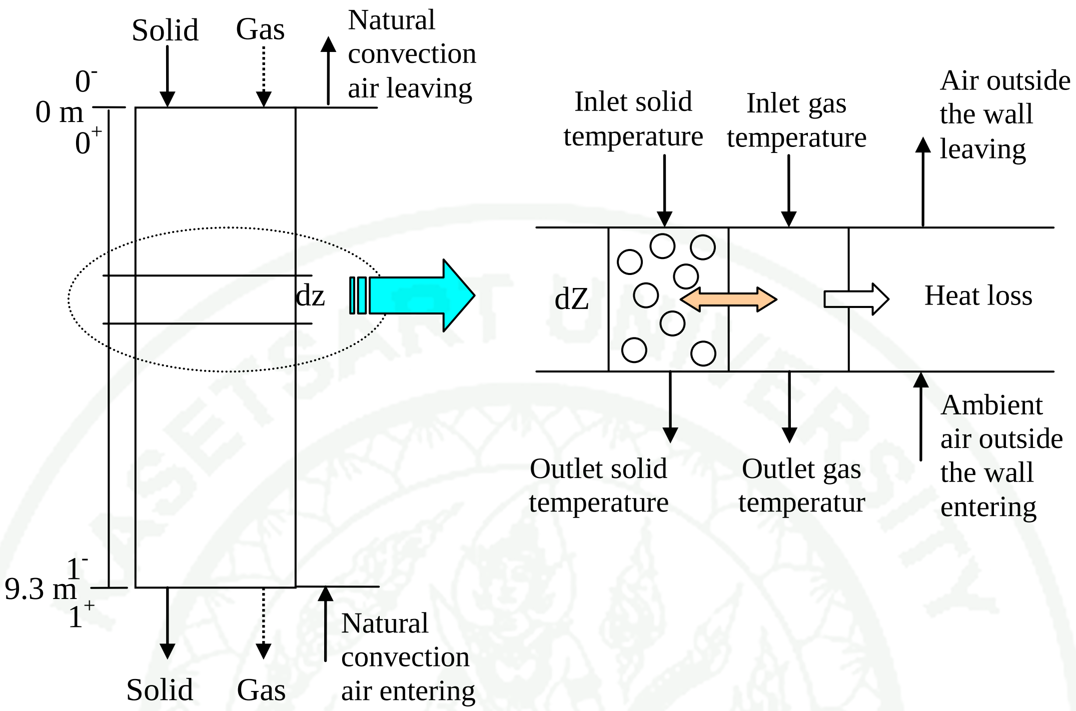

Figure 39 Diagram of heat transfer between gas-solid and heat loss through the wall in the downer reactor.

The energy balance equations of solid phase and gas phase are shown in equation (27) and equation (28).

Solid phase:

$$\frac{1}{Pe_{Hs}}\frac{d^2\theta_s}{dZ^2}-\frac{d\theta_s}{dZ}-\frac{haL}{G_sC_{ps}}\left(\theta_s-\theta_g\right)+\frac{(1-\varepsilon)\Delta H_A L}{G_sC_{ps}T_{s0}}r_A=0 \qquad (27)$$

Gas phase:

$$\frac{1}{Pe_{Hg}}\frac{d^2\theta_g}{dZ^2}-\frac{d\theta_g}{dZ}+\frac{haL}{G_gC_{pg}}\left(\theta_s-\theta_g\right)=0 \qquad (28)$$

The heat loss through the wall is added into the energy balance of dispersion model in gas phase (equation (28)). So, the energy balance equation of gas phase is shown as in equation (40).

$$\frac{1}{Pe_{Hg}}\frac{d^2\theta_g}{dZ^2}-\frac{d\theta_g}{dZ}+\frac{haL}{G_gC_{pg}}\left(\theta_s-\theta_g\right)+\frac{Ua_wL}{G_gC_{pg}}\left(\theta_g-\theta_j\right)=0 \qquad (40)$$

where $\theta_s, \theta_g, \theta_j$, and Z are the dimensionless temperature of solid, gas, outside air, and length of the reactor, respectively. They are:

$$\theta_s=\frac{T_s}{T_{s0}} \qquad \theta_g=\frac{T_g}{T_{s0}} \qquad \theta_j=\frac{T_j}{T_{s0}} \qquad Z=\frac{l}{L}$$

where T_{s0} is inlet solid temperature and L is total length of reactor.

The groups of Pe_{Hg} and Pe_{Hs} represent the dimensionless terms relating to properties of gas and solid including the effect of heat dispersion and convection term. They are:

$$Pe_{Hg}=\frac{G_gC_{pg}L}{\varepsilon k_{g,eff}} \qquad Pe_{Hs}=\frac{G_sC_{ps}L}{(1-\varepsilon)k_{s,eff}}$$

where $k_{g.eff}$ and $k_{s.eff}$ are the gas phase and solid phase heat dispersion coefficients, respectively.

The surface area of solid particles per unit volume of bed and surface area of wall per unit volume of bed are a and a_w , [m^2.m^{-3}], respectively. They can be shown as in equation (41) and (42).

$$a=\frac{6(1-\varepsilon)}{d_s} \qquad (41)$$

$$a_w = \frac{4}{D_t} \tag{42}$$

The boundary conditions at the inlet of the downer reactor ($Z = 0$) considered both convection and conduction terms including back mixin are shown follow as:

$$Z = 0 \qquad \frac{\mathrm{d}\theta_\mathrm{s}}{\mathrm{dZ}} = \mathrm{Pe_{Hs}}\left(\theta_\mathrm{s}|_{\mathrm{Z}=0^+} - \theta_\mathrm{s}|_{\mathrm{Z}=0^-}\right)$$

$$\frac{\mathrm{d}\theta_\mathrm{g}}{\mathrm{dZ}} = \mathrm{Pe_{Hg}}\left(\theta_\mathrm{g}\big|_{\mathrm{Z}=0^+} - \theta_\mathrm{g}\big|_{\mathrm{Z}=0^-}\right)$$

The boundary condition at the outlet of reactor, $Z = 1$ is fully developed. So the temperature of the gas and solid with no heat transfer occur after these points are shown as:

$$Z = 1 \qquad \frac{\mathrm{d}\theta_\mathrm{s}}{\mathrm{dZ}} = 0 \qquad \frac{\mathrm{d}\theta_\mathrm{g}}{\mathrm{dZ}} = 0$$

The heat transfer coefficient between solid and gas in the downer reactor is expressed in equation (15). (Kim *et al.*, 1999)

$$h = 12(p_{sus})^{0.43} \tag{15}$$

where $p_{sus} = \rho_s(1 - \varepsilon)$, p_{sus} is density of suspension (kg/m^3).

The overall heat transfer coefficients of heat loss through the wall of the downer reactor are calculated from the temperature profiles of experimental data. The heat loss through the wall occurs in gas phase only. The heat loss is considered in heat balance equations of gas phase and solid phase for each interval of reactor length as shown in equation (43) and (44).

Gas phase:

$$\dot{m}_g C_{p,g}\left(T_{g,out} - T_{g,in}\right) = UA_w\left(\Delta T_{lm,g-j}\right) + hA_s\left(T_g - T_s\right) \tag{43}$$

Solid phase:

$$\dot{m}_s C_{p,s}\left(T_{s,out} - T_{s,in}\right) = hA_s\left(T_g - T_s\right) \tag{44}$$

where T_g and T_s are gas and solid temperatures, $\dot{m}$ the mass flow rate, [kg/s], A_w the area of the wall, [m^2], $\Delta T_{lm,g-j}$ the logarithmic mean temperature between gas and outside air, [K], h heat convection between phases, [kw/m^2.K]. The T_g and T_s are the average value within the interval. In case of non solid flow, the overall heat transfer coefficient can be rewritten from equation (43) to equation (45).

$$U = \frac{\dot{m}_g C_{p,g}\left(\dot{T}_{g,out} - T_{g,in}\right)}{A_w\left(\Delta T_{lm,g-j}\right)} \tag{45}$$

where logarithmic mean temperature, $\Delta T_{lm,g-j}$ is shown in equation (46).

$$\Delta T_{lm,g-j} = \frac{\left(T_{g,in} - T_{j,out}\right) - \left(T_{g,out} - T_{j,in}\right)}{ln\frac{\left(T_{g,in} - T_{j,out}\right)}{\left(T_{g,out} - T_{j,in}\right)}} \tag{46}$$

2.3 Mass balance equation

The mass balance equations are used to simulate the mass distribution of catalytic cracking of heavy oil. The model resembles the work done previously (Promsan, 2005). The reaction is considered as heterogeneous reaction, with influence of mass transfer between gas phase and solid phase. The dispersion model mass balance includes the effect of diffusion and convection in the terms of Peclect number, *Pe*. The dispersion model is done in combination with the four-lump kinetic model of catalytic cracking of heavy oil. The conversion and yields are considered for individual gas phase and solid phase along the length of the reactor as shown in dimensionless equation (25) and (26).

Solid phase:

$$\frac{1}{Pe}\frac{d^2y_{is}}{dZ^2}-\frac{dy_{is}}{dZ}+\frac{k_{ig}aL}{u_s}\left(y_{ig}-y_{is}\right)+\frac{(1-\varepsilon)\rho_sL}{C_{A0}u_s}r_i=0 \tag{25}$$

Gas phase :

$$\frac{1}{Pe}\frac{d^2y_{ig}}{dZ^2}-\frac{dy_{ig}}{dZ}-\frac{k_{ig}aL}{u_g}\left(y_{ig}-y_{is}\right)=0 \tag{26}$$

The boundary conditions at the inlet $(Z=0)$ and outlet $(Z=1)$ of the downer reactor are expressed as:

$$Z=0 \qquad \frac{dy_{is}}{dZ}=Pe(y_{is}|_{Z=0^+}-y_{is}|_{Z=0^-})$$

$$\frac{dy_{ig}}{dZ}=Pe\left(y_{ig}\big|_{Z=0^+}-y_{ig}\big|_{Z=0^-}\right)$$

$$Z=1 \qquad \frac{dy_{is}}{dZ}=0 \qquad \frac{dy_{ig}}{dZ}=0$$

where y_i is dimensionless concentration or mass fraction of the reactant and products as shown in equation (47).

$$y_i=\frac{C_i}{C_{A0}} \tag{47}$$

where C_i is concentration of the reactant and products. C_{A0} is the initial concentration of gas A as show in equation (48).

$$C_{A0} = \frac{G_A P}{\sum_{n=A,i} G_n R T_g / M_{w,n}} \tag{48}$$

Mass transfer coefficient, k_{ig} can be obtained from the correlation as shown in equation (49). (Welty *et al.*, 1984)

$$S_h = \frac{k_{ig} d_s}{D_{im}} = 2 + 0.6 \left(\frac{d_s u \rho}{\mu}\right)^{0.5} \left(\frac{\mu}{\rho D_{im}}\right)^{1/3} \quad (49).$$

where S_h is Sherwood number, and D_{im} the diffusion coefficient of component i in gas mixture.

2.4 Kinetic model

The 4-lump kinetic model of heavy oil catalytic cracking reaction was used in this study. They are the same as used in the previous simulation (Promsan, 2005) as shown in Figure 32.

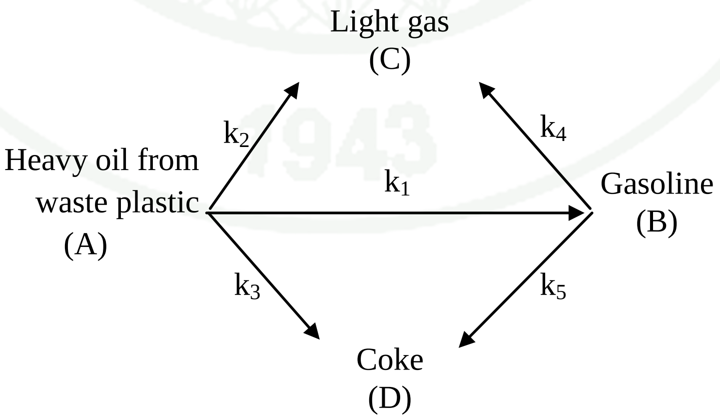

Figure 32 The kinetic model of heavy oil catalytic cracking.

Source: Songip *et al.* (1994)

The cracking reactions of heavy oil to gasoline, light gas, and coke are the second order reaction. The over cracking reactions of the gasoline to light gas and coke are the first order reaction. The reaction rates from equation (21) to (24) is included with mass fraction of heavy oil and gasoline from equation (57).Hence, the reaction rates of the four-lump model can be expressed in equations (50) to (53).

$$r_A = -(k_1 + k_2 + k_3)y_{As}^2 C_{A0}^2 \tag{50}$$

$$r_B = k_1 y_{As}^2 C_{A0}^2 - (k_4 + k_5) y_{Bs} C_{A0} \tag{51}$$

$$r_C = k_2 y_{As}^2 C_{A0}^2 + k_4 y_{Bs} C_{A0} \tag{52}$$

$$r_D = k_3 y_{As}^2 C_{A0}^2 + k_5 y_{Bs} C_{A0} \tag{53}$$

For the adiabatic and non- adiabatic with heat loss through the wall cases, the variation of temperature inside the downer leads to variation of the reaction rate constant. These reaction rate constants can be obtained from the Arrhenius equation from equation (20).

$$k = k_0 exp\left(\frac{-Ea}{RT}\right) \tag{20}$$

The frequency factors and activation energies for heavy oil catalytic cracking with 4-lump model is showing from Table 3.

2.5 Numerical Method

This dispersion model is used for co-current down flow fluidized bed reactor (downer). The model equation in energy balances are the second-order ordinary differential equations and nonlinear. The numerical solution is used for solving these equations. In this work, the orthogonal collocation method is applied with COLNEW software to solve the dispersion model. The solutions are calculated from the operating conditions and the boundary of dimensionless equations. The solutions are reported as the temperature distribution and mass fraction as a function of the length of reactor. The numerical methods of COLNEW software is shown in Figure 40 with the following steps.

1. Input and read the constant value, various parameters, and estimate the constant functions.

2. Set the boundary of calculations to equal section (interval) to calculate the variation in parameters.

3. Calculation of the first interval by generating the mesh and evaluate the matrix with Jacobi polynomial.

4. Solve the ODEs then check the tolerance of the solutions. If the tolerance is higher than a fixed value, go back and recalculate. If the tolerance is less than the fixed value, go to the next position.

5. Record the solutions.

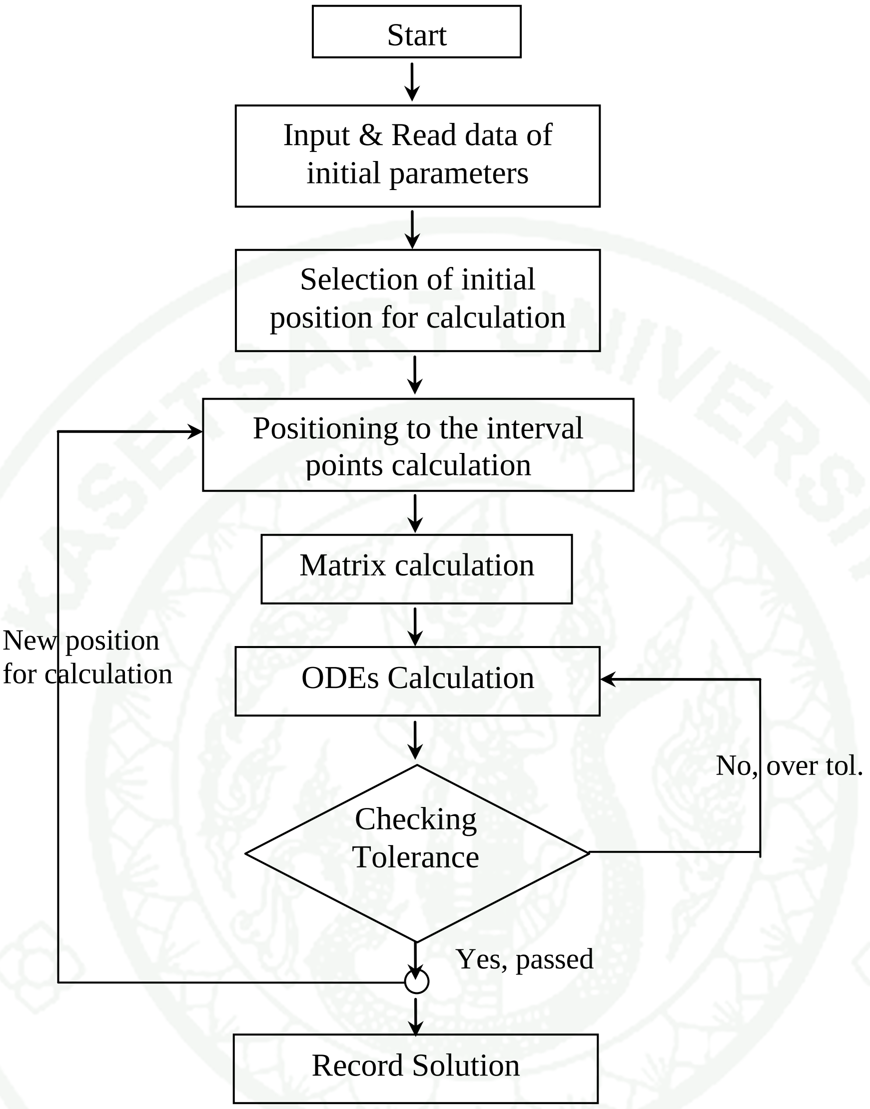

Figure 40 Diagram of numerical solution by COLNEW software of dispersion model.

The gas – solid heat transfer experiments with hot air were done under the operating conditions. The physical properties and experimental condition are shown in Table 7. From the experimental data, the correlation of heat loss though the wall from the downer reactor was created. This correlation was put into the mathematical model of catalytic cracking of heavy oil in the downer reactor. The simulation of catalytic cracking with heat loss through the wall was done under various operating condition. The physical properties of gas feed and simulation conditions are shown in Table 7 and 8.

Table 7 The physical properties of gas feed (air) and the heat loss experimental operating conditions.

Physical properties of air	Value
Thermal conductivity of air	(4.54 – 6.75) x 10^{-5} kJ/(K.m.s)
Heat capacity of air	1.04 - 1.14 kJ/kg.K
Viscosity of air	(2.95 - 4.15)x 10^{-5} Pa.s
Molar mass of air	29 kg/kmol
Density of air	0.8 – 1.1 kg/m^3
Catalyst density	1,800 kg/m^3
Operating conditions	**Range and value**
Inlet gas temperature, T_{g0}	380 – 560 ^{o}C
Inlet catalyst temperature, T_{s0}	35 ^{o}C
Outside air entrance temperature, $T_{j\ in}$	35 ^{o}C
Inlet pressure, P_0	1.01 atm
Solid flux, G_s	2.2 – 5.6 kg/m^2.s
Gas flux, G_g	3.8 – 5.8 kg/m^2.s
Reactor length	9.3 m
Reactor diameter	0.075 m

Table 8 The physical properties of gas feed (heavy oil) and solid catalyst and the simulation conditions.

Physical properties	Value
Thermal conductivity of gas	6.2×10^{-5} kJ/(K·m·s)
Thermal conductivity of solid	0.229 kJ/(K·m·s)
Heat capacity of gas	3.3 kJ/kg·K
Heat capacity of solid	1.087 kJ/kg·K
Heat of reaction	600 kJ/kg of feed
Viscosity of gas	1.4×10^{-5} kg/m·s
Average particle diameter	70×10^{-6} m
Catalyst density	1,800 kg/m^3
Molar mass of heavy oil	262 kg/kmol
Molar mass of gasoline	106.7 kg/kmol
Molar mass of light gases	40 kg/kmol
Molar mass of coke	14 kg/kmol
Molar mass of inert gas	28 kg/kmol
Operating conditions	**Range and value**
Inlet heavy oil gas temperature, T_{g0}	380 – 560 ^oC
Inlet solid temperature, T_{s0}	35 ^oC and 380 – 560 ^oC
Outside air entrance temperature, $T_{j\ in}$	35 ^oC
Inlet pressure, P_0	1.01 atm
Reactor length	9.3 m
Reactor diameter	0.075 m
Solid flux,G_s	2.2 – 5.6 kg/m^2·s and 180 kg/m^2·s
Gas flux, G_g	3.8 – 5.8 kg/m^2·s and 15 kg/m^2·s
Nitrogen feed	3.75 (%wt of feed)

Source: Berry *et al*. (2004)

RESULTS AND DISCUSSION

This study considered the effect of heat loss through the wall in the downer reactor to the catalytic cracking of heavy oil. The temperatures in the downer reactor (gas temperature) changes from the effects of heat transfer to the solids inside the reactor and the heat loss through the wall. The heat loss experiments were done at steady state with hot air without reaction to study the effects of inlet gas temperature, gas mass flux, and solid mass flux. The estimation the overall heat transfer coefficient (U) between the gas inside the reactor and the gas outside the wall was done from the heat loss experiments. These overall heat transfer coefficients are added into the energy balance of dispersion model for fluid catalytic cracking of heavy oil in the downer. The simulations were done to show the reactor performance to see the effect of heat loss.

The heat loss experiments with hot air feed were conducted in downer reactor. The gas temperature distributions led to the calculations of the heat loss to the surrounding system and the overall heat transfer coefficient. The experiments were divided into 2 parts: 1) heat transfer without solid particle in the system and 2) heat transfer with solid flow in the system.

1. The heat transfer experiments of hot air in the downer reactor without solid

1.1 The experimental effects of inlet gas temperature on the axial gas temperature distributions

These experiments were performed without solid flowing in the downer system. The inlet gas (hot air) at a constant temperature was fed into the top of the downer reactor. The hot gas was fed into the reactor for at least 400 minutes so that the gas temperature distributions did not change with time and approached to steady state. The effects of inlet gas temperature on the axial gas temperature distribution are shown in Figure 41.

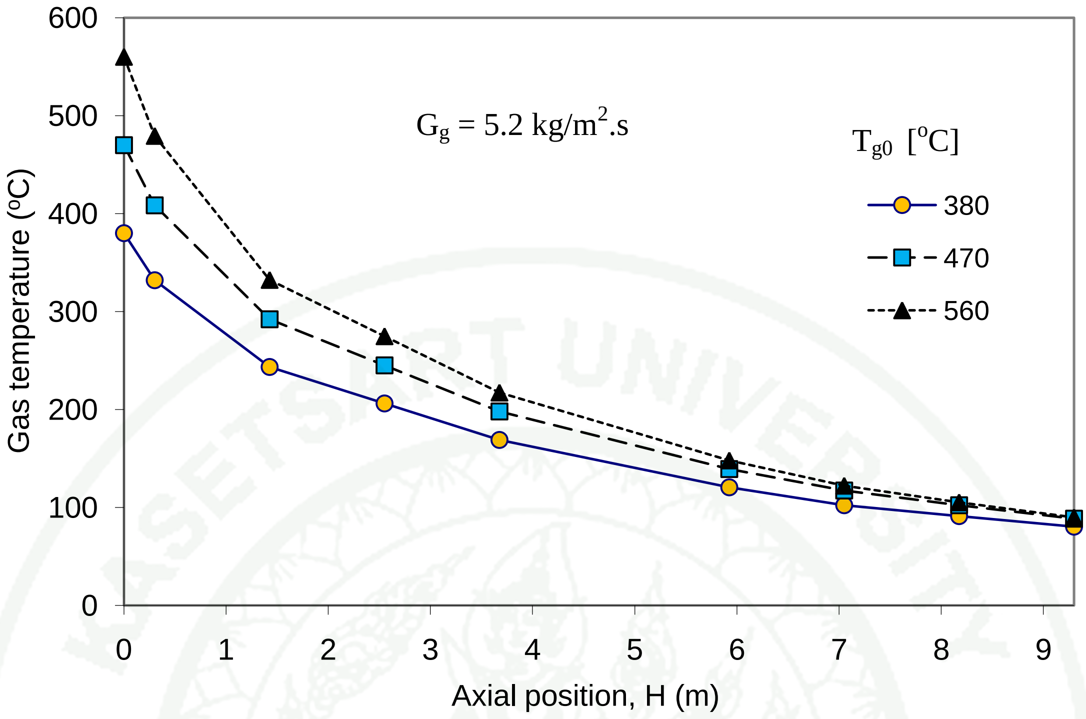

Figure 41 The experimental effect of inlet gas (hot air) temperature on the gas temperature profiles with the constant gas flux of 5.2 $kg/m^2.s$ in the downer reactor without solid flux.

In Figure 41, the gas temperature distributions are illustrated at various inlet gas temperatures (380, 470, and 560 ^oC) at the same 5.2 $kg/m^2.s$ of gas flux. All gas temperatures sharply decreased in the entrance zone (0-1.4 m.), then slowly decreased in the middle zone of the reactor. At the bottom of reactor, the gas temperature gradually decreased until they reached the exit of reactor. Higher inlet gas temperature gives higher gas temperature distribution along the length of reactor. The reduction in the gas temperature distributions of downer reactor are affected from the heat loss through the wall. In the entrance zone, the heat of inlet gas is rapidly transferred to surrounding system because the large difference in temperatures of the inlet gas and the outside system gives higher diving force. Then, the driving force smoothly reduces along the reactor length.

The overall heat transfer coefficient was calculated from the heat loss through the wall of the downer reactor by using equation (45). The overall heat transfer coefficients at various inlet gas temperatures as a function of gas temperature are shown in Figure 42.

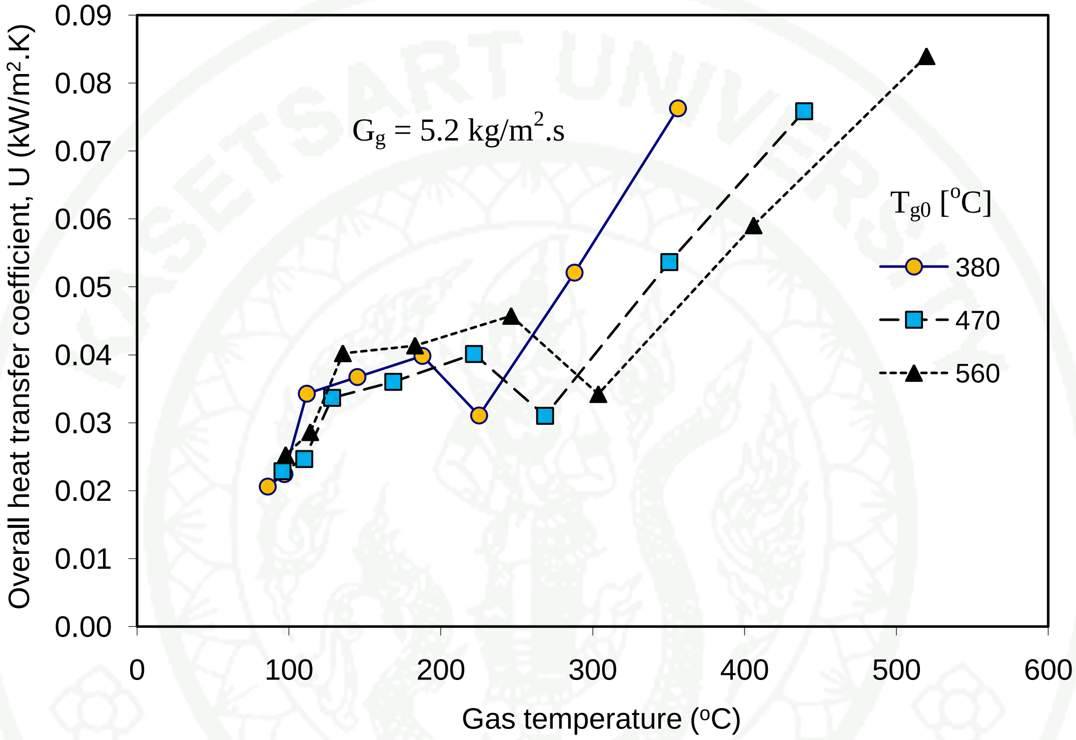

Figure 42 The experimental overall heat transfer coefficients at various inlet gas temperatures as a function of gas temperature in the downer reactor at constant gas flux without solid flux.

The overall heat transfer coefficients are high at the high gas temperature and decreases very fast. At the mid range of the gas temperature (120-250 °C), the overall heat transfer coefficients does not very much. At the low gas temperature (below 120 °C), the overall heat transfer coefficients decreases with temperature to minimum. The gas flux was fed into the top of reactor at various inlet gas temperatures in this experiment. It was noticed that the outside gas temperatures at the top of reactor increased with inlet gas temperature due to the effects of natural convection. The increase in outside gas temperature tends to give a lower overall heat transfer coefficients at the same gas temperature inside. Abnormality is observed at the mid range of temperature. This effect could be the result of the assumption of linear variation of outside air temperature at the mid range of temperature near the bottom of the reactor against the non linear variation of temperature driving force across the wall in actual system.

1.2 The experimental effect of gas flux on the axial gas temperature distributions

The effects of varying the mass flow rate of gas under a constant inlet gas temperature and without solid flux are shown in Figure 43.

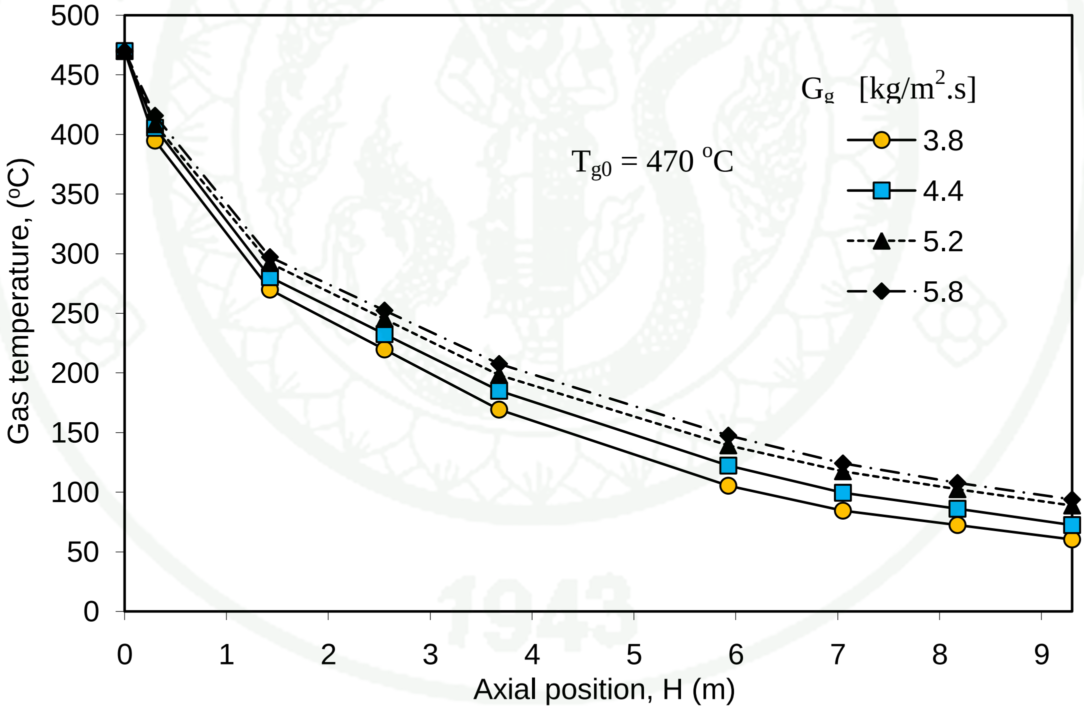

Figure 43 The experimental effect of gas mass flux on the gas temperature profiles with a constant inlet gas temperature of 470 °C in the downer reactor without solid flux.

Figure 43 shows the effect of various gas flux (3.8, 4.4, 5.2, and 5.8 kg/m^2.s) at 470 ^{o}C of inlet gas temperature on gas temperature distribution was shown. The gas temperature distributions decrease along the length of reactor. The lowest gas flux leads to the lowest gas temperature distribution. The gas temperature profiles increase with the gas flux because higher gas flux carries in more heat at the same inlet gas temperature.

The overall heat transfer coefficients at various gas fluxes as a function of gas temperature are shown in Figure 44.

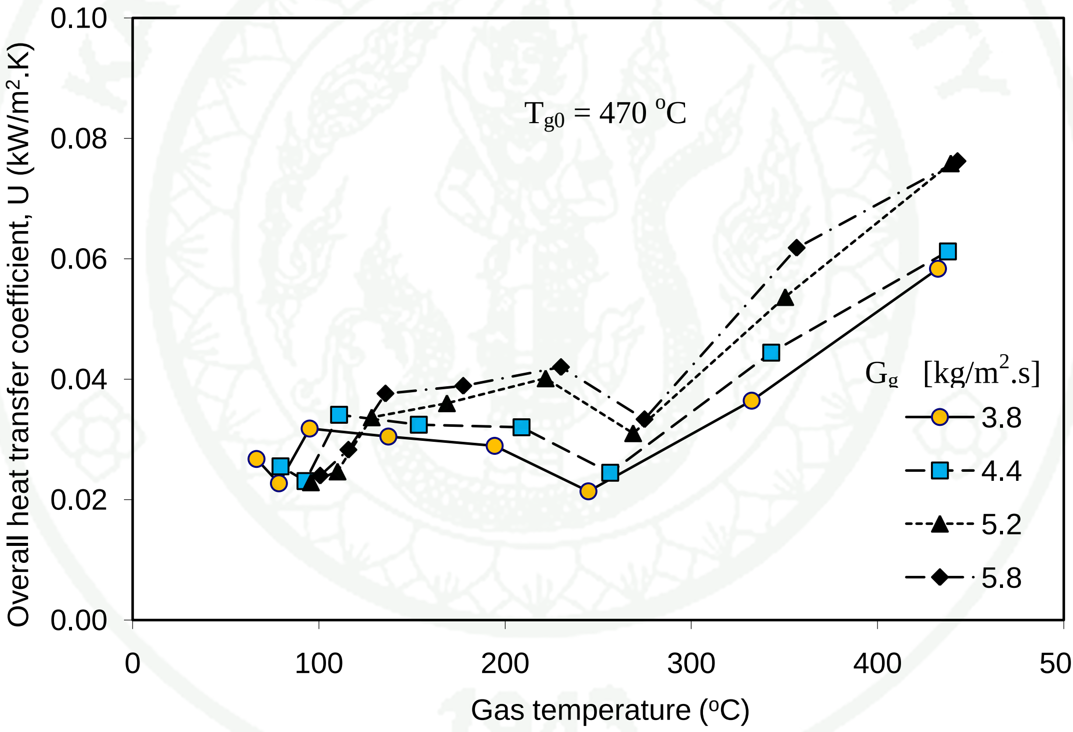

Figure 44 The overall heat transfer coefficients at various gas fluxes as a function of gas temperature in the downer reactor without solid flux

It is apparent that higher gas flux gives higher overall heat transfer coefficients. Higher gas flux gives higher gas velocity, thus higher convective heat transfer coefficient. At high gas temperature inside the reactor, the overall heat transfer coefficients increased.

2. The heat transfer experiments of hot air in the downer reactor with gas-solid.

2.1 The experimental effect of inlet gas temperature on the axial gas temperature distributions

The effects of inlet gas temperature on axial gas temperature at constant solid mass flux and constant gas mass flux are illustrated in Figure 45.

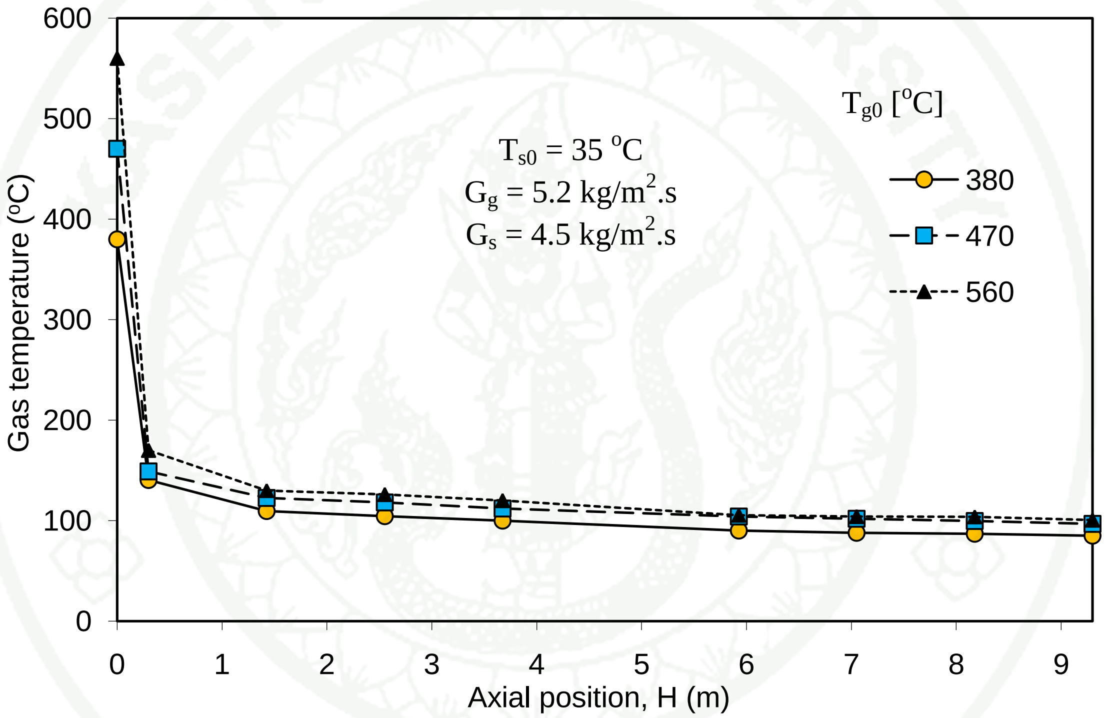

Figure 45 The experimental effect of inlet gas temperature on the axial gas temperature distributions under G_g= 5.2 kg/m^2.s and G_s = 4.5 kg/m^2.s in the downer reactor.

In Figure 45, 5.2 kg/m^2.s of gas mass flux was fed into the downer reactor with various inlet gas temperatures. A constant solid flow rate (4.5 kg/m^2.s) at 35 °C was fed by a distributor. Gas and solid mixed together at the entrance zone. Then gas-solid flew downward together. The gas temperature decreased very fast at the beginning of the solids flow. At the middle and bottom sections, the gas temperatures gradually decreased and approached to some constant values. The higher inlet gas temperature gives higher gas temperature profiles because there are higher quantities of heat supplied into the reactor. The quick reduction of gas temperature in the solid flowing experiment comes from 2 main mechanisms: the heat loss through the wall and the heat transferred to the solid phase. The heat loss through the wall is represented by overall heat transfer coefficient. The overall heat transfer coefficient at various inlet gas temperatures as a function of gas temperature in the downer are shown in Figure 46.

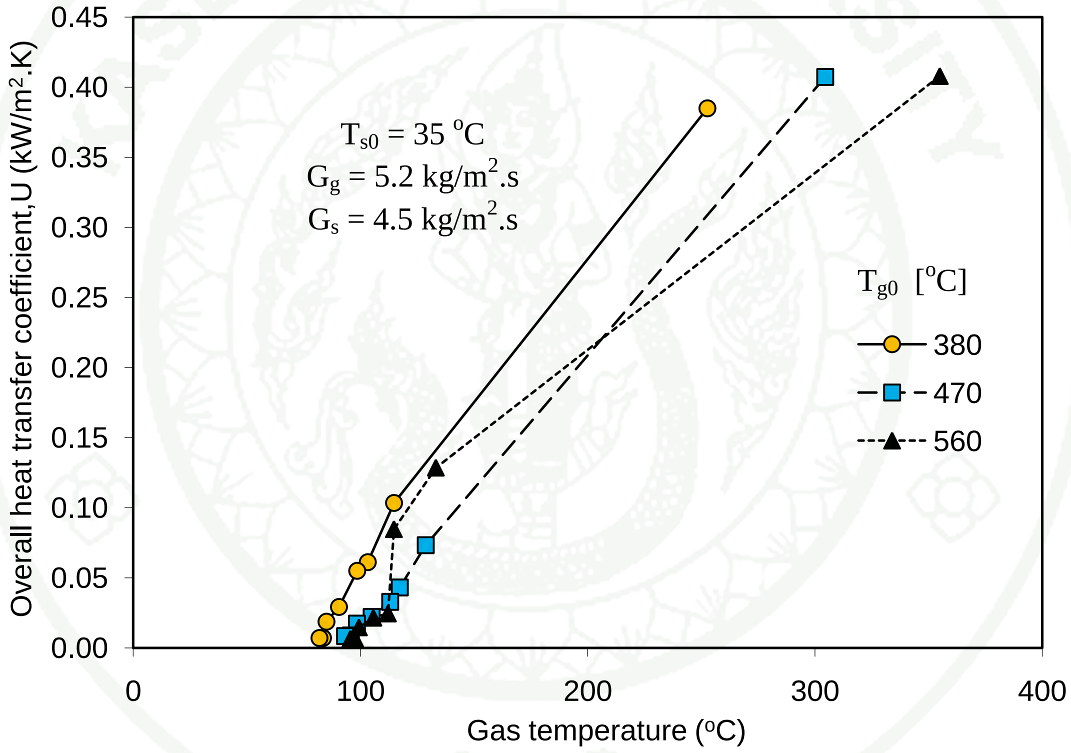

Figure 46 The overall heat transfer coefficients at various inlet gas temperatures as a function of gas temperature in the downer reactor with constant gas flux and solid flux.

The overall heat transfer coefficients were obtained at various reactor lengths and then were plotted as a function of gas temperatures inside the reactor. The overall heat transfer coefficients increase with the gas temperature. The lower gas temperature indicates lower overall heat transfer coefficients at all inlet gas temperatures. Approximately the same value of overall heat transfer coefficients (at the entrance) are obtained at various inlet gas temperatures. However, at the same gas temperature inside the downer, variations of overall heat transfer coefficients are shown. The effect could come from higher heat transferred to the solid than heat loss through the wall. The inlet gas temperatures are insignificant to the overall heat transfer coefficients with the solid flow inside the downer.

2.2 The experimental effect of gas flux on the axial gas temperature distributions

The effects of gas flux on the axial gas temperature with gas solid flow at constant inlet temperature and solid flux are illustrated in Figure 47.

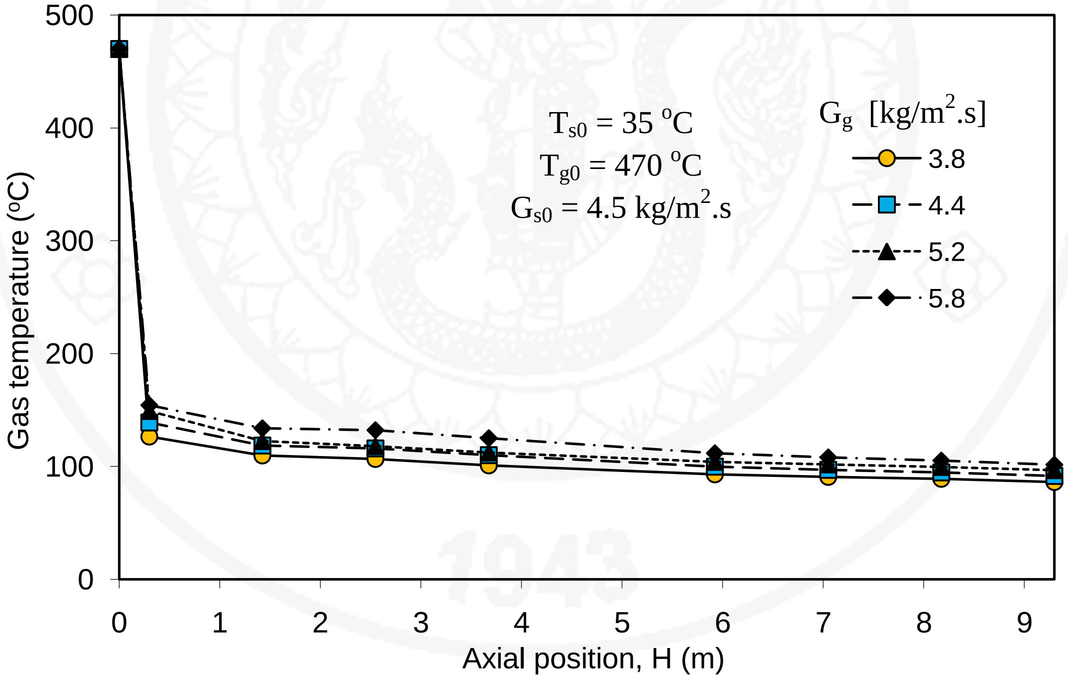

Figure 47 The experimental effect of gas flux on the axial gas temperature distributions under T_{g0} = 470 °C and G_s = 4.5 kg/m^2.s in the downer reactor.

In Figure 47, gas at inlet temperature of 470 °C was fed into the downer reactor at the various gas flow rates with fixed solid mass flux at a temperature of 35 °C. The gas temperature dropped very fast at the entrance. After that, gas temperature smoothly decreased along the length of the downer reactor. The gas temperature profiles increase with gas flux. The decrease of gas temperature is influenced from the heat transfer to the solid phase and the heat loss through the wall. The overall heat transfer coefficients at various gas fluxes as a function of gas temperature are shown in Figure 48. The overall heat transfer coefficients were obtained at various reactor lengths and then were plotted as a function of the gas temperatures inside the downer.

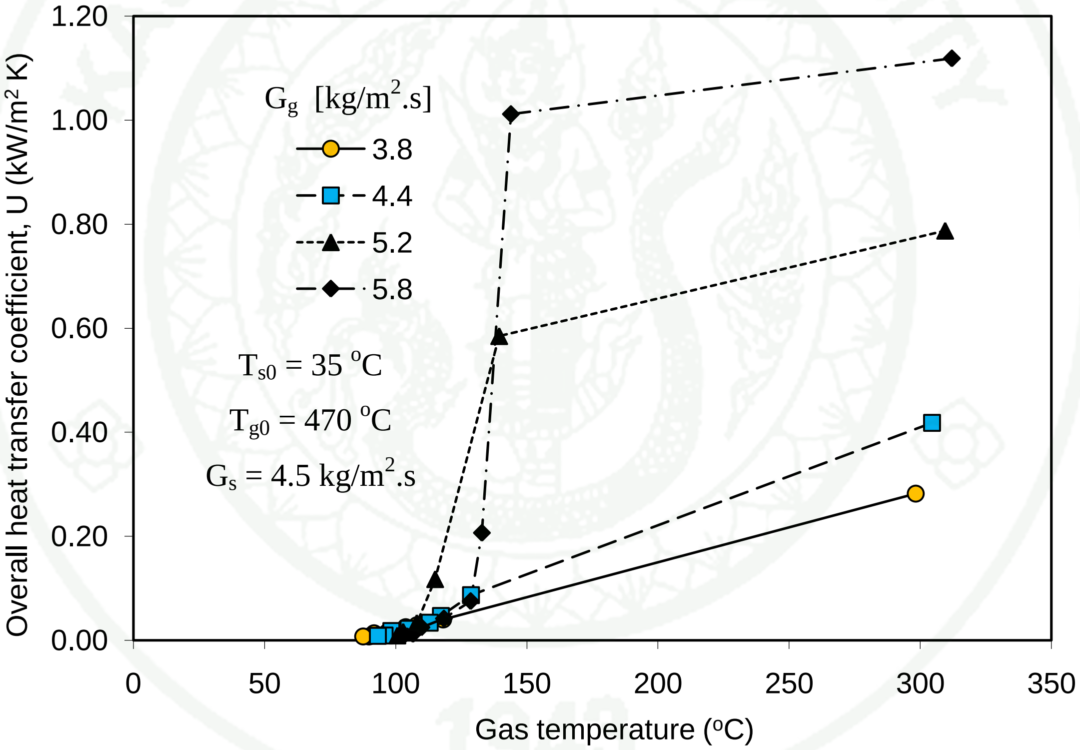

Figure 48 The overall heat transfer coefficients at various gas fluxes as a function of gas temperature in the downer reactor with constant solid flux and inlet gas temperature.

The overall heat transfer coefficients increase with gas mass flux. The overall heat transfer coefficients decreased slightly in the high range of gas temperature (130 – 300 °C). At the lower gas temperature, the overall heat transfer coefficients were low comparing with the high gas temperature range. These lower values could be the result of lower gas velocity at the lower temperature at constant axial gas mass flux. The increasing of gas flux increases overall heat transfer coefficients at the same gas temperature due to higher gas velocity.

2.3 The experimental effect of solid flux on the axial gas temperature distributions

The effects of varying solid flux under the constant gas flux and inlet gas temperature of 470 ^oC are shown in Figure 49.

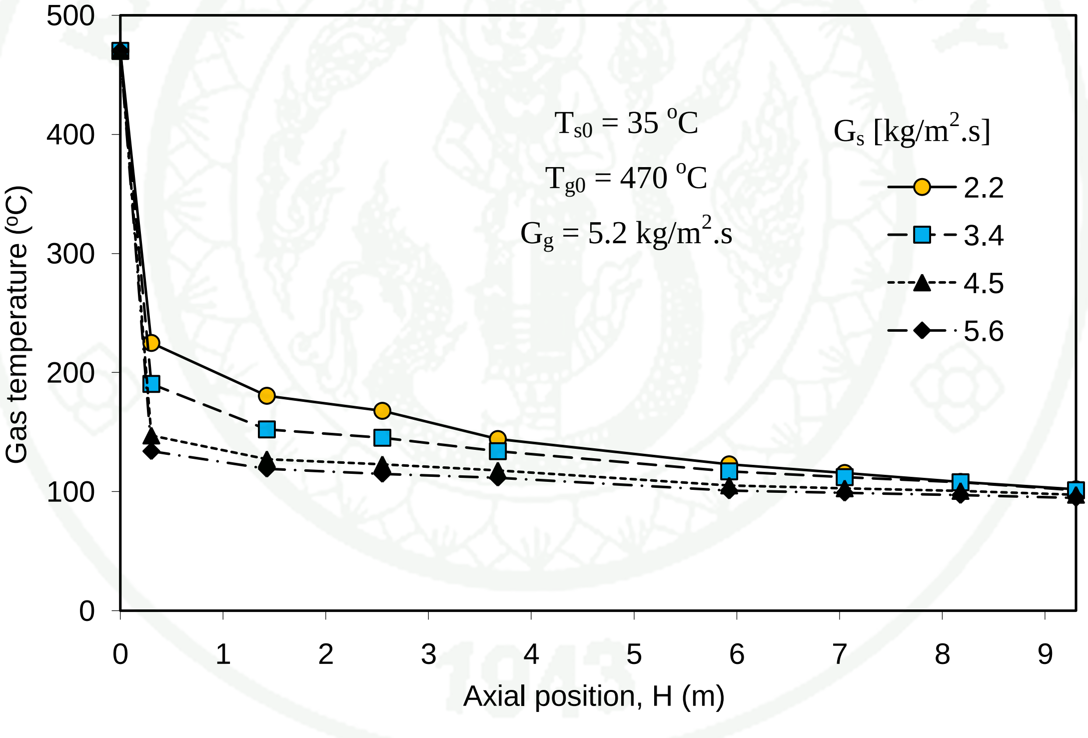

Figure 49 The experimental effect of solid flux on the axial gas temperature distributions under T_{g0} = 470 ^oC and G_g = 5.2 kg/m^2.s in the downer reactor.

In Figure 49, all gas temperature profiles decreased very fast at the entrance. In high solid mass flux (5.6 and 4.5 kg/m^2.s), the gas temperature deeply decreases and then approaches to some constant temperature at the middle of reactor. Then the gas temperature was fairly constant to the exit of reactor. For the lower solid mass flux (3.4 and 2.2 kg/m^2.s), the gas temperature distribution continually decreased along the downer reactor after the fast decreasing at the entrance because the heat transfer rate to solid did not overwhelm the total heat transfer from the gas. The lower solid mass flux gave the higher gas temperature distributions. The overall heat transfer coefficients at various solid mass fluxes as a function of gas temperature are shown in Figure 50.

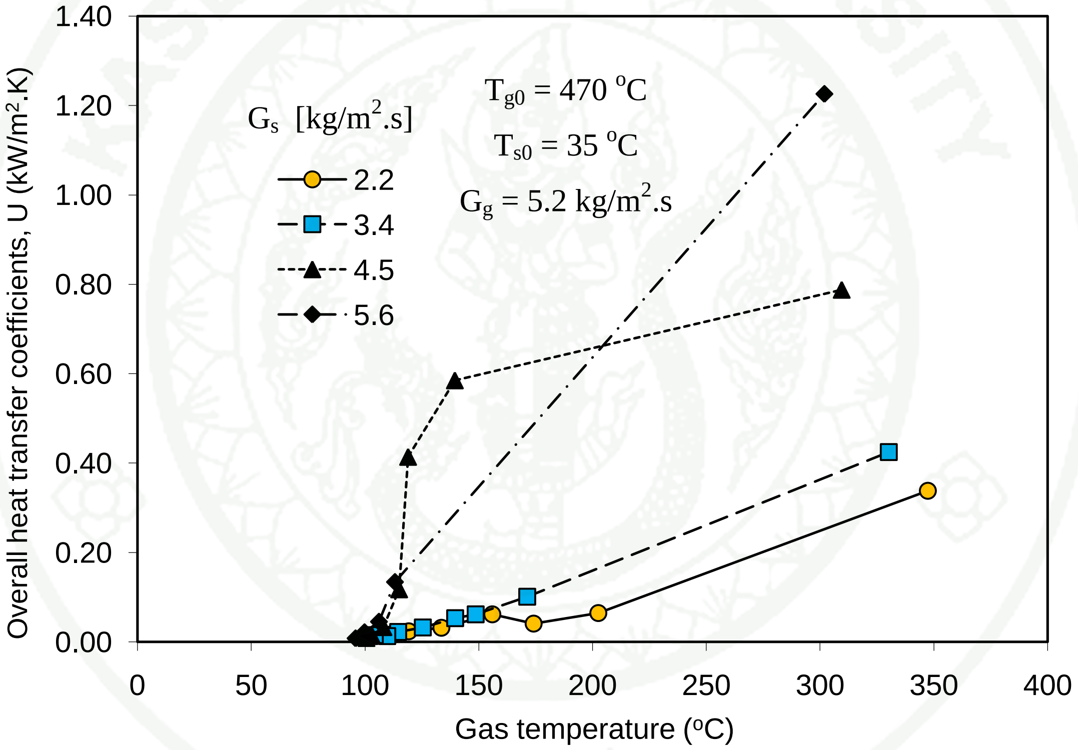

Figure 50 The overall heat transfer coefficients at various solid fluxes as a function of gas temperature in the downer reactor with constant gas flux and inlet gas temperature.

The overall heat transfer coefficients increase with gas temperature. In high gas temperature range (200 – 350 °C), the high solid flux gives high overall heat transfer coefficients. The overall heat transfer coefficients increase with solid flux. At high solid flux, the gas velocity increase and gives higher heat transfer coefficient.

3. The correlation of overall heat transfer coefficients in the downer reactor

The rate of heat loss through the wall of the downer reactor was calculated in terms of the overall heat transfer coefficients. From the experiments, the overall heat transfer coefficients were obtained with variations in inlet gas temperature, gas mass flux, and solid flux. From experimental data, variation in inlet gas temperature did not significantly affect the overall heat transfer coefficients at the gas temperature higher than 300 ^{o}C. The gas mass flux and solid mass flux had more effects to the overall heat transfer coefficients. A simple empirical correlation for overall heat transfer correlation is developed as:

$$U = f(G_g, G_s)$$

$$U = kG_g^a G_s^b \tag{54}$$

where k, a, and b are constants.

From the experimental data, all the constants in equation (54) are obtained and the correlation of overall heat transfer coefficients is:

$$U = 0.000408\left(G_g^{3.31}\right)\left(G_s^{1.37}\right) \tag{55}$$

where U is in kW/m^2.K, G_g and G_s are in kg/m^2.s. This correlation is obtained from experimental data at a temperature range of 300 – 560 ^{o}C, a gas mass flux range of 3.8 kg/m^2.s and a solid flux range of 2.2 – 5.6 kg/m^2.s.

The comparison of overall heat transfer coefficients from the experimental data and the correlation (equation (55)) are illustrated in Figure 51 and 52. Comparison of the overall heat transfer obtained from equation (55) to experimental data gives average errors of 9% with the highest error of 21 %. The numerical value of the over heat transfer coefficients are shown in Appendix A Table A2.

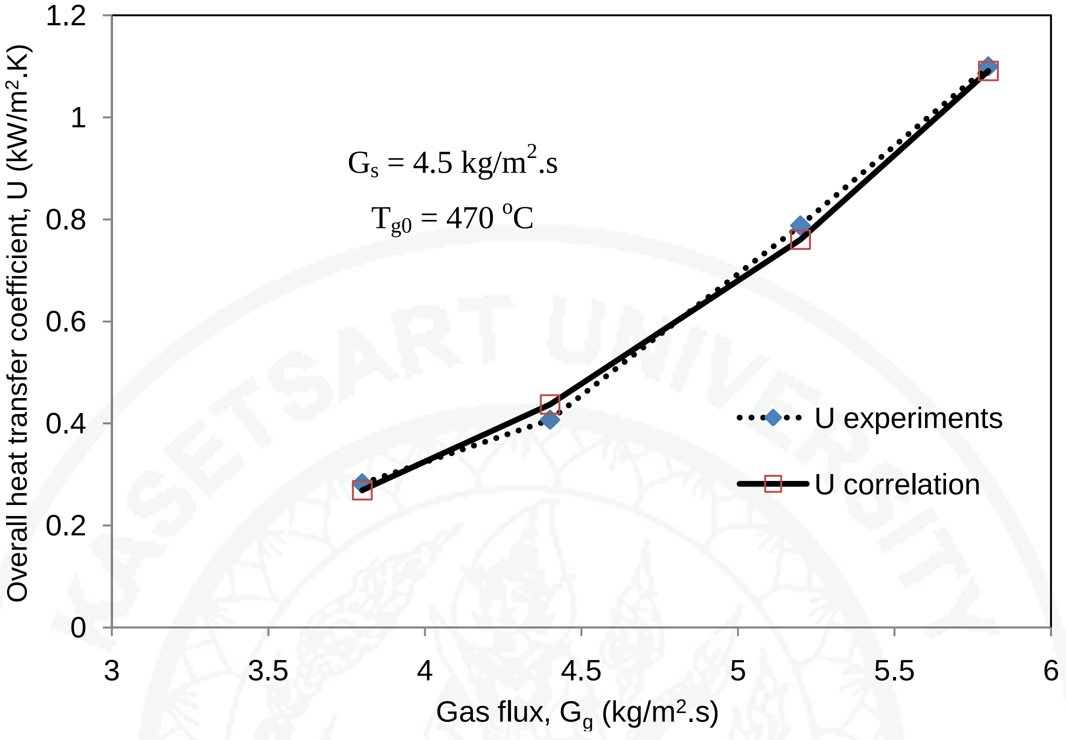

Figure 51 Comparison of the overall heat transfer coefficients from the experimental data and the correlation (equation (55)) as a function of gas flux under a constant solid flux and inlet gas temperature in the downer reactor.

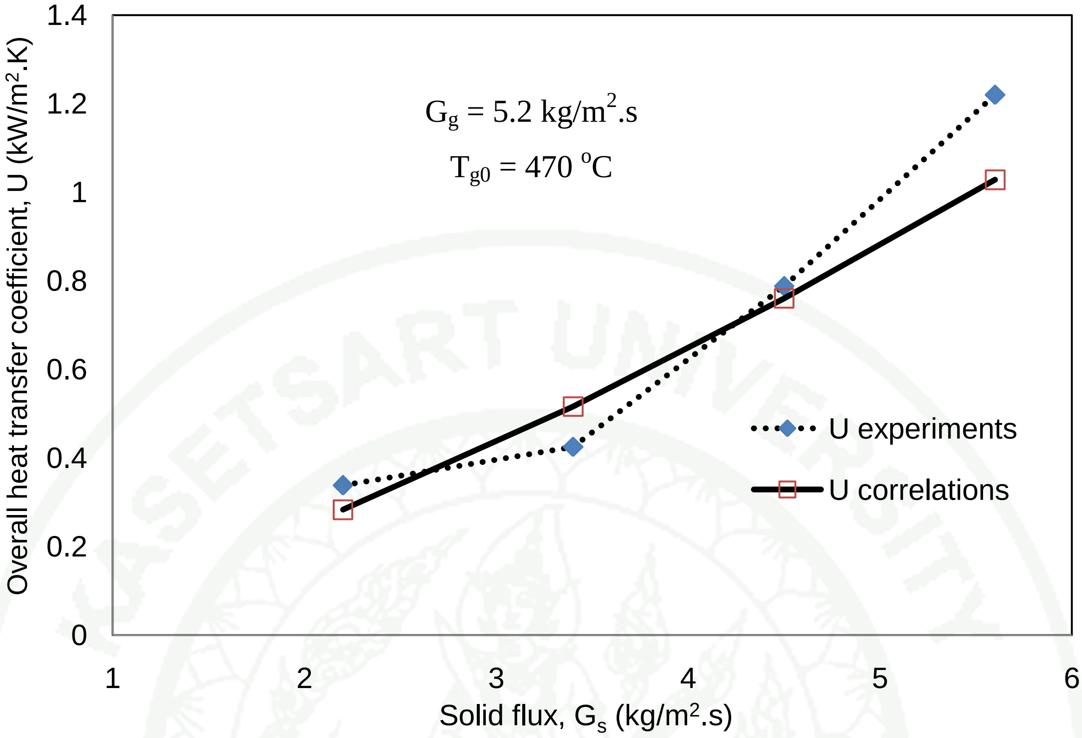

Figure 52 Comparison of the overall heat transfer coefficients from the experimental data and the correlation (equation (55)) as a function of solid flux under a constant gas flux in the downer reactor.

This correlation of U from equation (55) is applicable under following range of conditions: gas flux of 3.8 - 5.8 kg/m^2.s, solid mass flux of 2.2 - 5.6 kg/m^2.s, and inside temperature of the downer reactor of 300 - 560 °C.

4. Simulation of temperature profiles with heat loss through the wall without reaction

To verify the calculation of heat transfer within the downer reactor, the simulation of reactor temperature profiles at steady state with gas-solid heat transfer and heat loss through the wall without reaction. The hot gas fed into the top of the reactor is the air. The rate of heat loss is calculated using the correlation of overall heat transfer coefficient, equation (55). The simulation results are shown as the gas temperature profiles along the length of reactor comparing to the experimental results. The ambient temperature is set as 35 ^{o}C in these simulations. The gas inlet temperature, gas fluxes, and solid fluxes are at the heat transfer experimental conditions. The outside gas temperature of the gas rising along the outside wall of the reactor is assumed to decrease linearly with reactor length from reactor top to bottom. The temperature at the top is set at the experimental temperature. The outside gas temperature at the bottom is set to 35 ^{o}C.

4.1 Gas temperature profiles from simulations and experiments at various inlet gas temperature in the downer reactor

The result of gas temperature profiles from experiment and simulation with heat loss through the wall at various inlet gas temperatures are shown in Figure 53. The simulated solid temperature profiles are also shown.

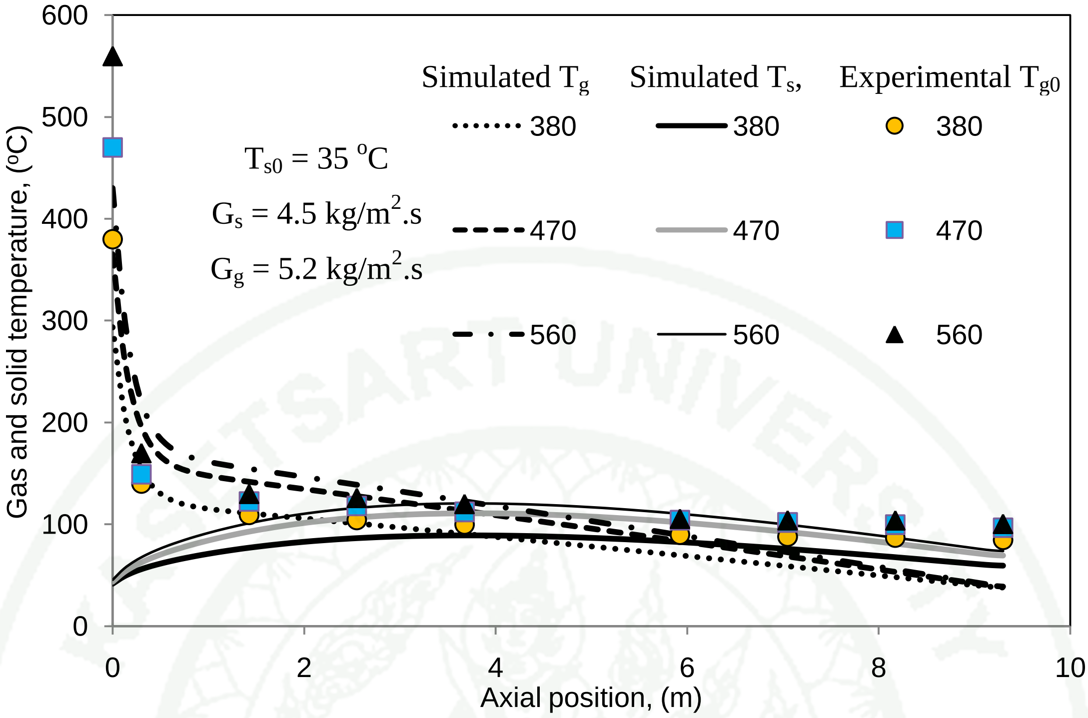

Figure 53 Comparison gas temperature distributions from experiments and simulation with heat loss through the wall without reaction at various inlet gas temperature and G_g = 5.2kg/m^2.s, G_s = 4.5kg/m^2.s, and T_{s0}=35 °C in the downer reactor. The simulated solid temperatures are also presented.

From Figure 53, the gas temperature decreases very fast at the entrance and then continually decreases along the length of the reactor to the ambient temperature. At the entrance, the heat of the gas is transferred to the solid phase and also losses through the wall. The temperatures of the solid are increase. After that, the heat is transferred from the solid to the gas and then through the wall. Finally, the gas temperature approaches the ambient temperature of 35 °C. The outside gas adjacent to the wall is in natural convection from the bottom to the top of the reactor. The experimental data gave the outside gas temperatures of 85 – 100 °C which are higher than the simulation results. Higher gas temperature profiles are obtained with higher inlet gas temperature because higher energy is supplied into the reactor.

Difference results of the gas temperature profiles between the experiment and simulations was obtained because the correlation of overall heat transfer coefficient is in the range of 300 – 560 °C while a large portion of gas inside the reactor is well under 300 °C. The results show that the heat loss is higher than the experimental data at low gas temperature in the 100 – 130 °C region. However, at the high temperature range of 300 – 560 °C the value of overall heat transfer coefficient is a little lower than what it should be which resulted in a little higher inside gas temperature near the inlet region.

4.2 Gas temperature profiles from simulations and experiments at various gas flux in the downer reactor

The gas temperature profiles with heat loss through the wall from experiments and simulations at various gas fluxes are shown in Figure 54.

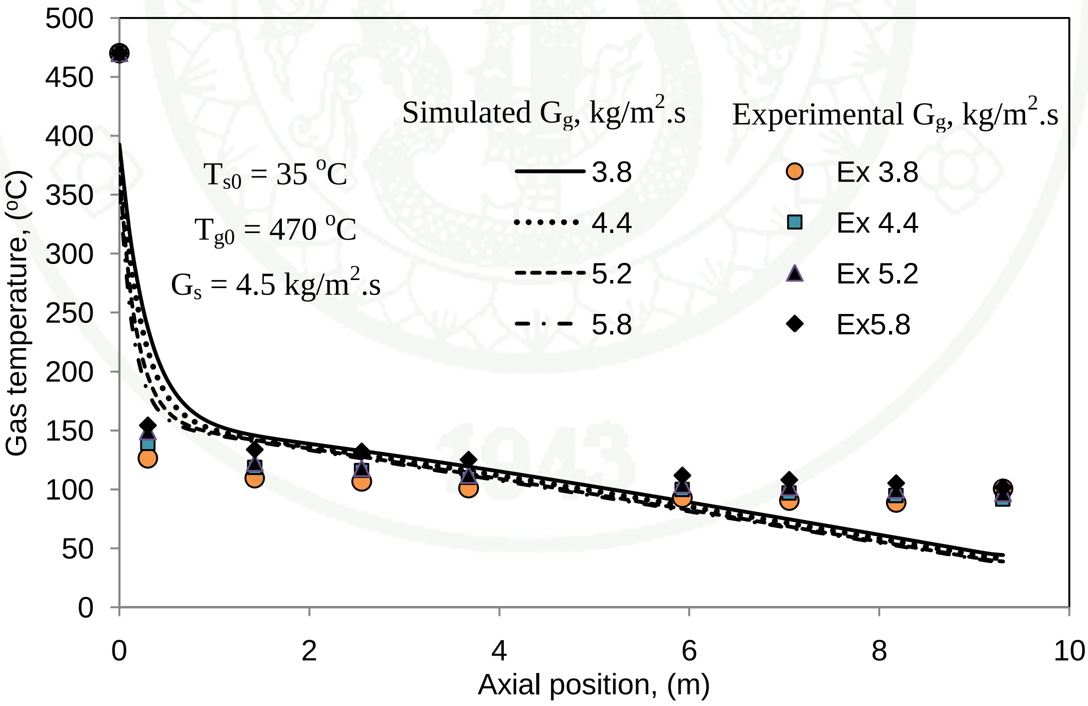

Figure 54 Comparison of gas temperature profiles from experiments and simulation with heat loss through the wall at various gas flux under T_{g0} = 470 °C, G_s = 4.5 kg/m^2.s, and T_{s0} = 35 °C in the downer reactor.

In Figure 54, inlet gas temperature drops very fast at the entrance. In the middle and bottom sections, gas temperature gradually decreases and approaches the ambient gas temperature. The experiment gas temperature profiles increases with gas flux because higher gas flux give higher heat input rate. However, the simulation gives the reverse result which shows too strong dependency of heat loss through the wall to gas flux. The discrepancy results in small temperature difference.

The simulated gas temperature is higher than the experimental result at the inlet region but lower than the experimental result at low temperature range. That is, the value of overall heat transfer coefficient is a little too low at 300 – 560 ^{o}C, and the correlation of overall heat transfer coefficient is a little too high at below 120 ^{o}C range. These results confirm heat transfer coefficient in the range of 300 – 560 ^{o}C as in Figure 53.

4.3 Comparison of gas temperature profiles from simulations and experiments at various inlet solid flux in the downer reactor

The gas temperature profiles with heat loss through the wall of experiments and simulations at various solid fluxes are shown in Figure 55.

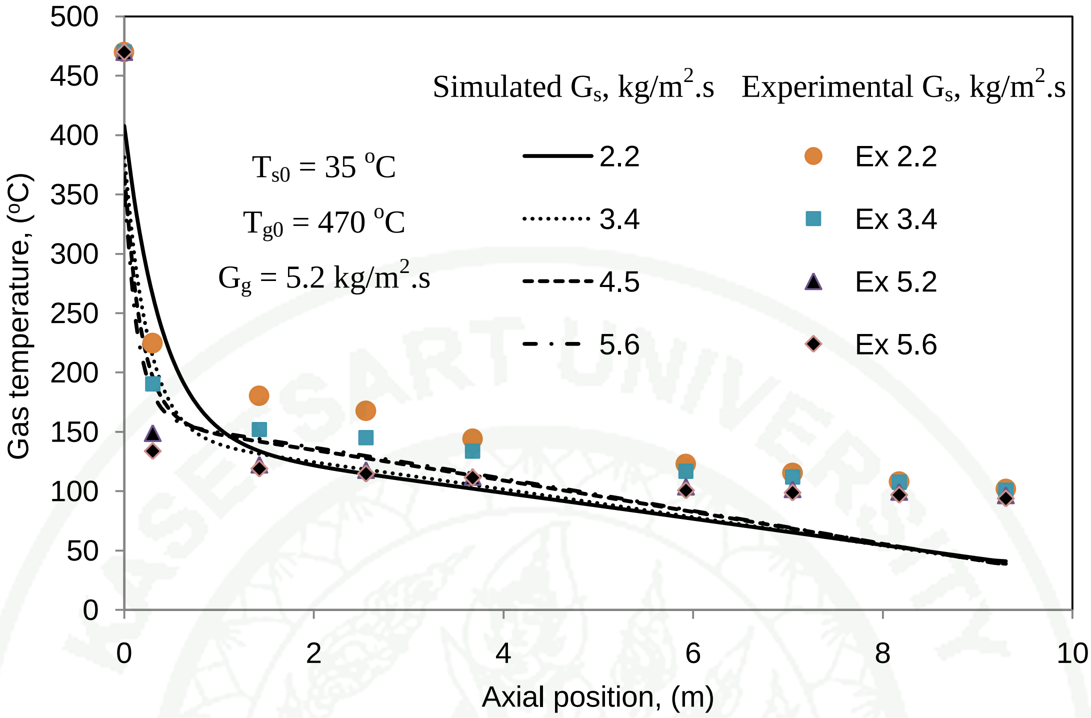

Figure 55 Comparison gas temperature profiles from experiments and simulation with heat loss through the wall without reaction at various solid flux under T_{g0} = 470 °C, G_g = 5.2 kg/m^2.s and T_{s0} = 35 °C in the downer reactor.

In Figure 55, the gas temperature profiles decreases very fast at the entrance. Then gas temperature slowly decreases in the middle section. The simulated gas temperature approaches the outside wall temperature due to the high overall heat transfer coefficients at low temperature. It also shows that at the entrance region the gas temperature profiles decrease while solid flux increases, resulting from increasing overall heat transfer coefficient with solid flux.

Here again, the simulation temperature is higher than experimental value due to too low heat transfer coefficient at the entrance region but simulated temperature is lower than the experiment resulting from too high heat transfer coefficient at low temperature. Above 200 °C, the simulated results fit quite well with the experimental results. However, under 200 °C, the deviations are shown due to too high heat transfer coefficient. The maximum temperature difference is 62 °C at the reactor outlet.

5. Simulation of catalytic cracking of heavy oil with heat loss through the wall

The simulation of catalytic cracking of heavy oil in the downer reactor is done using dispersion model with the effect of heat loss through the wall. The correlation of overall heat transfer coefficients is added to calculate the rate of heat loss in the energy balance equation. The simulated temperature distribution of heavy oil catalytic cracking with heat loss through the wall is shown in Figure 56.

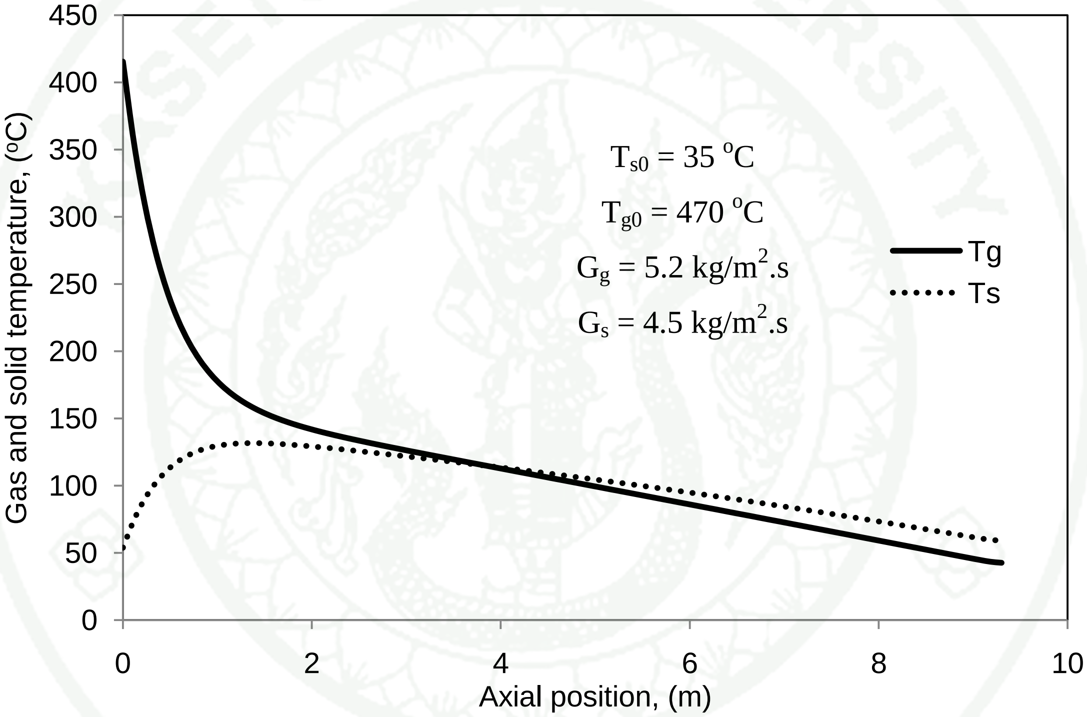

Figure 56 Simulated temperature distributions of catalytic cracking of heavy oil with heat loss through the wall at ambient solid temperature in the downer reactor with T_{g0} = 470 °C, G_g = 5.2 kg/m^2.s, and G_s = 4.5 kg/m^2.s.

In Figure 56, the simulation conditions is T_{g0} = 470 °C, G_g = 5.2 kg/m^2.s, T_{s0} = 35 °C, and G_s = 4.6 kg/m^2.s. The heat carried into the reactor by the gas feed in this model is transferred from gas phase to the solid phase and loss through the wall. At the same time, the heat disappears at the solid due to the endothermic reaction at the catalyst surface.

At the entrance section, the solid temperature increases along the reactor length because solid receives the heat from the hot gas. At the middle of reactor, after the solid and gas temperature are equal at approximately 100 ^oC, the gas temperature still continues to decrease down due to the heat loss effect while the solid temperature is higher than gas temperature because heat loss through the wall has higher effect than the heat transferring between phases. For this low inlet solid temperature, the reactions occur minimally because the solid (catalyst) temperature is not high enough. The result of cracking reaction using 4-lump kinetic can be checked from the decomposition of heavy oil component (A) in Figure 57.

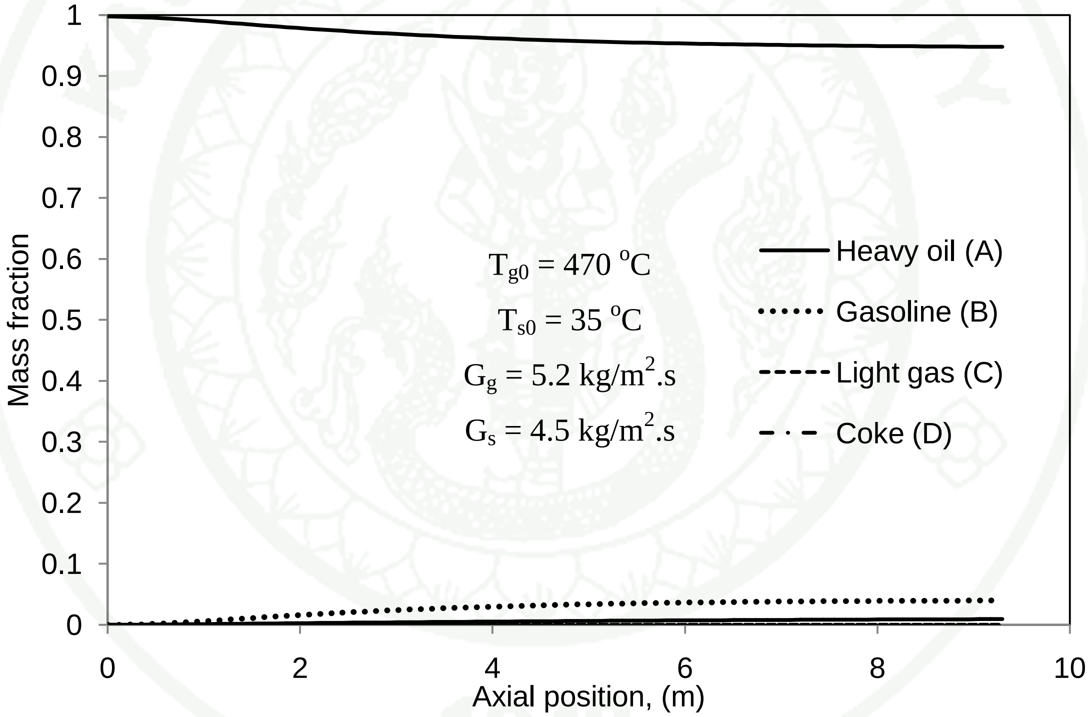

Figure 57 The mass fraction distributions of heavy oil (A), gasoline (B), light gas (C), and coke (D) of catalytic cracking with heat loss through the wall at ambient solid temperature feed under T_{g0} = 470 ^oC, G_g = 5.2 kg/m^2.s, and G_s = 4.5 kg/m^2.s in the downer reactor.

In Figure 57, the heavy oil (A) does not change significantly along the axial positions of the downer reactor because the temperature on the surface of catalyst is not high enough for cracking reaction. So the mass distributions of the products are minimal in this simulating condition.

6. Simulation of catalytic cracking of heavy oil with the heat loss through the wall at high solid temperature

This section presents the temperature and mass distribution in catalytic cracking of heavy oil with heat loss through the wall at high inlet solid temperature (300 - 560°C). The case studies are at 470 °C which is more common in the cracking reaction. Heat loss through the wall is considered in the energy balance equation of gas phase in the dispersion model. The results are shown in Figure 58 and 59.

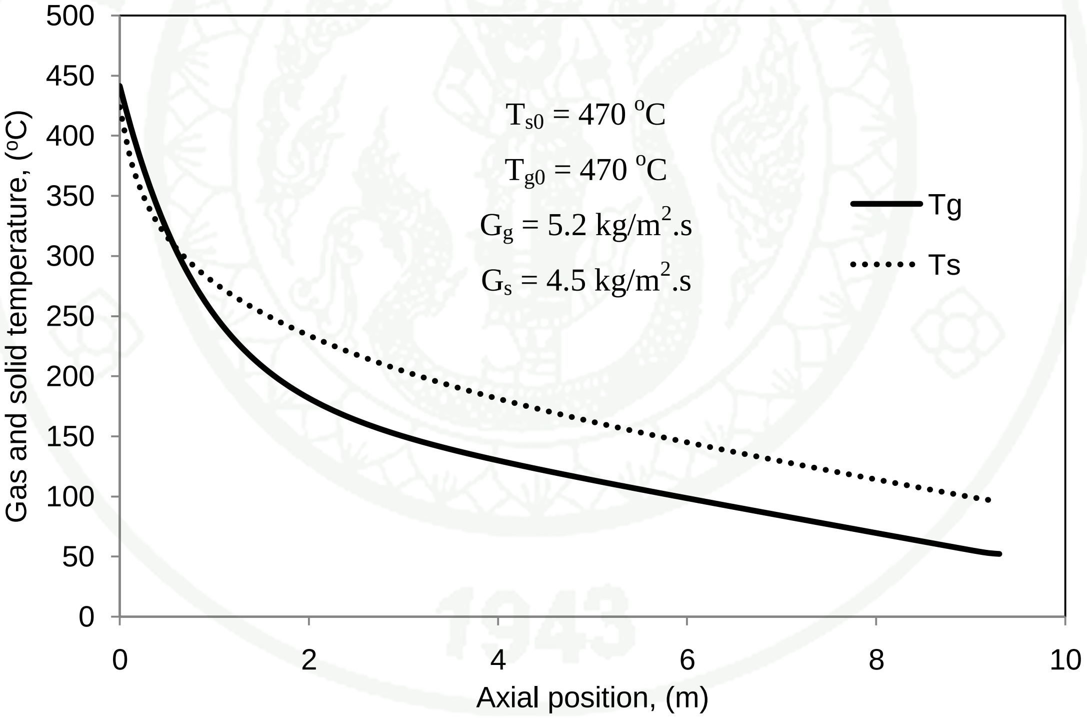

Figure 58 The temperature distributions of catalytic cracking of heavy oil with heat loss through the wall at high inlet solid temperature feed under T_{g0} = 470 °C, G_g = 5.2 kg/m^2.s, and G_s = 4.5 kg/m^2.s in the downer reactor.

In Figure 58, the gas and solid temperature profiles decrease very fast at the entrance. The solid temperature decreases faster than gas temperature because of the endothermic heat of reaction. At the same time, the heat from gas is transferred to solid phase and losses though the wall. After entrance region, the solid temperature gradually decreases due to the low heat of cracking reaction as the reaction rate is lower at lower temperature. The gas temperature continually decreases because of the heat loss through the wall.

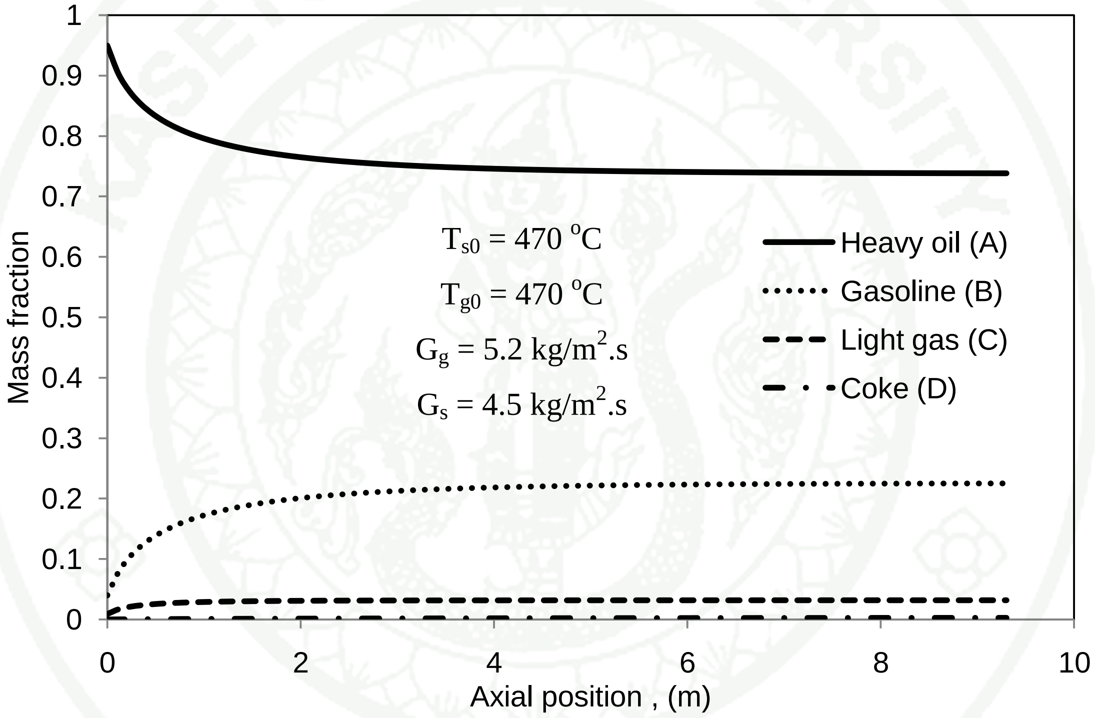

Figure 59 The mass fraction distributions of heavy oil (A), gasoline (B), light gas (C), and coke (D) of catalytic cracking with heat loss through the wall at high inlet solid temperature feed under T_{g0} = 470 ^oC, G_g = 5.2 kg/m^2.s, and G_s = 4.5 kg/m^2.s in the downer reactor.

In Figure 59, the mass distribution of heavy oil decreases very fast at the entrance and gradually decreases until the exit of reactor because the reaction rate is depleted with the catalyst surface temperature. After the entrance section, solid temperature decreases down to lower than 300 ^oC where the reaction rate is reduced according to the Arrhenius equation. At the same time, the yield of the products (gasoline, light gas, and coke) increase with the axial length of the reactor. The most desired product is gasoline. From this simulation, the mass fraction of gasoline is approximately 0.22 of total products and reactant. Most of reaction occurs at the entrance of the reactor. The total conversion of heavy oil (A) is 26%.

6.1 The effect of inlet gas temperature on the temperature and conversion distribution in downer reactor

The effect of the inlet gas temperature on the gas and solid temperature distribution and mass fraction in catalytic cracking of heavy oil with heat loss through the wall at the constant gas flux, solid flux, and inlet solid temperature are shown in Figure 60 to 64.

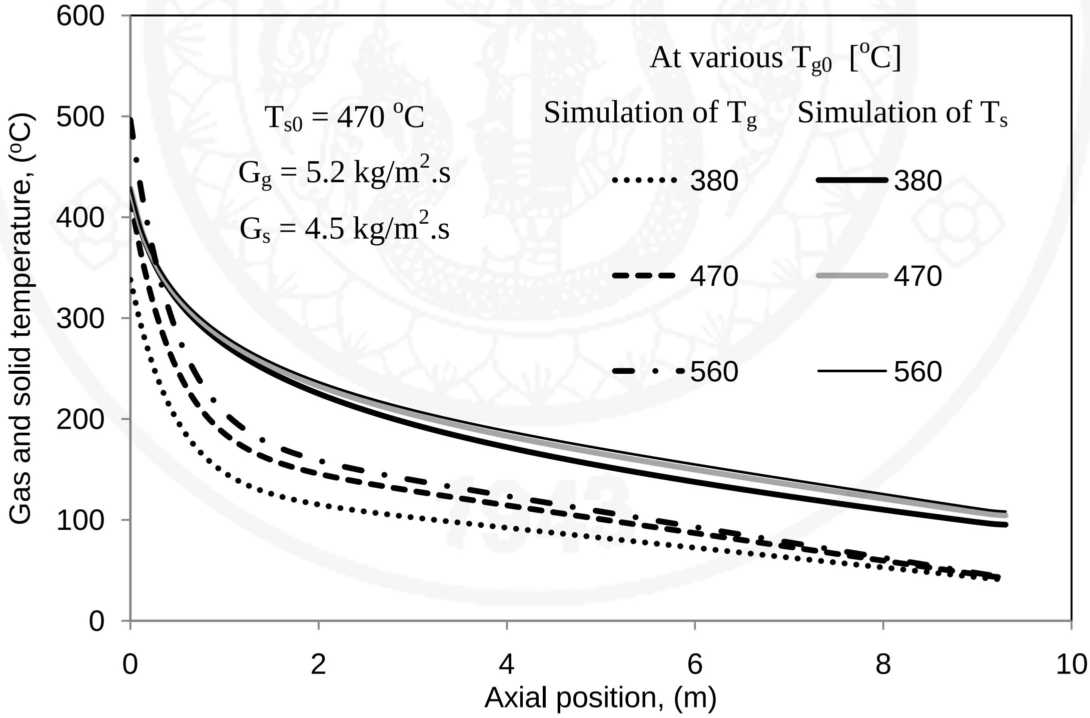

Figure 60 The effect of inlet gas temperature on gas and solid temperature distributions with heat loss through the wall of catalytic cracking in the downer reactor.

The effect of varying inlet gas temperature under the constant gas flux, solid flux, and inlet solid temperature are shown. The trends of gas and solid temperatures are the same as in Figure 58 and 59. The conversion increases with the inlet gas temperature. The increasing of inlet gas temperature enhanced the yield of gasoline product.

At the entrance, the solid temperature decreases very rapidly than the gas temperature because of the endothermic reaction (Figure 61). After entrance region, the solid temperature gradually decreases due to low heat of reaction. The conversion of heavy oil (A) decreases fast at the entrance and slowly decreases after 2 m of the reactor length because of the higher solid temperature at the entrance but much lower later on. So, the conversion of heavy oil is about 0.82 – 0.84 (Figure 62). At the same time, the product yields are also low according to the low solid temperature.

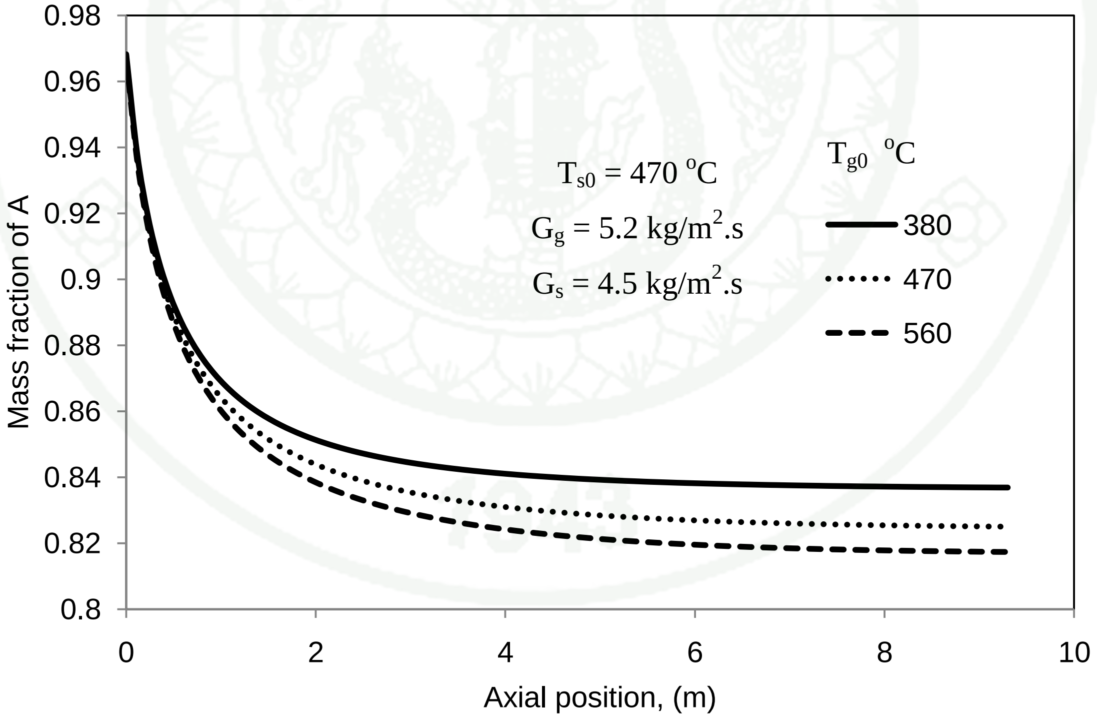

Figure 61 The effect of inlet gas temperature on mass fraction of heavy oil (A) with heat loss through the wall of catalytic cracking in the downer reactor.

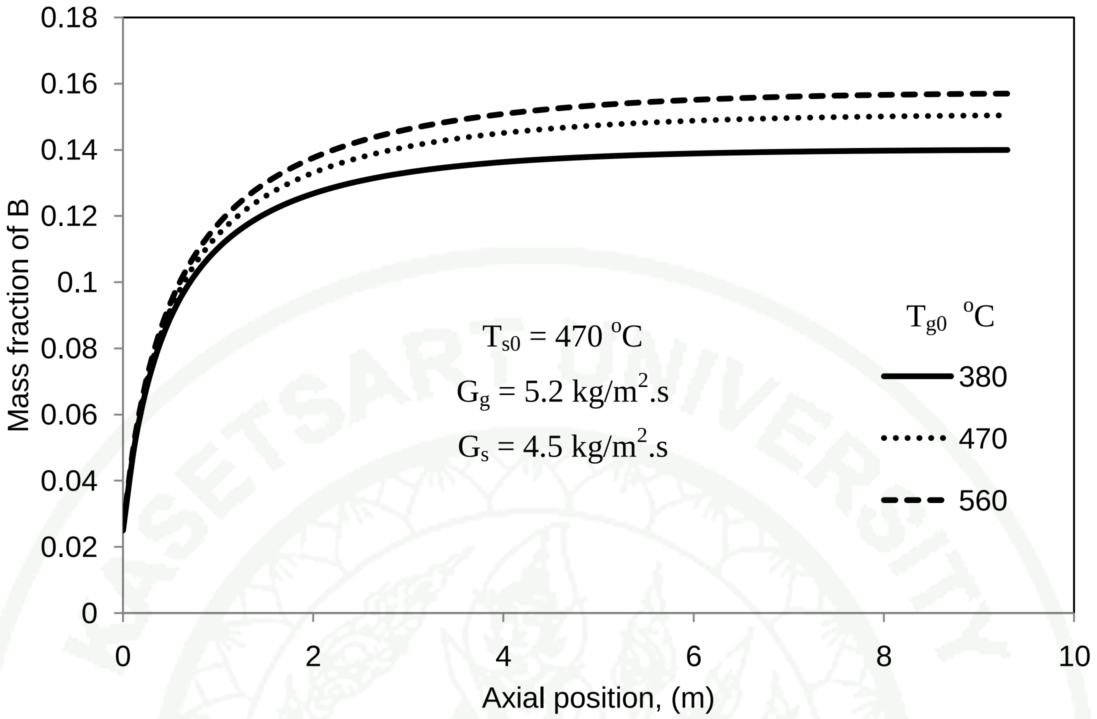

Figure 62 The effect of inlet gas temperature on mass fraction of gasoline (B) with heat loss through the wall of catalytic cracking in the downer reactor.

The gasoline (B) yield increases fast at the entrance of the reactor and slowly increases after 1 m (Figure 62). The high inlet gas temperature gives higher gasoline yield because high inlet gas temperature gives more heat to the solid catalyst so the reactions proceed better.

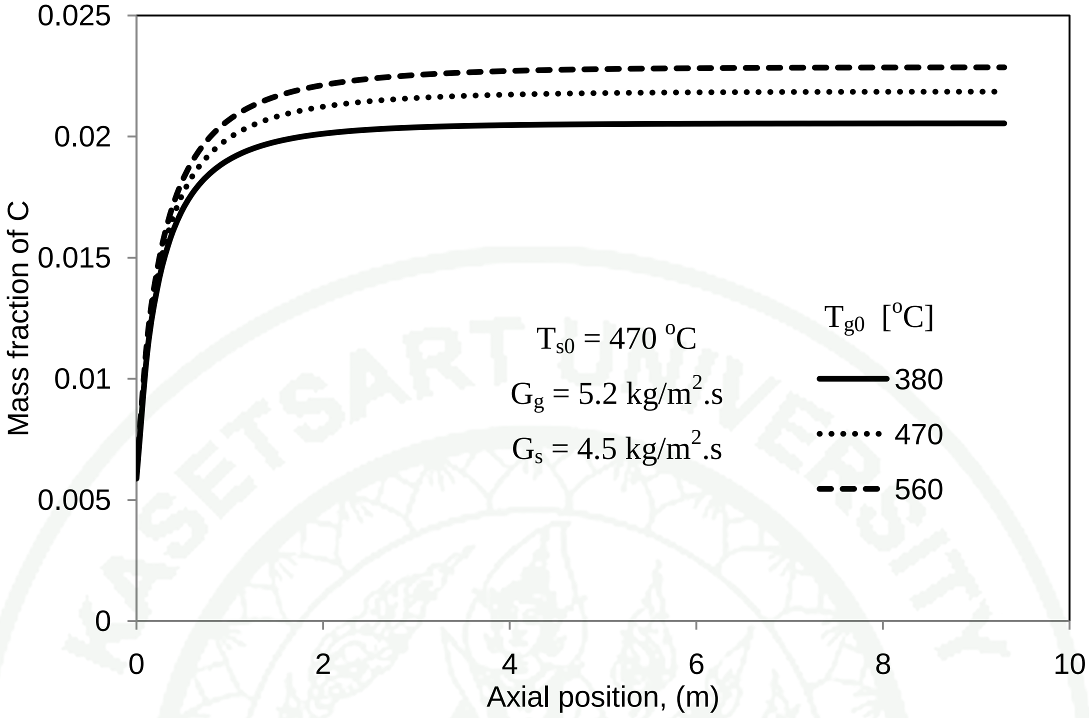

Figure 63 The effect of inlet gas temperature on mass fraction of light gas (C) with heat loss through the wall of catalytic cracking in the downer reactor.

The trend of light gas yield is similar to the trend of gasoline from the same reason as in Figure 63. The increase in light gas selectivity due to higher activation energy than gasoline is small as the temperature increases. The reaction rate of light gas production is very small comparing to the gasoline. Thus effect of increasing temperature on light gas selectivity is not much.

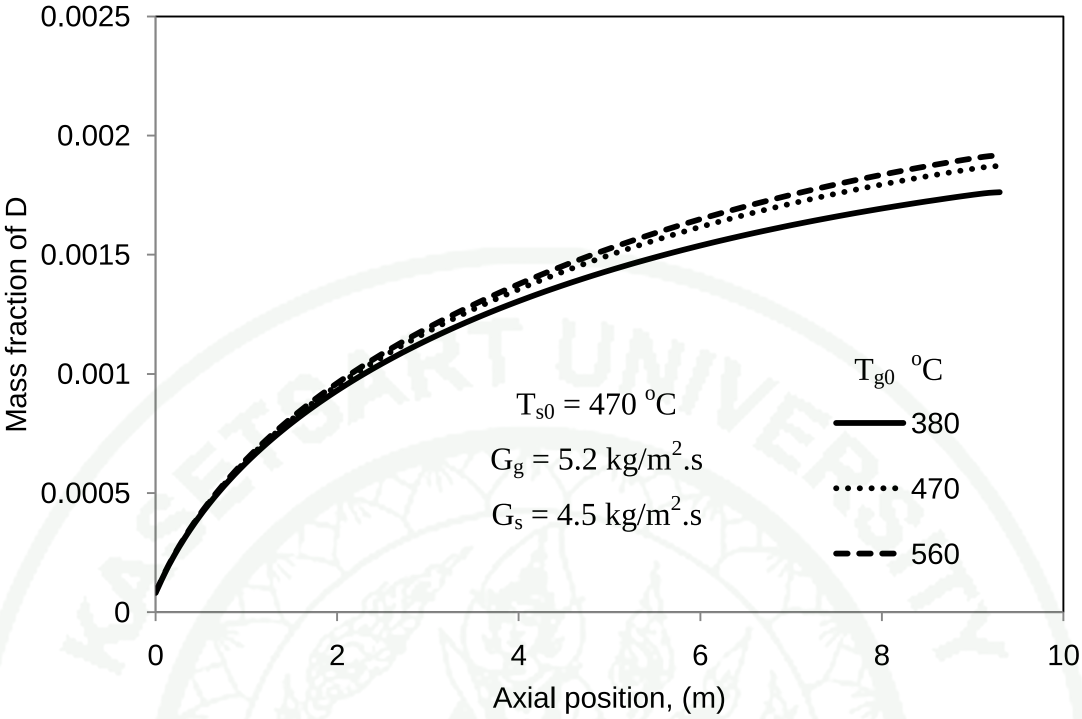

Figure 64 The effect of inlet gas temperature on mass fraction of coke (D) with heat loss through the wall of catalytic cracking in the downer reactor.

The yield of coke is low when compared with the gasoline and light gas (Figure 64). The trend of coke shows an increase along the length of the reactor. High inlet gas temperature leads to high amount of coke product as the reaction rate goes faster because of the heat transferring from gas to solid.

6.2 The effect of inlet solid temperature on the temperature and conversion distribution in downer reactor

The effect of the inlet solid temperature on the gas and solid temperature distribution and mass fraction in catalytic cracking of heavy oil with heat loss through the wall at the constant gas flux, solid flux, and inlet gas temperature are shown in Figure 65 to 69.

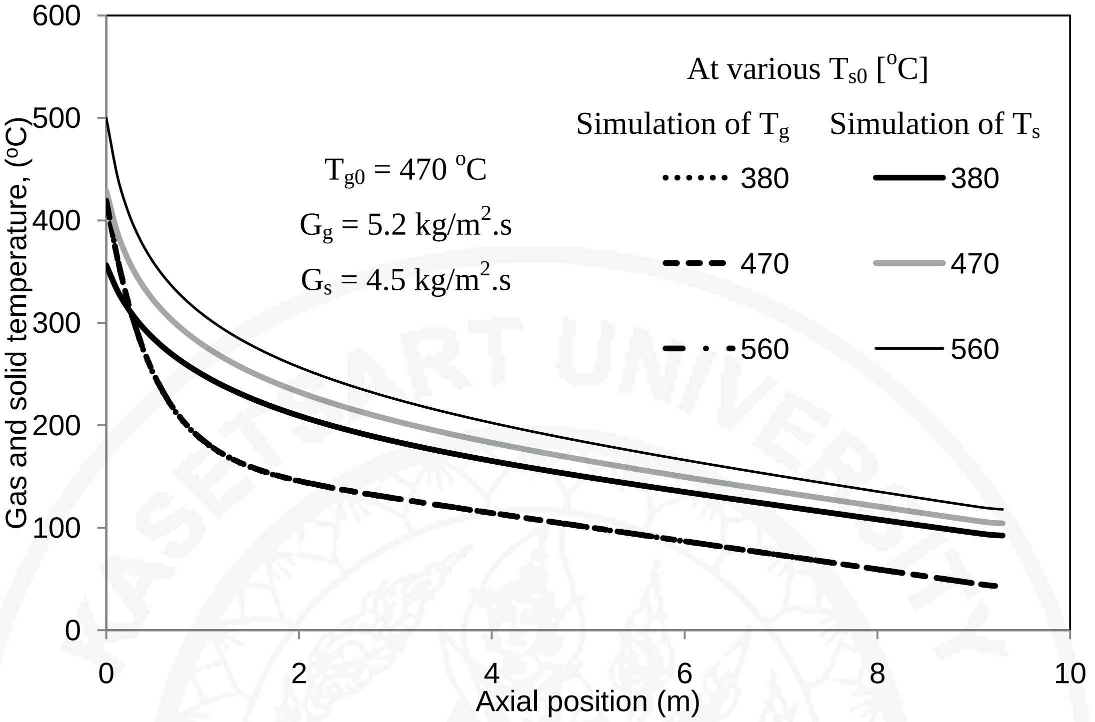

Figure 65 The effect of inlet solid temperature on gas and solid temperature distributions with heat loss through the wall of catalytic cracking in the downer reactor.

The gas temperature profiles are the same with the different inlet solid temperature (380 – 560 °C) because the heat loss through the wall has much higher effect than the heat transfer between phases. The solid temperature decreases with the endothermic reaction. Higher solid temperature gives higher kinetic rate, thus higher product yields.

The effect of inlet solid temperature is minimal. The result Tg’s coincide with each other in the simulation range of inlet solid temperature. Heat transfer to solid is small comparing to heat loss through the wall. Apparently, the heat loss through the wall dominates the heat transfer of the gas.

The endothermic reactions are occurring on solid phase. The temperature of solid are drops fast. Heat transfer to solid is slow. At low solid temperature, the reaction is less. The effect of heat loss through the wall is significantly higher.

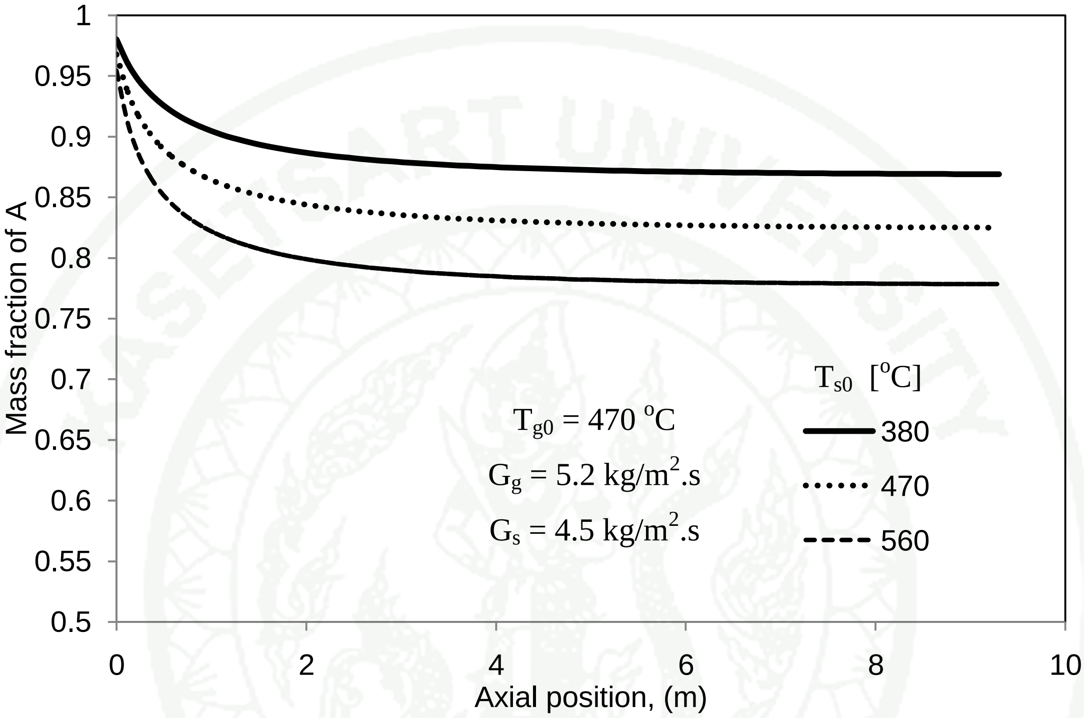

Figure 66 The effect of inlet solid temperature on mass fraction of heavy oil (A) with heat loss through the wall of catalytic cracking in the downer reactor.

The reaction occurs at entrance with high solid temperature. At lower solid temperature. At lower solid temperature within 1 m of reactor, the reaction is slow and the conversion is almost constant.

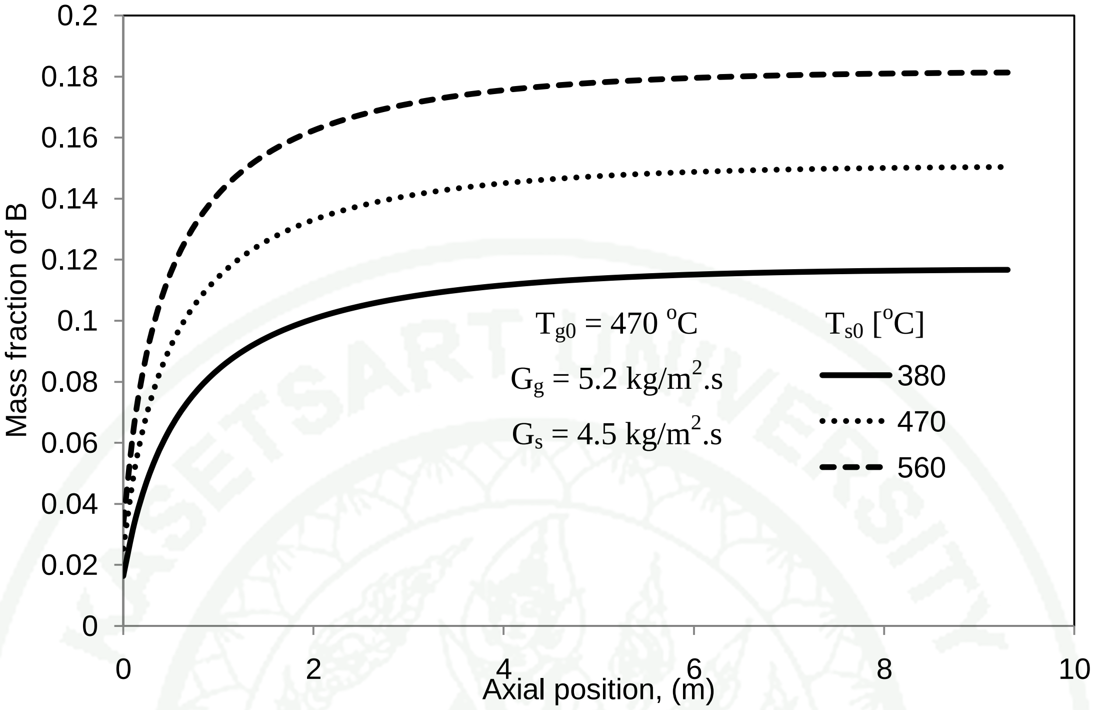

Figure 67 The effect of inlet solid temperature on mass fraction of gasoline (B) with heat loss through the wall of catalytic cracking in the downer reactor.

Gasoline is produce at the entrance with high solid temperature. At low solid temperature after 1 m. length, the conversion rate is low and gasoline production rate is low also.

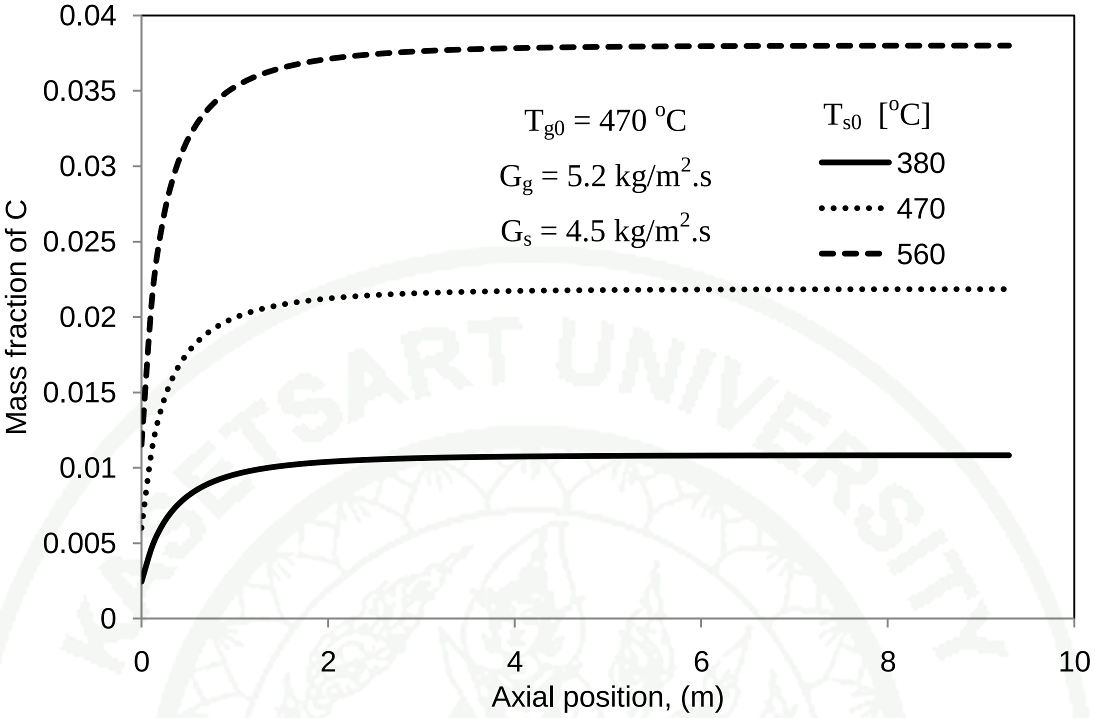

Figure 68 The effect of inlet solid temperature on mass fraction of light gas (C) with heat loss through the wall of catalytic cracking in the downer reactor.

A phenomenon of light gas yield is the same for gasoline. At low solid temperature, heavy oil cracking to light gas is very slow and very small amount of light gas is obtained due to the low reaction.

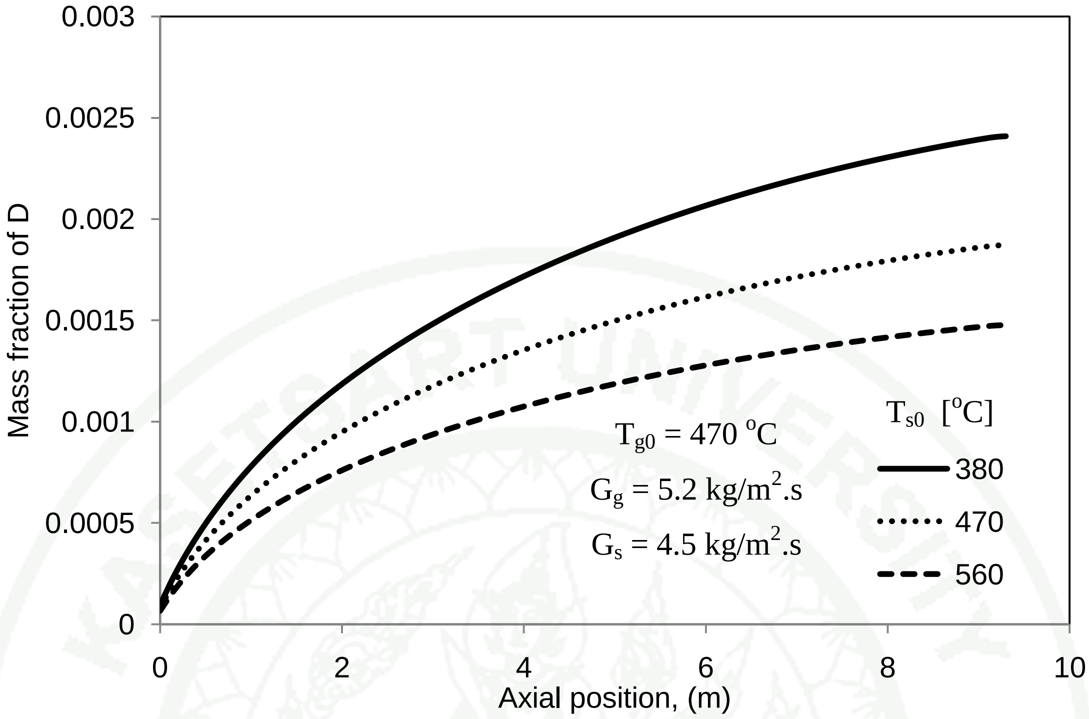

Figure 69 The effect of inlet solid temperature on mass fraction of coke (D) with heat loss through the wall of catalytic cracking in the downer reactor.

Result shows minimal amount of coke resulting for low solid temperature in the reactor. In these simulations, the solid flux is fixed at 4.5 kg/m2.s which is low. Therefore, the reaction rate per unit volume of reaction is low too.

6.3 The effect of gas flux on the temperature and conversion distribution in downer reactor

The effect of the gas flux on the gas and solid temperature distribution and mass fraction in catalytic cracking of heavy oil with heat loss through the wall at the constant gas flux, solid flux, and inlet solid temperature are shown in Figure 70 to 74.

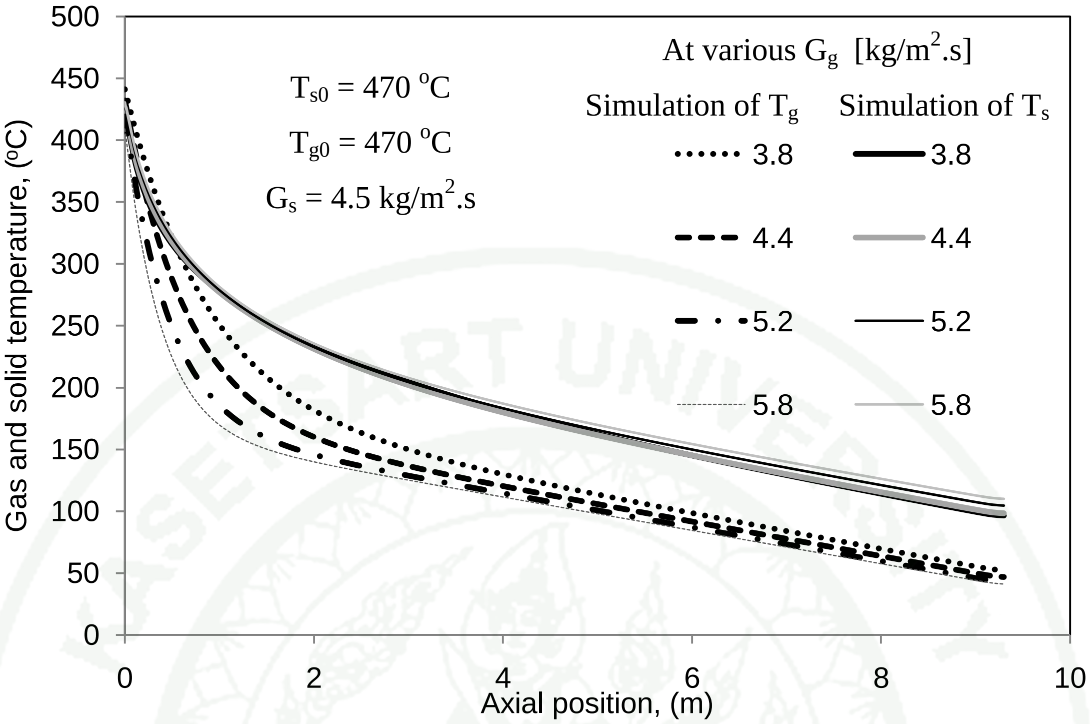

Figure 70 The effect of gas flux on gas and solid temperature distributions with heat loss through the wall of catalytic cracking in the downer reactor.

The effect of gas flux can be seen. The higher gas flux gives lower temperature because of higher convective heat loss through the wall. The conversion profile is lower at higher gas flux because the resident time is lower.

The temperature of gas and solid drop fast at the entrance region of the reactor as the heat of reaction on the solid dominates from high reaction temperature. After the entrance region where the temperature drop below 250 °C, the reaction is slow and the temperature drop slowly until the reactor exit. High gas flow rate gives lower gas temperature because heat transfer rate is higher according to higher gas velocity.

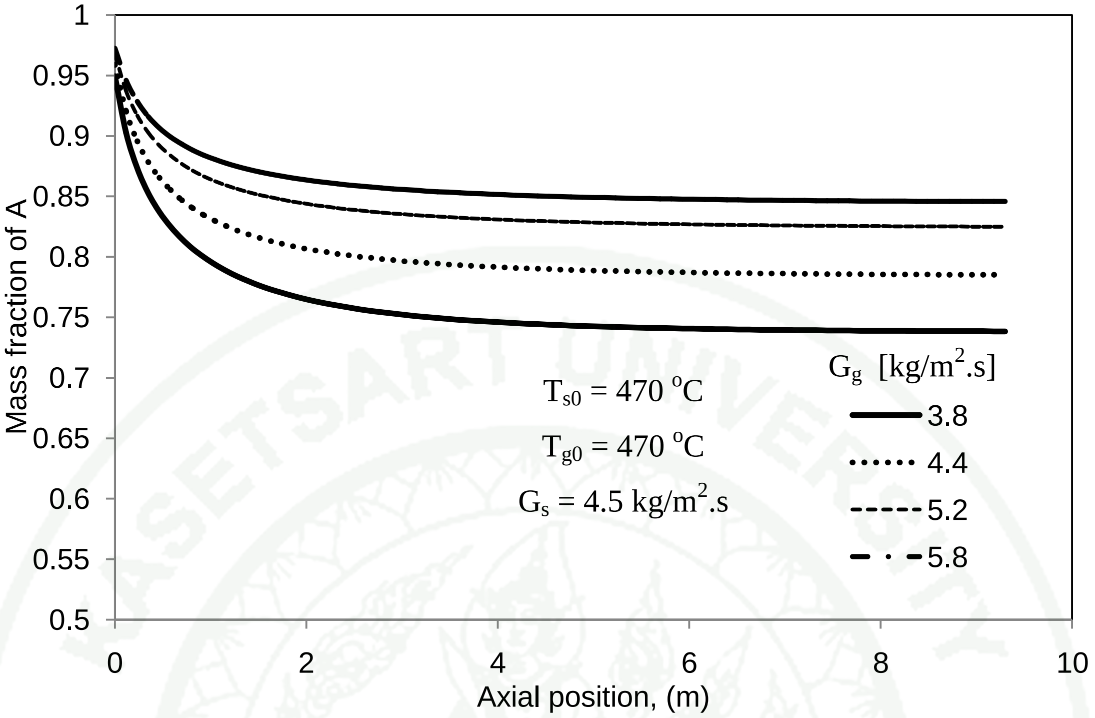

Figure 71 The effect of gas flux on mass fraction of heavy oil (A) with heat loss through the wall of catalytic cracking in the downer reactor.

The reaction occurs at the entrance region due to the high solid temperature. After 1m of reactor length, the solid temperature is low which minimize the reaction rate. High gas mass flux gives less conversion as the retention time is reduced.

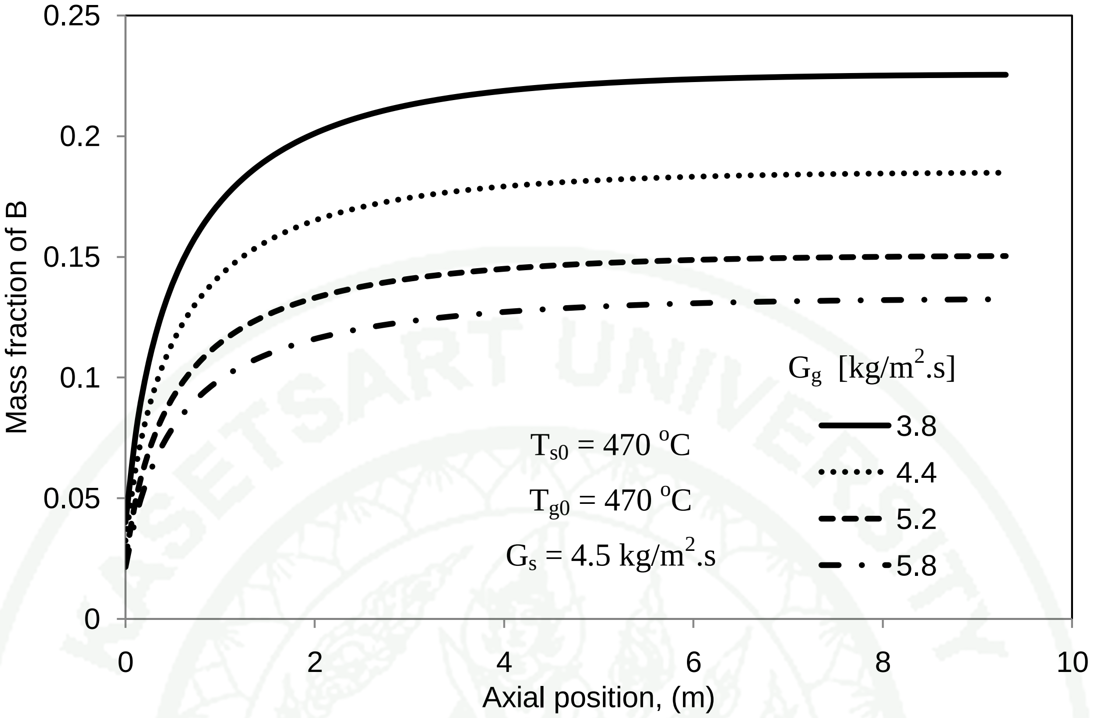

Figure 72 The effect of gas flux on mass fraction of gasoline (B) with heat loss through the wall of catalytic cracking in the downer reactor.

The result is the same as with the conversion of heavy oil. Gasoline is produced mainly at the entrance region. Higher gas mass flux reduces the gasoline fraction from 23% to 13% due to less conversion of heavy oil.

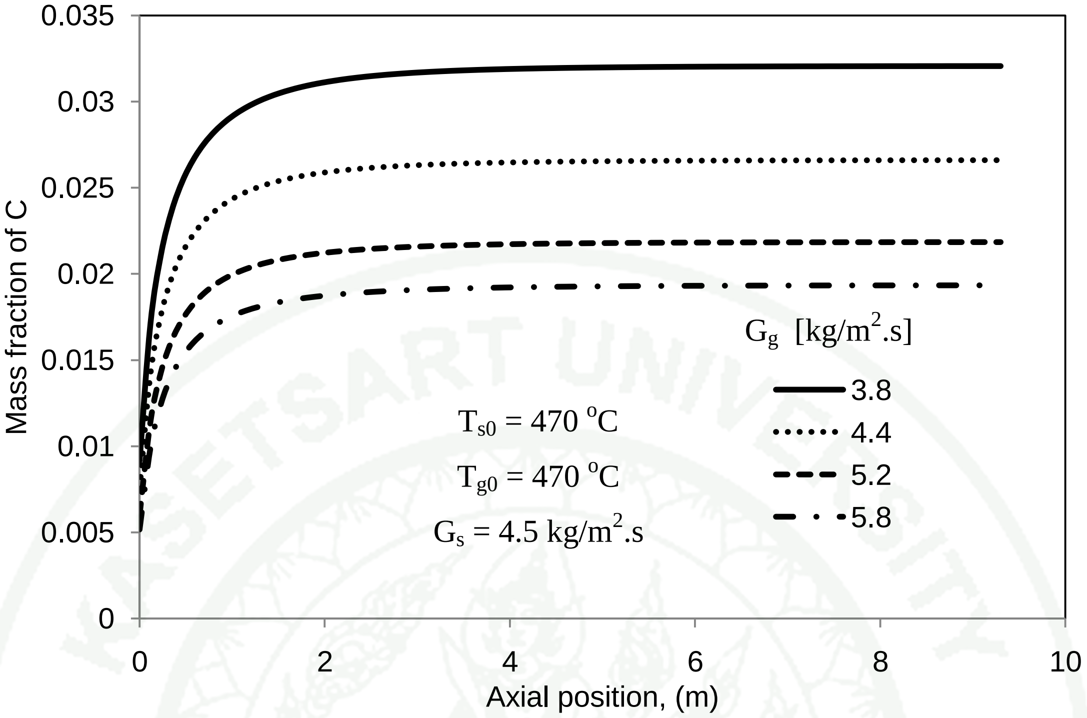

Figure 73 The effect of gas flux on mass fraction of light gas (C) with heat loss through the wall of catalytic cracking in the downer reactor.

The result of light gas is the same trend as in gasoline mass fraction but at much lower value because the reaction rate of light gas is lower than gasoline.

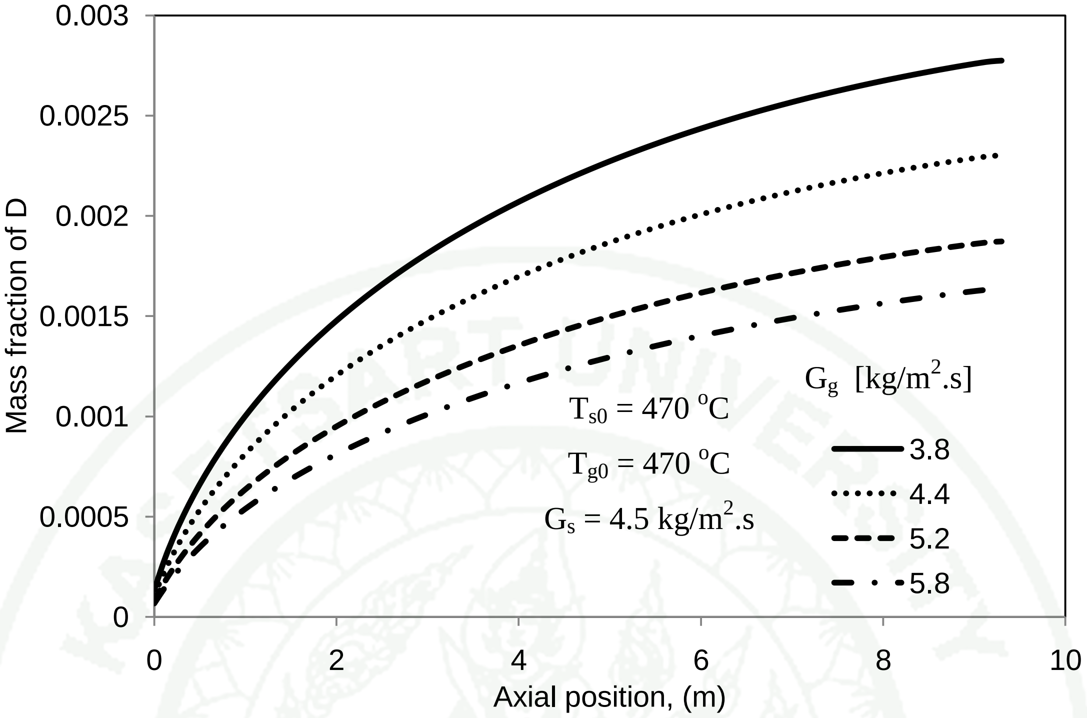

Figure 74 The effect of gas flux on mass fraction of coke (D) with heat loss through the wall of catalytic cracking in the downer reactor.

The concentration of coke from catalytic cracking of heavy is very low due to the kinetic reaction rate of coke very low. For the low gas flux gives high mass fraction of coke because lower gas flux is high residence time in the reactor.

6.4 The effect of solid flux on the temperature and conversion distribution in downer reactor

The effect of the solid flux on the gas and solid temperature distribution and mass fraction in catalytic cracking of heavy oil with heat loss through the wall at the constant gas flux, solid flux, and inlet solid temperature are shown in Figure 75 to 79.

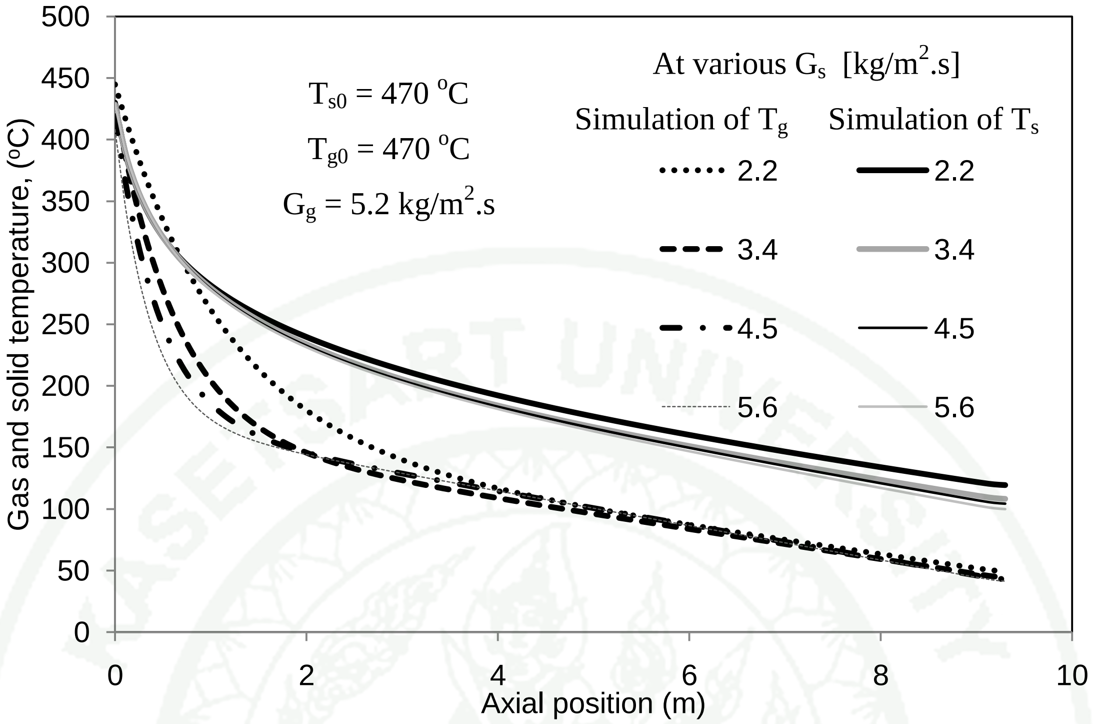

Figure 75 The effect of solid flux on gas and solid temperature distributions with heat loss through the wall of catalytic cracking in the downer reactor.

The temperature profiles decrease with increasing solid flux because of higher solid flux lead to higher the overall heat transfer coefficient. The rate of disappearance of heavy oil increases with solid flux because the rate of reaction depended on the solid catalyst quantity. The higher solid flux gave higher mass distributions.

The results show fast gas temperature drops at the entrance region due to high solid temperature. The solid temperature drops from endothermic cracking reaction on its surface and heat transferred from the gas is slow. After the entrance region, the solid temperature is low and the reaction is less. Therefore, the temperature drop slowly and more from the heat loss through the wall.

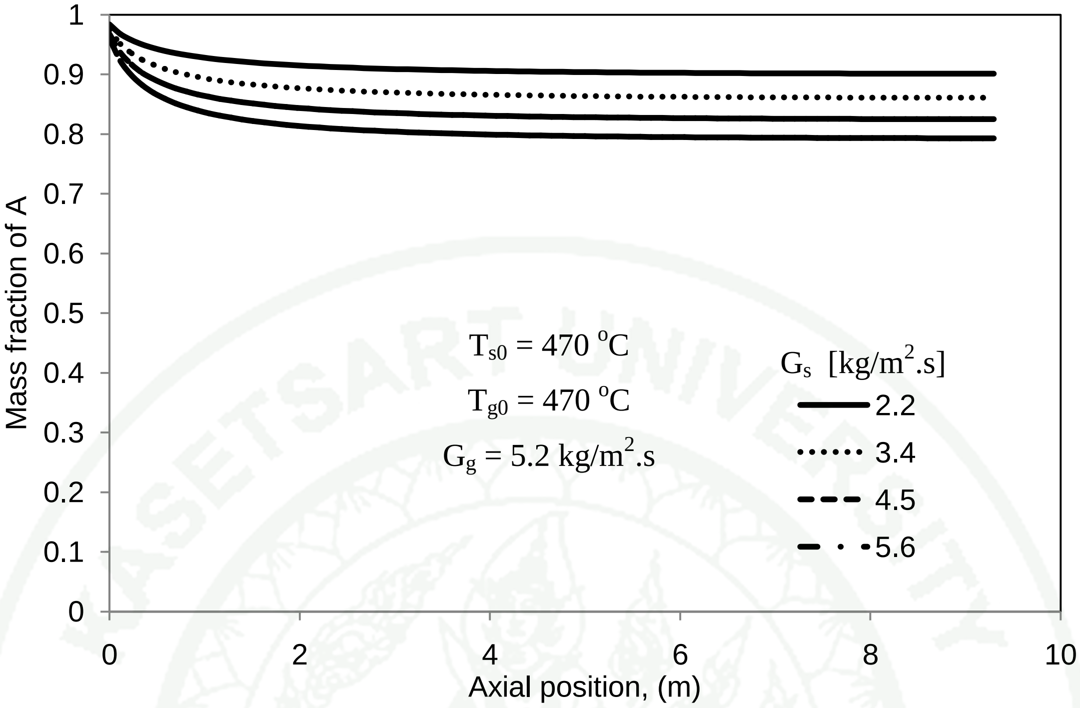

Figure 76 The effect of solid flux on mass fraction of heavy oil (A) with heat loss through the wall of catalytic cracking in the downer reactor.

The conversion rate of heavy oil is slow at low solid flow rate due to smaller amount of catalyst in the reaction.

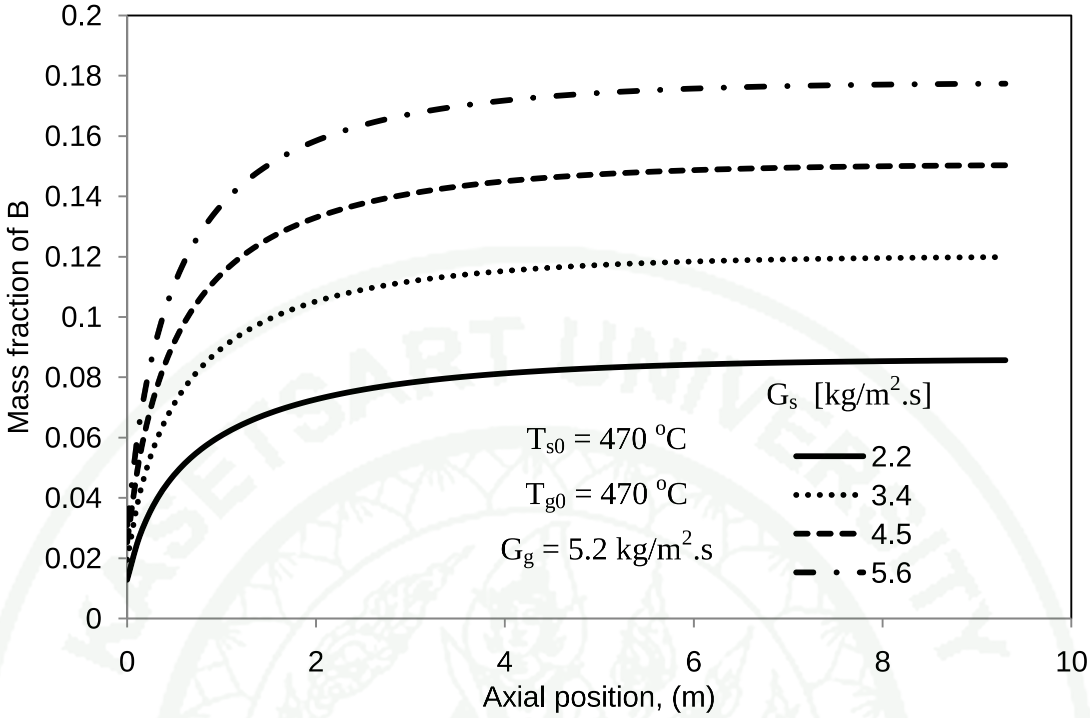

Figure 77 The effect of solid flux on mass fraction of gasoline (B) with heat loss through the wall of catalytic cracking in the downer reactor.

Here again, production rate of gasoline is high at the entrance region and decrease to almost negligible as the solid temperature drops.

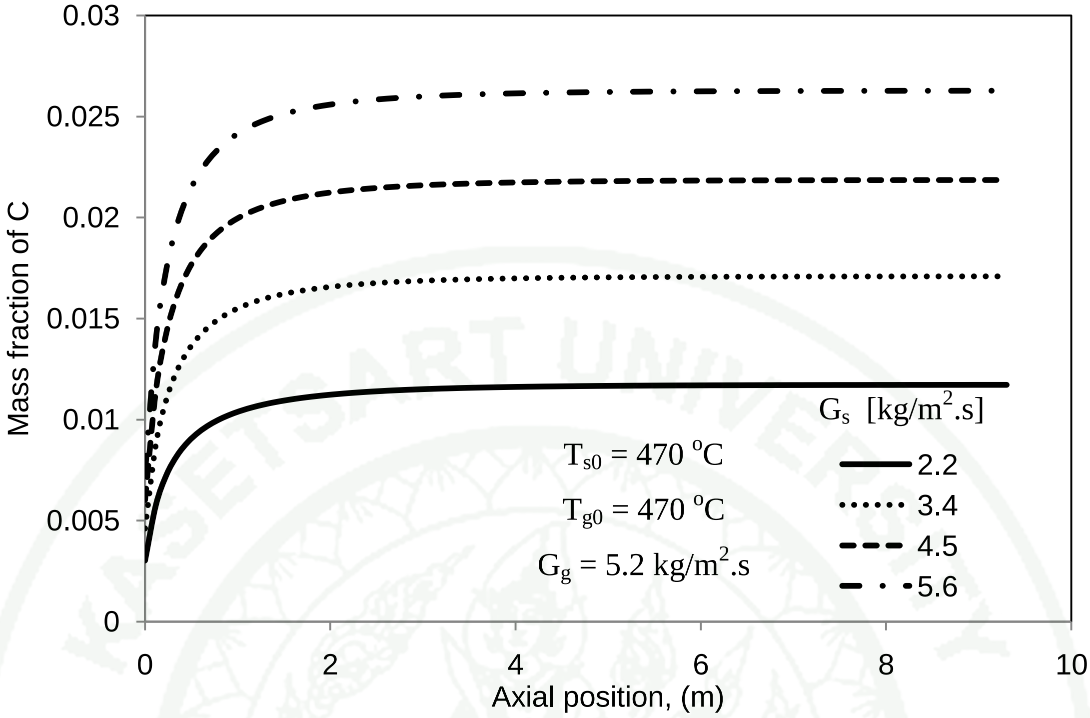

Figure 78 The effect of solid flux on mass fraction of light gas (C) with heat loss through the wall of catalytic cracking in the downer reactor.

Through the light gas production rate is high at the entrance region, the mass fraction of gas is very low due to the minimal overall reaction rate from low solid catalyst mass flux.

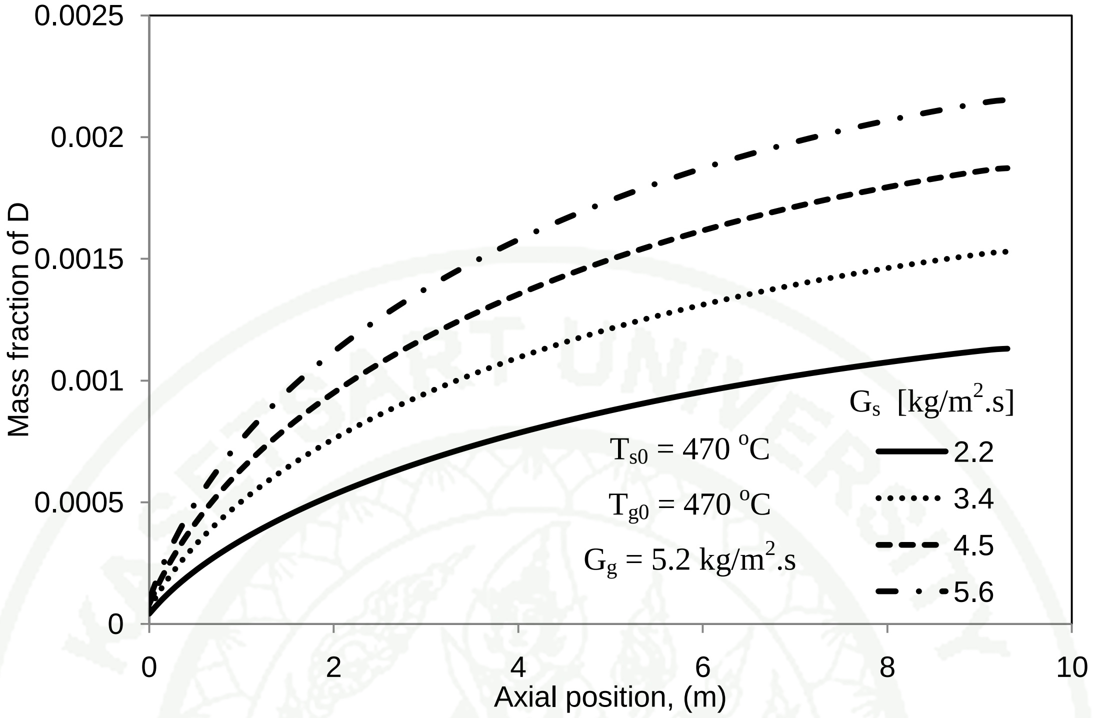

Figure 79 The effect of solid flux on mass fraction of coke (D) with heat loss through the wall of catalytic cracking in the downer reactor.

Almost negligible coke is formed from the cracking reaction due to small amount of solid catalyst mass flux.

7. Simulation of catalytic cracking of heavy oil with heat loss through the wall at high operating condition.

The most common operating condition of downer reactor is solid mass flux between 50 – 300 $kg/m^2.s$. This section shows the simulation of catalytic cracking of heavy oil at high solid catalyst mass flux for high performance operations. The results of temperature and mass fraction profiles are shown in Figure 80 and 81.

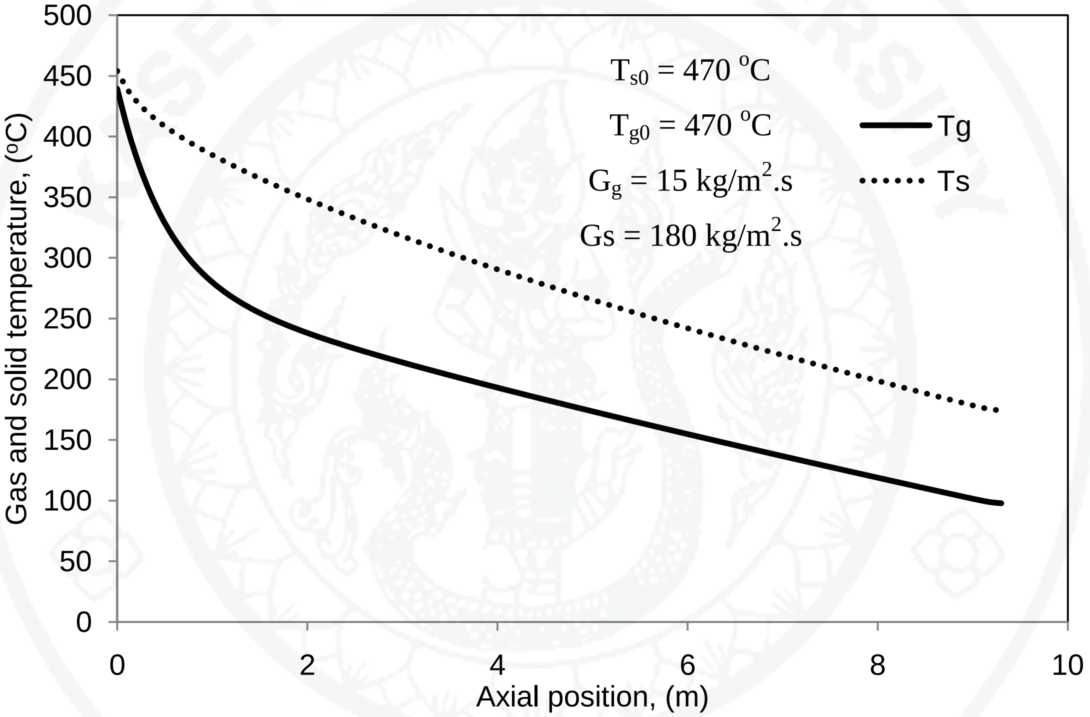

Figure 80 Simulated gas and solid temperature distributions of catalytic cracking of heavy oil with heat loss through the wall at T_{s0}=470 °C, T_{g0} = 470 °C, G_g = 15 $kg/m^2.s$, and G_s = 180 $kg/m^2.s$ in the downer reactor.

At the high operating condition (G_g = 15 $kg/m^2.s$ and G_s = 180 $kg/m^2.s$), the simulated temperature profiles gradually decrease along the length of the reactor. The decreasing rate of temperature is lower and exit temperature is higher than those at lower operating conditions (G_g = 5 $kg/m^2.s$ and G_s = 4.5 $kg/m^2.s$) because the high amount of heat carried in with the solid phase is transferred to the gas phase.

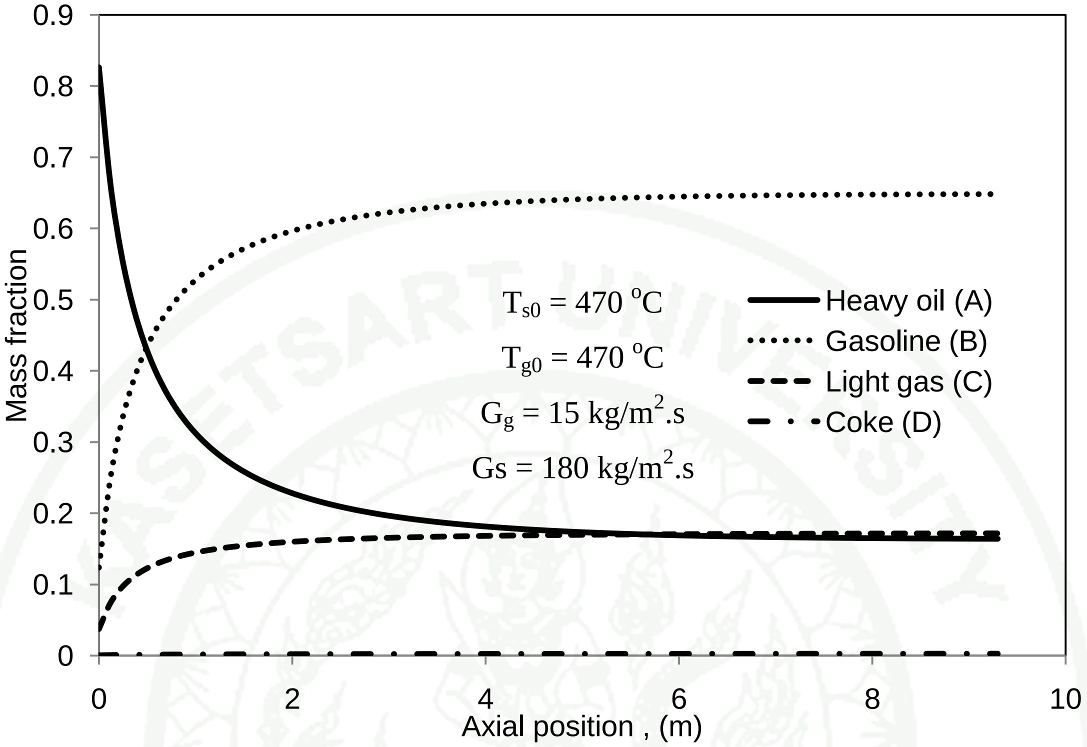

Figure 81 The mass fraction distributions of heavy oil (A), gasoline (B), light gas (C), and coke (D) of catalytic cracking with heat loss through the wall at T_{s0} = 470 ^{o}C, T_{g0} = 470 ^{o}C, G_g = 15 kg/m^2.s, and G_s = 180 kg/m^2.s in the downer reactor.

The concentration of heavy oil decreases faster and greater than those at low operating conditions (in Figure 59) because of higher solid catalyst quantity. This high conversion produces more of product yields especially the gasoline (B) because the temperature of 470 ^{o}C is not too high to overcrack into light gas. Under this operating condition, a reactor length of 3 m is enough to carry out the reaction. After 3 m, not much of heavy oil is left and the temperature is too low to carry out the cracking reactions.

8. Comparison of downer reactor performance in adiabatic, isothermal, and non adiabatic operation

The operations of downer reactor in catalytic cracking are adiabatic, isothermal, and non-adiabatic with heat loss through the wall. The mathematical model with heat loss through the wall is modified to adiabatic operation without heat loss through the wall and isothermal operation at constant gas and solid temperature. Simulation is done at the same operating condition. The results in temperature and mass fraction profiles are shown in Figure 82, 83, and 84.

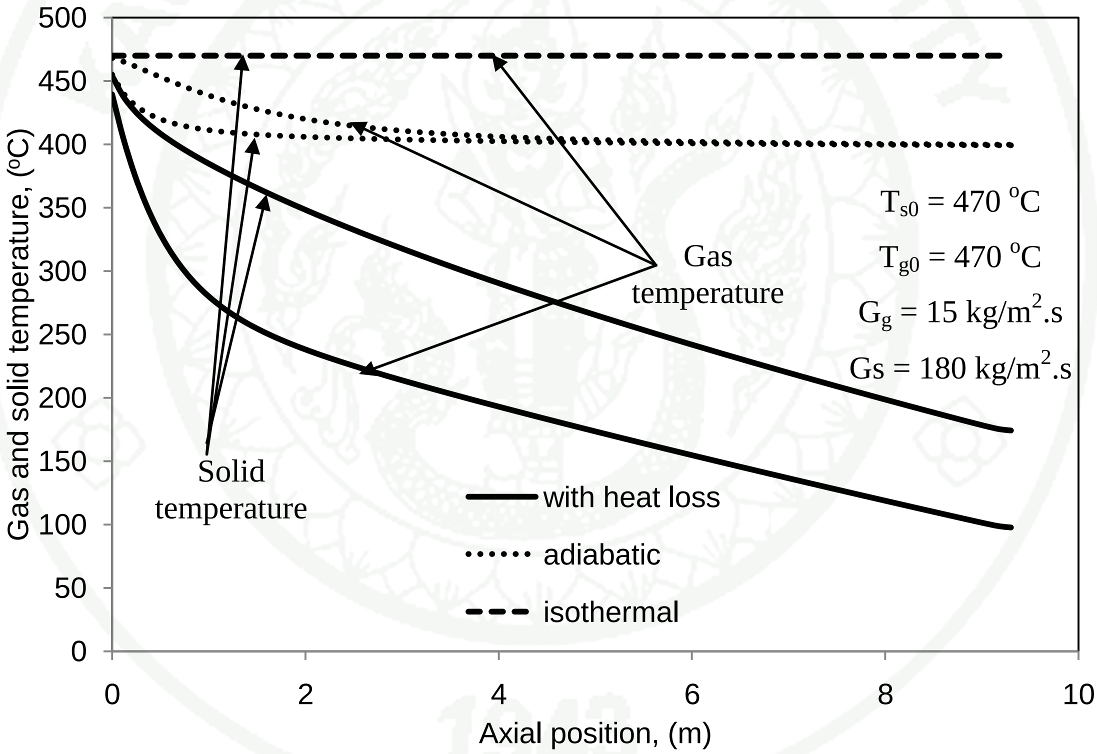

Figure 82 Temperature profiles of the downer reactor in catalytic cracking of heavy oil under various operations of adiabatic, isothermal, and non-adiabatic with heat loss through the wall.

The temperature profiles in isothermal case are constant at the inlet temperature of 470 °C. The solid temperature profile in adiabatic case decreases from the effect of endothermic reaction at the solid catalyst surface. The gas temperature also decreases from transferring the heat to the solid phase. After the entrance region, the solid temperature is a little under the practical cracking temperature range of 425 °C and the heavy oil concentration is low (see Figure 83). Thus the temperature profiles of adiabatic case are flat due to negligible reaction occurs. Whiles the non-adiabatic with heat loss through the wall case, the gas temperature profile decreases faster when compare with solid temperature profile because the heat loss through the wall occurs in gas phase. After the entrance region, the gas temperature decreases with the effect of heat loss through the wall. The solid temperature decreases from the heat transfer to the gas.

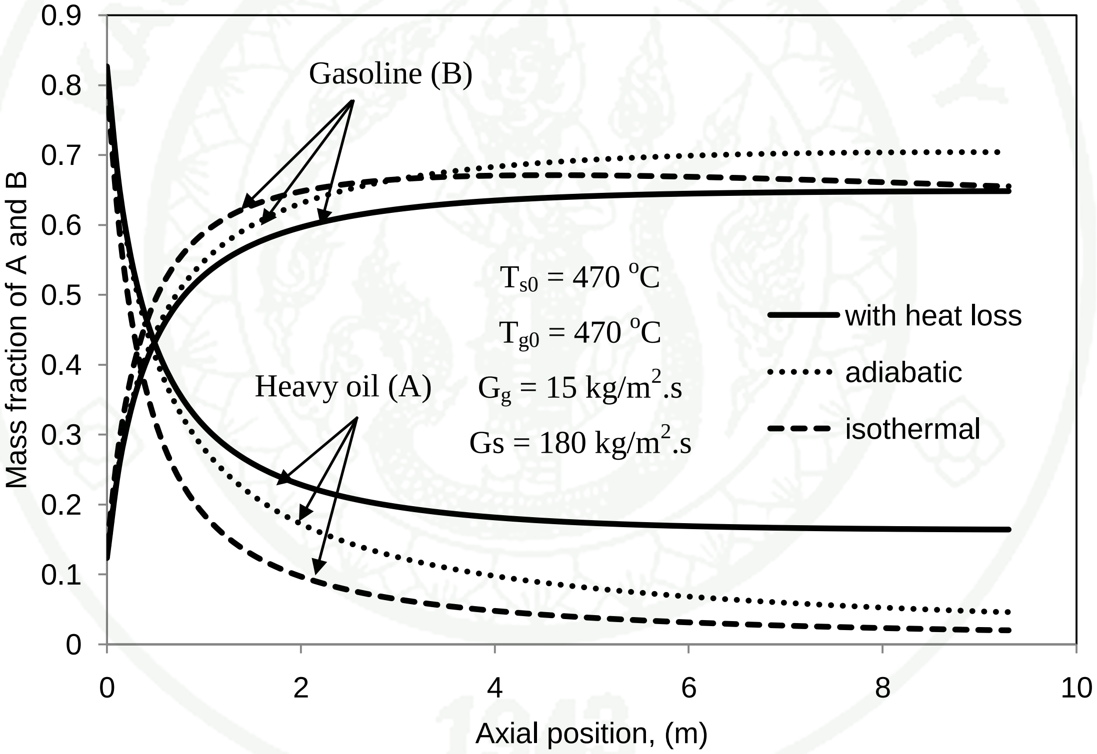

Figure 83 Comparison mass fraction of heavy oil (A) and gasoline (B) in adiabatic, isothermal, and non-adiabatic with heat loss through the wall under similar operating condition in the downer reactor.

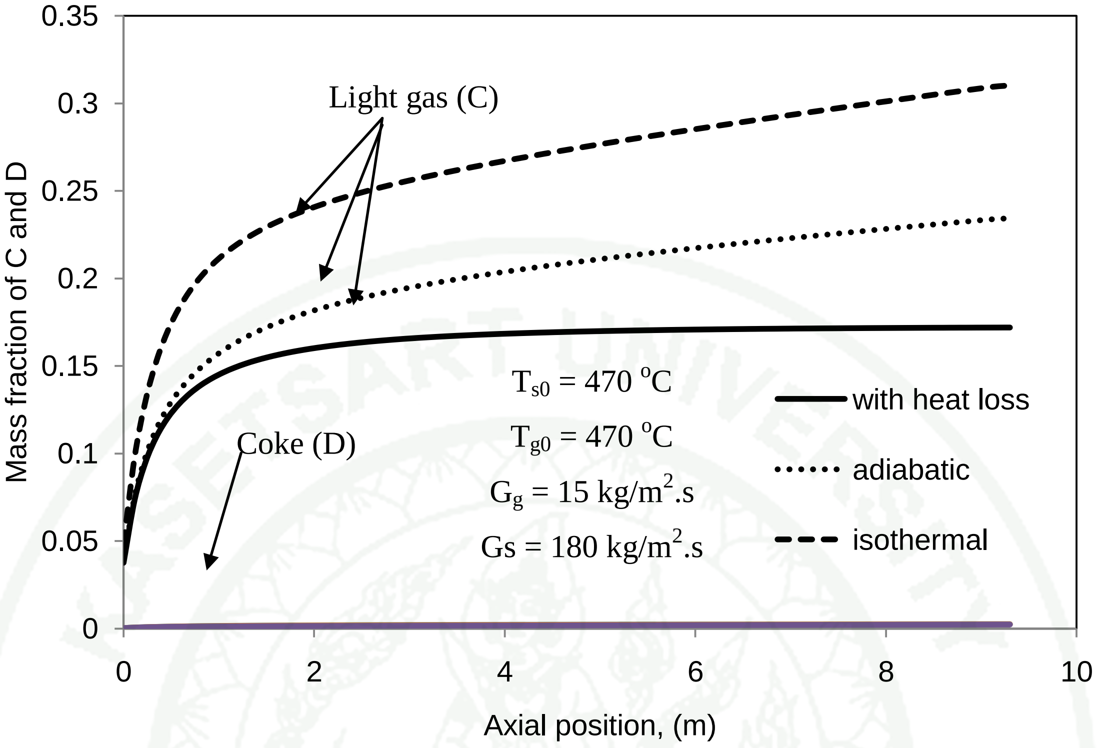

Figure 84 Comparison mass fraction of light gas (C) and coke (D) in adiabatic, isothermal, and non-adiabatic with heat loss through the wall under similar operating condition in the downer reactor.

The high operating flux condition gives high conversion and yields in every cases. The Isothermal case gives the highest rate of gasoline production but in moving to the reactor exit, the gasoline yield decreases a little due to the overracking. So, the light gas yield from the isothermal case is the highest. For the adiabatic case, the conversion and yield is the second high and follow by the heat loss through the wall case. The heat losing through the wall has an important roll in gas and solid temperatures which result in the heavy oil conversion and gasoline yield. The coke occurs minimally. At this simulated condition, a reactor length of 3 m should be used to minimize the overcracking.

CONCLUSION AND RECOMENTATIONS

1. The rate of heat loss through the wall of the downer reactor was obtained from the heat transfer experiment and the overall heat transfer coefficients (U) was estimated.

2. The correlation of overall heat transfer coefficient ($U_{correlation}$) is calculated from the overall heat transfer coefficients obtained from the experiments. This correlation of overall heat transfer coefficient is $U = 0.000408 G_g^{3.31} G_s^{1.37}$ kW/m^{2}K for the temperature range of 300 - 560 ^{o}C, solid flux range of 2.2 – 5.6 kg/m^2.s, and the gas flux range of 3.8 - 5.8 kg/m^2.s.

3. The average errors between the correlation and experiment of overall heat transfer coefficient is 9% and the maximum error is 21 %.

4. The correlation of overall heat transfer coefficient is a little low at the entrance and a little high at the exit of the reactor when compare with experimental data. The average error of temperature at the exit is about 60 ^{o}C.

5. The correlation of overall heat transfer coefficient is added into the energy balance equation for simulation of temperature and mass distribution of catalytic cracking of heavy oil. The simulation of heavy oil catalytic cracking with heat loss through the wall at T_{s0} = 35 ^{o}C gives minimal conversion and yield because solid temperature is not enough for cracking reaction.

6. At high T_{s0}, the simulated gas and solid temperature profiles decrease fast due to the endothermic reaction, heat transfer between phase, and heat loss through the wall. The mass fractions of heavy oil decrease fast at the entrance and then slowly decrease because the reaction can be occurs only at high temperature at notice at the entrance of the reactor.

7. At high feeding condition, (G_g = 15 kg/m^2.s, G_s = 180 kg/m^2.s, and Ts0 = 470 ^{o}C), the simulated temperature and mass profiles are higher than at low feeding condition because large quantity of solid catalyst is available. The product yield is also higher because there are higher surface area for reaction.

8. The temperature profiles at the various downer reactor operating modes are obtained from simulations. The isothermal case gives constant gas and solid temperature at 470 ^{o}C along the length of the reactor. In the adiabatic case, the temperature profiles decrease from the effect of endothermic reaction. The temperature profiles of non-adiabatic case shows the effected of heat loss through the wall.

9. The simulated isothermal case gives the highest rate of gasoline production at the entrance and decreases a little at the exit of reactor because of overcracking. So, the light gas yield from the isothermal case is the highest. For the simulated adiabatic case, the conversion and yield is the second highest and the simulated case with heat loss through the wall is the lowest because the rates of reaction depend significantly on the solid temperature. The isothermal reactor can be reduced to 3 m. of length for the maximum yield gasoline.

LITERATURE CITED

Ministry of natural resource and environment. 2004. **Pollution of Waste in Thailand**. Ministry of natural resource and environment, Bangkok.

Aguado, J., D.P. Serrano, G.S. Miguel, M.C. Castro and S. Madrid. 2007. Feed stock recycling of polyethylene in a two-step thermo-catalytic reaction system. **J. Anal. Appl. Pyrolysis**. 79: 415-423.

Ascher, U., J. Christiansen and R.D. Russell. 1981. Collocation Software for Boundary-Value ODEs, pp.209-222. *In* **ACM Transactions on Mathematical Software**. 7: 209.

Berry, T.A., T.R. McKeen, T.S. Pugsley and A.K. Dalai. 2004. Two-dimensional reaction engineering model of the riser section of a fluid catalytic cracking unit. **Ind. Eng. Chem**. **Res**. Vol 43: 5571-5581.

Bolkan, Y., F. Berruti, J. Zhu and B. Milne. 2003. Modeling circulating fluidized bed downers. **Powder Technology.** 132: 85–100.

Chen, H. and H. Li. 2004. Characterization of a high-density downer reactor. **Powder Technology.** 146: 84–92.

Cheng, Y., C. Wu, J. Zhu, F. Wei and Y. Jin. 2008. Downer Reactor: From Fundamental Study to Industrial Application. **Powder Technology.** 183: 364–384.

Cullis, C. F. and M.M. Hirschler. 1981. **The Combustion of Organic Polymer**. Clarendon Press. New York.

Deng, R., F. Wei, T. Liu and Y. Jin. 2002. Radial behavior in riser and downer during the FCC process. **Chemical Engineering Process**. 41: 259-266.

Huang, C., Z. Qian, M. Zhang and F. Wei. 2005. Solid mixing in a down-flow circulating fluidized bed of 0.418-m in diameter. **Powder Technology**. 161: 48-52.

Kim, Y.J., J.H. Bang and S.D. Kim. 1999. Bed to wall heat transfer in downer reactor. **The Canadian Journal of Chemical Engineering**. 77: 207-212.

Klomkom, P. 2009. **Performance of Polypropylene Cracking in a Fluidized Bed Reactor.** Master of Engineering (Chemical Engineering), Department of Chemical Engineering. Kasetsart University, Bangkok, Thailand.

Levenspiel, O. 1999. **Chemical Reaction Engineering**. 3rd ed. John Wiley & Sons, Inc., New York.

Lie, F., F. Wei, Y. Zheng and Y. Jin. 2006. CFD simulation of fluid catalytic cracking in downer reactors. **China Particuology**. Vol. 4, 160-166.

Lin, Y-H. and M-H. Yang. 2007. Catalytic pyrolysis of polyolefin waste into valuable hydrocarbon over reused catalyst from refinery FCC units. **Applied Catalysis A.** 328: 132-139.

Liu, W., K.-B. Luo, J.-X. Zhu and J.M. Beeckmans. 2001. Characterization of high-density gas–solids downward fluidized flow. **Powder Technology**. 115: 27–35.

Ma, Y. and J.-X. Zhu. 1999. Experimental study of heat transfer in a co-current downflow fluidized bed (downer). **Chemical Engineering Science**. 54: 41-50.

Pum-in, C. 2006. **Kinetics Rate of Polypropylene Catalytic Cracking**. Master of Chemical Engineering, Kasetsart University, Bangkok, Thailand.

Promsarn, S. 2005. **The Dispersion Model for Fluid Catalytic Cracking of Heavy Oil from Waste Plastic in Circulating Fluidized Bed Downer Reactor**. Master of Chemical Engineering, Kasetsart University, Bangkok, Thailand.

Rice, R.G. and D.D. Do. 1995. **Applied Mathematics and Modeling for Chemical Engineering.** John Wiley & Sons, Inc., New York.

Shoeter, J.G. and Buekens. 1979. A pyrolysis of plastics in stream fluidized bed. n.p

Songip, A.R., Masuda, T. Masuda, H. Kuwahara and K. Hashimoto. 1993. Kinetic studies for catalytic cracking of heavy oil from waste plastics over REY Zeolite. **Energy and Fuels**. 8: 131-135.

Weekman, V.W. 1969. Kinetic study for catalytic cracking of heavy oil. **Ind. Eng. Chem. Process Des**. Dev. 8(3): 385.

Welty, J. R., C. E. Wicks and R. E. Wison. 1984. **Fundamentals of Momentum, Heat, and Mass Transfer**. 3rd ed. John Wiley & Sons, Inc., New York.

Wu, B., J.-X. Zhu and H. Zhang. 2007. Flow dynamic in a four-inch downer using solids concentration measurements. **Powder Technology**. 178: 187-193.

Xie, D., B.D. Bowen, J.R. Grace and C. J. Lim. 2003. Two-dimensional model of heat transfer in circulating fluidized beds. Part II: Heat transfer in a high density CFB and sensitivity analysis. **International Journal of Heat and Mass Transfer**. 46: 2193-2205.

Zhang, M., Z. Qian, H. Yu and F. Wei. 2003. The near wall dense ring in a large-scale down-flow circulating fluidized bed. **Chemical Engineering Journal**. 92: 161–167.

Zhang, H., W.-X. Huang and J.-X. Zhu. 2000. Gas-solid flow behavior: CFB riser vs downer. **AlChE J.** 47: 2000-2011.

Zhu, J.-X., Y. Ma and H. Zhang. 1999. Gas-solids contact efficiency in the entrance region of a co-current downflow fluidized bed (downer). **Trans IChemE.** 77: 151-158.

______,_____, Z. Q. Yu Y. Jin, J. R. Grace and A. Issangya. 1995. Co-current downflow circulating fluidized bed (downer) reactor. **The Canadian Journal of Chemical Engineering.** 73: 662-677.

APPENDICES

Appendix A

Results data

Appendix Table A1 The gas temperature data of heat transfer experiment as a function of the operating time at T_{g0} = 470 ^oC, T_{s0} = 35 ^oC, G_g = 5.2 kg/m^2.s, and G_s = 4.5 kg/m^2.s in the downer reactor.

Time (min)	T_1 (^{o}C)	T_2 (^{o}C)	T_3 (^{o}C)	T_4 (^{o}C)	T_5 (^{o}C)	T_6 (^{o}C)	T_7 (^{o}C)	T_8 (^{o}C)	T_9 (^{o}C)	Jacket (^{o}C)
0	28	28	28	29	29	29	30	30	31	32
20	40	47	48	57	108	95	159	180	264	51
40	52	61	67	84	160	138	213	233	353	83
60	59	68	76	95	173	149	221	243	367	100
80	63	73	81	100	180	155	226	249	374	113
100	66	76	85	105	185	160	230	254	378	123
120	68	79	88	108	190	165	233	258	382	133
140	70	81	91	112	194	168	237	262	385	141
160	72	84	94	115	197	172	239	266	389	148
180	74	86	96	117	200	175	241	268	391	154
200	76	87	99	120	202	178	243	272	394	162
220	77	89	101	122	205	181	246	275	396	167
240	79	91	103	125	207	183	247	277	398	172
260	80	93	105	127	209	185	249	280	400	176
280	82	95	107	129	212	188	251	282	402	181
300	83	96	109	131	214	190	252	284	403	185
320	84	97	111	132	215	192	254	286	404	188
340	86	99	112	134	217	193	255	288	405	191
360	87	100	114	136	219	195	256	289	406	194
380	88	101	115	137	220	196	257	290	407	196
400	88	102	117	139	221	198	258	291	408	198
420	90	102	110	114	124	128	133	140	176	177
440	91	102	104	107	115	119	125	130	154	162
460	92	99	102	104	112	117	123	127	147	155

where T_1 to T_9 are the position of thermocouples from the bottom to the top of the downer reactor.

Appendix Table A2 The comparison of overall heat transfer coefficients from the experimental data and the correlation.

G_g (kg/m^2.s)	G_s (kg/m^2.s)	T_{g0} (^{o}C)	T_{gi} (^{o}C)	$U_{experiment}$ (kW/m^2.K)	$U_{correlation}$ (kW/m^2.K)	% error
4.4	4.5	380	280	0.385	0.440	14.28998
4.4	4.5	470	300	0.407	0.437	7.46366
4.4	4.5	560	350	0.407	0.437	7.46366
3.8	4.5	470	298	0.282	0.269	-4.53102
4.4	4.5	470	305	0.407	0.437	7.46366
5.2	4.5	470	310	0.788	0.760	-3.51217
5.8	4.5	470	312	1.10	1.091	-0.78401
5.2	2.2	470	347	0.338	0.283	-16.21
5.2	3.4	470	330	0.425	0.516	21.51152
5.2	4.5	470	310	0.788	0.760	-3.51217
5.2	5.6	470	302	1.22	1.028	-15.7238

where T_{gi} is the temperature inside the downer reactor.

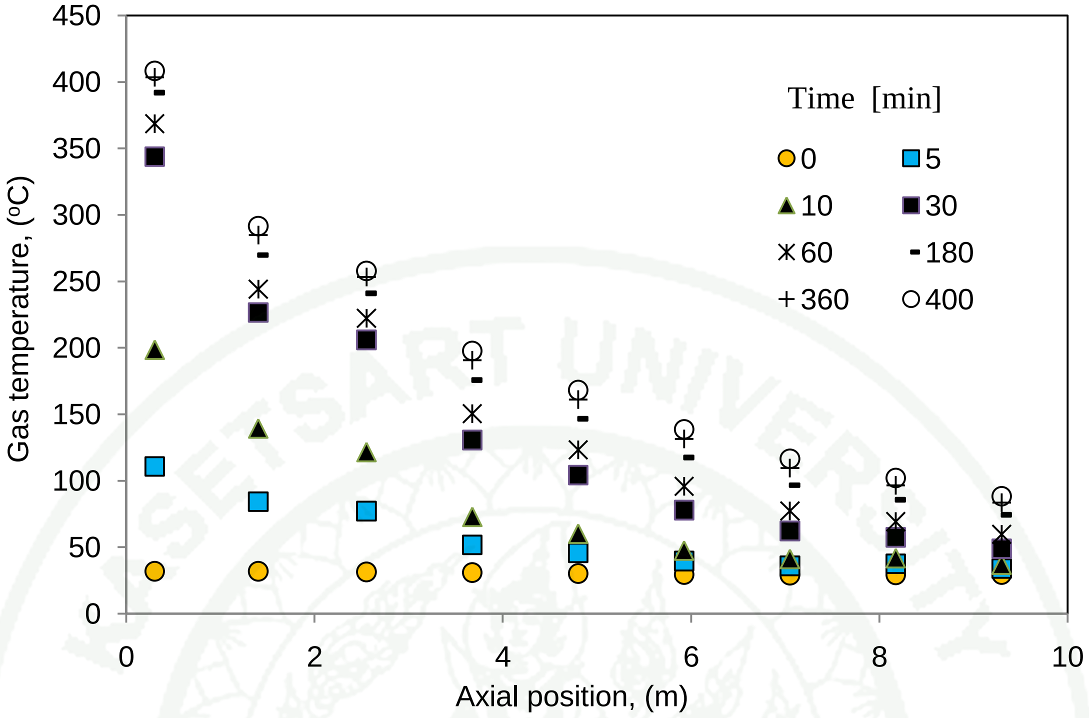

Appendix Figure A1 Temperature profiles with heat loss through the wall at various operating time, T_{g0} = 470 °C, G_g 5.2 kg/m^2.s, and without solid flow in downer reactor. After 360 min, the temperature profile changes minimally.

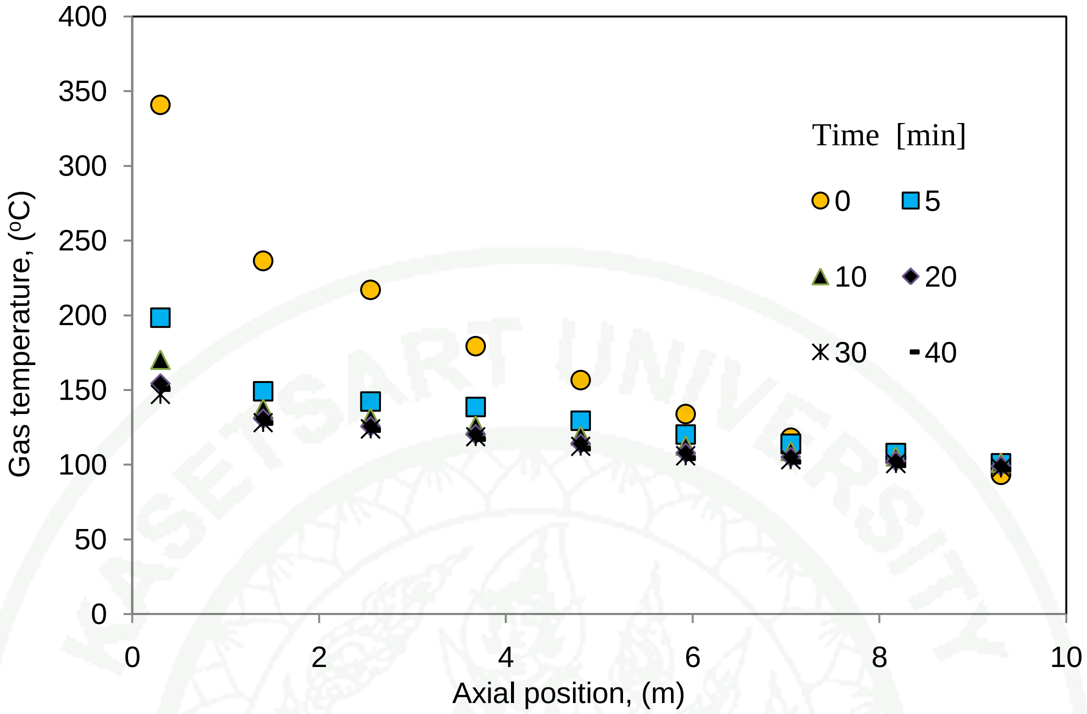

Appendix Figure A2 Temperature profiles with heat loss through the wall at various operation time, T_{g0} = 470 °C, G_g 5.2 kg/m^2.s, and G_s = 4.5 kg/m^2.s in downer reactor. After 30 min, the temperature profile reaches steady state.

Appendix B

Calculations

1. Find the inlet gas temperature of the downer reactor

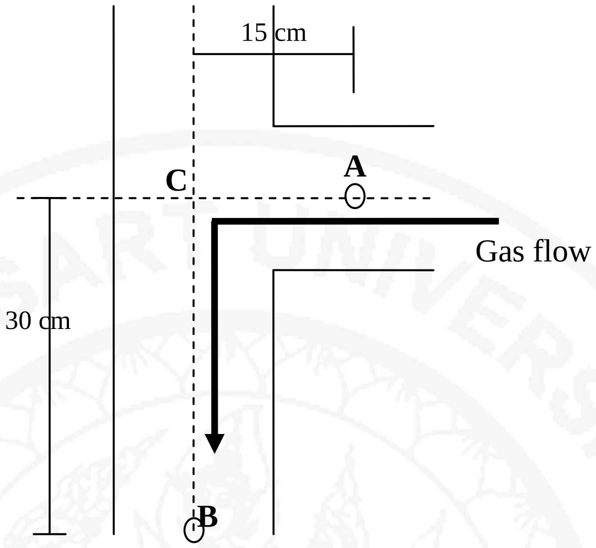

Appendix Figure B1 Schematic diagram of gas flow through the entrance region of the downer reactor.

where

A is the temperature set point.
B is the first temperature measurement.
C is the estimated inlet gas temperature of downer.

The temperature from A to B decreases linearly with the distance. The estimated inlet gas temperature is point C. Example: A = 500 ^{o}C, B = 400 ^{o}C

$$C = A - \frac{(A-B)(15)}{(15+30)}$$

$$C = 500 - \frac{(500-400)(15)}{(15+30)}$$

$$C = 467\ ^{o}\mathrm{C}$$

The inlet temperature at the entrance is 467 ^{o}C.

2. Calculation of overall heat transfer coefficient (U) in without solid flow

Example: Operating condition without solid flow at the 2nd section (l=1.125 m) from the top of downer is show as:

G_g = 5.2 kg/m^{2}s $T_{g,in}$ = 409 ^oC $T_{g,out}$ = 292 ^oC

C_{pg} = 1.09 kJ/kg.K $T_{j,in}$ = 128^oC $T_{j,out}$ = 140 ^oC A_{sec} =0.00456 m^2

A_w = 0.265 m^2

Logarithmic mean temperature across the second section ($\Delta T_{lm,g-j}$) can be calculate by equation (46).

$$\Delta T_{lm,g-j} = \frac{\left(T_{g,in} - T_{j,out}\right) - \left(T_{g,out} - T_{j,in}\right)}{ln\dfrac{\left(T_{g,in} - T_{j,out}\right)}{\left(T_{g,out} - T_{j,in}\right)}} \tag{46}$$

$$= \frac{(409 - 140) - (292 - 128)}{ln\dfrac{(409 - 140)}{(292 - 128)}}$$

= 212 ^oC = 212 K

Calculate the overall heat transfer coefficient with equation (45).

$$U = \frac{\dot{m}_g C_{p,g}\left(T_{g,out} - T_{g,in}\right)}{A_w\left(\Delta T_{lm,g-j}\right)} \tag{45}$$

$$U = \frac{\left(\dfrac{5.2kg}{m^2.s}\right)(0.00456m^2)\left(\dfrac{1.09kJ}{kg.K}\right)\left((409 - 292) \quad {}^oC\right)}{(0.265\,m^2)(212 \quad {}^oC)}$$

$$U = 0.584\ \frac{kW}{m^2K}$$

The overall heat transfer coefficient at the 2nd section of the downer reactor without solid flow is 0.584 kW/m^2.K

3. Calculation of overall heat transfer coefficient (U) in without solid flow

Example: Operating condition with solid flow at the 2nd section (l=1.125 m) from the top of downer is show as:

G_g = 5.2 kg/m^{2}s $T_{g,in}$ = 149 ^{o}C $T_{g,out}$ = 130^{o}C
C_{pg} = 1.09 kJ/kg.K G_s = 4.5 kg/m^{2}s $T_{s,in}$ = 136 ^{o}C A_s = 2.66 m^2
C_{ps} = 1.08 kJ/kg.K $T_{j,in}$= 128^{o}C $T_{j,out}$ = 140 ^{o}C A_{sec}=0.00456 m^2
ρ_s=1,800 kg/m^3 ε=0.9987 $T_{j,in}$= 128^{o}C $T_{j,out}$ = 140 ^{o}C
A_{sec}=0.00456 m^2 A_w = 0.265 m^2

T_g is the average temperature between the gas inlet and gas outlet temperature can be calculated follow:

$$T_g = \frac{T_{g,in} + T_{g,out}}{2} = \frac{149 + 130}{2} = 139.5^o C$$

The heat transfer between phases inside the reactor is calculated by equation (15).

$$h = 12\big((1-\varepsilon)\rho_s\ \big)^{0.43} \tag{15}$$

$$h = 12\big((1-0.9987)1{,}800\ \ \big)^{0.43}$$

h=0.0173 kW/m^2.K

From the energy balance of solid as in equation (44) can be derived the outlet solid temperature of interval section as shows.

$$\dot{m}_s C_{p,s}\big(T_{s,out} - T_{s,in}\big) = hA_s\big(T_g - T_s\big) \tag{44}$$

$$T_{s,out} = 129\ ^{o}\mathrm{C}$$

The calculation of overall heat transfer coefficient is derived from the equation (43)

$$\dot{m}_g C_{p,g}\left(T_{g,out} - T_{g,in}\right) = UA_w\left(\Delta T_{lm,g-j}\right) + hA_s\left(T_g - T_s\right) \tag{43}$$

$$U = 0.585\,\frac{kW}{m^2K}$$

The overall heat transfer coefficient at the 2nd section of the downer reactor with solid flow is 0.585 kW/m^2.K

Appendix C

Experimental setup

Appendix Figure C1 The downer reactor with 9.3 m of length and 3 inches of diameter and cover with the jacket.

Appendix Figure C2 Hot air feeding unit for the heat loss experiments.

Appendix Figure C3 The solid catalyst feeding unit.

Appendix Figure C4 The gas-solid separator unit.

Appendix Figure C5 The via of air inlet through the jacket unit.

Appendix Figure C6 The via of air outlet fromthe jacket unit (exhaust).

CURRICULUM VITAE

NAME : Mr. Chanin Sraphet

BIRTH DATE : September 5, 1982

BIRTH PLACE : Chumphon, Thailand

EDUCATION :

YEAR	INSTITUTION	DEGREE/DIPLOMA
2005	Prince of Songkla Univ.	B.Eng. (Chem. Eng.)

SCHOLARSHIP/ AWARDS: Kasetsart University Research and Development Institute (KURDI)
National Research Council of Thailand (NRCT), and Research Development Program in